

# Higgs production via gluon fusion in association with two or three jets in supersymmetric models

Zur Erlangung des akademischen Grades eines  
DOKTORS DER NATURWISSENSCHAFTEN  
der Fakultät für Physik der  
Universität Karlsruhe (TH)

genehmigte

DISSERTATION

von

Dipl.-Phys. Michael Kubocz  
aus Ruda Slaska

Tag der mündlichen Prüfung: 06. November 2009  
Referent: Prof. Dr. D. Zeppenfeld  
Korreferent: Prof. Dr. M. Mühlleitner



## Abstract

Within the Minimal Supersymmetric Standard Model neutral Higgs bosons, the  $\mathcal{CP}$ -odd Higgs  $A$ , a light and a heavy  $\mathcal{CP}$ -even Higgs,  $h$  and  $H$ , can be efficiently produced via gluon fusion in high energy hadronic collisions. Real emission corrections to Higgs production, at order  $\alpha_s^4$  and  $\alpha_s^5$ , lead to a Higgs plus two- and three-jet final state. This thesis presents the calculation of scattering amplitudes, as induced by triangle-, box-, pentagon- and hexagon-loop diagrams. Furthermore, the analytic expressions for the amplitudes were implemented into the Monte Carlo program *VBFNLO*, with which the numerical analysis was performed. Finally, resulting hadronic cross sections are discussed and phenomenologically relevant distributions for the Large Hadron Collider are shown.

## Zusammenfassung

Innerhalb des Minimal Supersymmetrischen Standardmodells können neutrale Higgsbosonen, wie das  $\mathcal{CP}$ -ungerade Higgsboson  $A$ , das leichte und schwere  $\mathcal{CP}$ -gerade Higgsboson  $h$  und  $H$ , effizient durch Gluonfusion in hochenergetischen hadronischen Kollisionen erzeugt werden. Reelle Emissionskorrekturen zur Higgsproduktion der Ordnung  $\alpha_s^4$  und  $\alpha_s^5$ , führen zu einem Endzustand mit zwei oder drei Jets. In dieser Dissertation wird die Berechnung von Streuamplituden, induziert durch Dreieck-, Box-, Pentagon- und Hexagonschleifendiagramme präsentiert. Desweiteren wurden die analytischen Ergebnisse in das Monte-Carlo Programm *VBFNLO* implementiert und mit dessen Hilfe die numerische Auswertung durchgeführt. Anschliessend werden resultierende hadronische Wirkungsquerschnitte diskutiert und phänomenologisch wichtige Verteilungen für den LHC gezeigt.



# Contents

---

<b>1</b>	<b>Introduction</b>	<b>3</b>
<b>2</b>	<b>Basics</b>	<b>7</b>
2.1	Standard Model and Higgs Mechanism . . . . .	7
2.2	Higgs mechanism in the MSSM . . . . .	10
2.3	Masses and mixing patterns of squarks . . . . .	13
2.4	Quantum Chromo-Dynamics . . . . .	14
<b>3</b>	<b>Higgs production processes in association with two and three jets</b>	<b>17</b>
3.1	Introduction and motivation . . . . .	17
3.2	Outline of the calculation . . . . .	19
3.3	Higgs production in association with two jets . . . . .	22
3.3.1	$qQ \rightarrow qQ\Phi$ and $qq \rightarrow qq\Phi$ . . . . .	23
3.3.2	$qg \rightarrow qg\Phi$ . . . . .	25
3.3.3	$gg \rightarrow gg\Phi$ . . . . .	27
3.4	Higgs production in association with three jets . . . . .	34
3.4.1	$qQ \rightarrow qQg\Phi$ and $qq \rightarrow qqg\Phi$ . . . . .	37
3.4.2	$qg \rightarrow qgg\Phi$ . . . . .	40
3.4.3	$gg \rightarrow ggg\Phi$ . . . . .	46
<b>4</b>	<b>Numerical implementation and checks</b>	<b>49</b>
<b>5</b>	<b>Applications to LHC physics</b>	<b>53</b>
5.1	Introduction . . . . .	53
5.2	Production of the $\mathcal{CP}$ -odd Higgs boson $A$ in association with two jets . . . . .	54
5.3	Production of a $\mathcal{CP}$ violating Higgs boson $\Phi$ in association with two jets . . . . .	59

5.4	Production of the $\mathcal{CP}$ -even Higgs bosons $h$ and $H$ in association with two jets with additional squark contributions . . . . .	61
5.5	Production of the Higgs bosons $\Phi$ in association with three jets	67
<b>6</b>	<b>Conclusions</b>	<b>71</b>
<b>A</b>	<b>Higgs vertices to fermions and sfermions</b>	<b>73</b>
A.1	Higgs couplings to fermions . . . . .	73
A.2	Higgs couplings to sfermions . . . . .	75
<b>B</b>	<b>Loop tensors</b>	<b>79</b>
B.1	Three-point functions (Triangles) . . . . .	79
B.1.1	Fermion-triangle with Higgs vertex . . . . .	79
B.1.2	Fermion-triangle with $\mathcal{CP}$ -odd Higgs vertex . . . . .	80
B.1.3	Fermion-triangle with $\mathcal{CP}$ -even Higgs vertex . . . . .	81
B.1.4	Sfermion-triangle with $\mathcal{CP}$ -even Higgs vertex . . . . .	82
B.1.5	Sfermion-triangle with $\mathcal{CP}$ -even Higgs vertex and $\tilde{q}\tilde{q}gg$ -vertex . . . . .	84
B.1.6	Sfermion-triangle with $\mathcal{CP}$ -even Higgs vertex and two $\tilde{q}\tilde{q}gg$ -vertices . . . . .	85
B.2	Four-point functions (Boxes) . . . . .	86
B.2.1	Fermion-box with Higgs vertex . . . . .	86
B.2.2	Fermion-box with $\mathcal{CP}$ -odd Higgs vertex . . . . .	88
B.2.3	Fermion-box with $\mathcal{CP}$ -even Higgs vertex . . . . .	89
B.2.4	Sfermion-box with $\mathcal{CP}$ -even Higgs vertex . . . . .	90
B.2.5	Sfermion-box with $\mathcal{CP}$ -even Higgs vertex and $\tilde{q}\tilde{q}gg$ -vertex	91
B.3	Five-point functions (Pentagons) . . . . .	94
B.3.1	Fermion-pentagon with Higgs vertex . . . . .	94
B.3.2	Sfermion-pentagon with $\mathcal{CP}$ -even Higgs vertex . . . . .	95
B.4	Six-point functions (Hexagons) . . . . .	96
<b>C</b>	<b>SU(N) identities</b>	<b>99</b>
C.1	SU( $N$ ) tensors . . . . .	99
C.2	Traces of color generators . . . . .	99
C.3	Convolutions of $d^{a_1 a_2 a_3}$ and $f^{a_1 a_2 a_3}$ with $t^a$ . . . . .	100
C.4	Jacobi identities . . . . .	100

<b>D</b>	<b>QCD- and SQCD Vertices</b>	<b>101</b>
	D.1 QCD vertices . . . . .	101
	D.2 SQCD vertices (only squarks) . . . . .	102
<b>E</b>	<b>Effective Lagrangian</b>	<b>103</b>
<b>F</b>	<b><math>gg \rightarrow ggg\Phi</math></b>	<b>107</b>
	F.1 Remaining color factors for diagrams with pentagons . . . . .	107
	<b>Bibliography</b>	<b>111</b>
	<b>Acknowledgements</b>	<b>117</b>





# Chapter 1

## Introduction

---

In today's modern physics, the process of gaining knowledge proceeds in a close cooperation of theory and experiment. By empirical research, claiming objectivity and reproducibility of the observation, theoretical assumptions are verified. Afterwards, the empirical models of experimental physics are attributed in a mathematical way to the known theoretical basis. Or, if that is not possible, a new theoretical model has to be invented, which fulfills the experimentally measured data. However, a theoretical model should not only reproduce experimental data, but also make predictions beyond the experimentally investigated region of the nature or the considered system respectively, which have not yet been discovered. With the discovery of quantum mechanics (QM) and its improved development to quantum field theory (QFT), the proof of renormalizability of non-Abelian gauge theories by G. 't Hooft and Veltman, the basic building blocks were set to the best experimentally verified and theoretically well established model, applicable over a wide range of conditions, the Standard Model (SM).

The Standard Model is based on the gauge group  $SU(3)_C \otimes SU(2)_L \otimes U(1)_Y$  and provides a unified framework to describe phenomena of the electro-weak as well as of the strong interaction. In spite of the successful description of elementary particle physics, the SM still has some crucial problems, which spoil the elegance of this theoretical framework. It starts already with the absence of gravity. But, ok, for this problem one can turn a blind eye, because gravitational effects can be safely neglected at the level of elementary particle interactions, due to very tiny effects. The introduction of a scalar field, whose vacuum expectation value breaks the gauge symmetry  $SU(2)_L \otimes U(1)_Y \rightarrow U(1)_Q$  spontaneously to generate masses for leptons, quarks and electro-weak gauge boson, seems to be a smart step for the first

glance. These masses are generated in a natural way without spoiling gauge invariance and other symmetries of the theory, and only one new particle, the Higgs boson, has to be found in experiments at particle colliders. However, to this day neither the LEP nor the Tevatron collider has found any evidence for the Higgs boson. But, they could provide a lower limit of 114.4 GeV for the SM Higgs boson mass. Unfortunately, the introduction of this scalar particle introduces a further problem, the so called "hierarchy problem". To guarantee unitarity of the scattering amplitude of electro-weak gauge bosons, the Higgs mass cannot be larger than 1 TeV. Though, quantum corrections spoil this limit, since they are proportional to a scale, which can be arbitrary large. A further problem of the SM is the extrapolation of gauge couplings to a high energy scale using methods of the renormalization group, that, however, does not lead to a unification. Furthermore, the absence of describing and providing candidates for dark matter does not make a lasting impression on the SM... Roughly speaking, there is still enough space for extensions. Many interesting extensions are already available on the market of elementary particle physics: extended Techni-color models, models with extra dimensions, Little Higgs models,... and of course supersymmetric models, like the minimal supersymmetric extension of the SM, the MSSM. It features the extended Higgs sector of a two-Higgs-doublet model: a light and a heavy neutral  $\mathcal{CP}$ -even Higgs,  $h$  and  $H$ , a  $\mathcal{CP}$ -odd Higgs  $A$  and two charged Higgs bosons  $H^\pm$ , and, of course, additional particles, which are referred as super-partners to the particle content of the SM. It attracted attention due to possible candidates for dark matter, and the extended particle content provides solutions to the above mentioned hierarchy problem. In addition, the much more constrained Higgs sector of the MSSM sets a limit for the mass of the light scalar  $h$  to  $m_h \lesssim 135$  GeV, which points towards  $m_h \approx 120$  GeV at the 95 % CL. The search for the Higgs bosons of the SM and its extensions, as well as the investigation of their couplings, is the main motivation for the construction of the Large Hadron Collider (LHC) at CERN with 14 TeV center-of-mass energy . The experimental evidence of Higgs bosons would confirm the idea of electro-weak unification and also show indication for theory beyond the SM.

The most copious sources of the Higgs boson production at the LHC are electro-weak boson fusion and gluon fusion. Higgs production via fusion of

electro-weak gauge bosons in association with two tagging jets provide an adequate possibility to measure the Higgs boson couplings. Small radiative corrections and, hence, small systematic errors characterize this process. Gluon fusion gives also rise to a Higgs plus two jet final state and constitutes a large background, which cannot be neglected. Furthermore, in gluon fusion the azimuthal angle  $\phi_{jj}$  between the more forward and more backward of the two tagging jets is sensitive to the  $\mathcal{CP}$ -character of the Higgs coupling to fermions.

The subjects of this thesis are the calculation and the discussion of the phenomenological implications on the production of neutral Higgs bosons with two and three additional jets in final state via gluon fusion in high energy hadronic collisions at the LHC. These are processes like  $pp \rightarrow \text{Higgs} + jjX$  and  $pp \rightarrow \text{Higgs} + jjjX$ . As theoretical basis, the minimal supersymmetric extension of the Standard Model (MSSM) is used. In the following, charged Higgs bosons are not considered and all neutral Higgs bosons are denoted by the shorthand  $\Phi$ . The contributing sub-processes to the  $\Phi jj$  and  $\Phi jjj$  production include quark-quark, quark-gluon and gluon scattering. At leading order, the coupling of the neutral Higgs bosons to gluons is mediated by a massive loop, whose particle content is restricted in this thesis to the third generation of quarks and its supersymmetric scalar partners, the squarks. Thus the requirement of a massive loop is justified, since the Higgs boson couples only to massive particles and the gluon, carrier of the strong force, has no mass. The loop-topologies, appearing in the calculation of the amplitudes, range from triangles, boxes, up to pentagons and hexagons, which make the calculation quite involved. Additionally, Quantum Chromodynamics (QCD) provides a complicated color structure for the scattering amplitudes. First results of double real emission corrections to the production of the  $H_{\text{SM}}$ , which lead to a Higgs plus two-jet final state at order  $\alpha_s^4$ , were already presented in Refs. [1, 2]. A further calculation with the same final state was performed for the  $\mathcal{CP}$ -odd Higgs boson  $A$  and is available in Ref. [3].

The results of the calculation, presented in this thesis, were implemented into the gluon fusion part *GGFLO* of the parton-level Monte Carlo program *VBFNLO* [4]. The thesis is organized as follows:

Chapter 2 gives a brief outline of the Standard Model and its particle content,

as well as the Higgs mechanism in the SM and in the supersymmetric extension, the MSSM. Furthermore, the masses and mixing patterns of squarks are preparatively introduced. And finally, the basics of perturbative QCD and the calculation of the cross section in hadronic collisions are reviewed.

Chapter 3 provides a detailed description of the calculation of the scattering amplitudes for the two processes  $pp \rightarrow \text{Higgs} + jjX$  and  $pp \rightarrow \text{Higgs} + jjjX$ . Further details on various loop contributions are relegated to the Appendices.

Chapter 4 describes analytical and numerical consistency checks of the calculation and implementation.

The main phenomenological results are presented in Chapter 5, for  $pp$  scattering at the LHC with a center of mass energy of  $\sqrt{s} = 14$  TeV. Integrated cross sections and differential distributions for the production of the  $\mathcal{CP}$ -odd Higgs boson  $A$  are shown, as well as arbitrary  $\mathcal{CP}$ -violating couplings to the third generation of quarks for general  $\Phi jj$  events. Furthermore, differential distributions and integrated cross sections are presented for the production of the  $\mathcal{CP}$ -even Higgs bosons  $h$  and  $H$  including fermionic and scalar loop-contributions of the third generation of quarks and squarks. The last part provides preliminary results for  $\Phi jjj$  production, showing de-correlation effects of the azimuthal angle distribution, in comparison to  $\Phi jj$  events.

Final conclusions are drawn in Chapter 6.

Vertices of the neutral Higgs bosons to fermions and sfermions are given in Appendix A. The Appendix B provides a detailed description of the calculated and implemented loop topologies. In Appendix C useful identities of the  $SU(N)$ -algebra are collected. Vertices of the QCD and SUSY-QCD (SQCD) are illustrated in Appendix D. The Appendix E gives a short introduction to the effective Lagrangian and its correspondence to the full theory. Finally, Appendix F contains some stored color structures of the sub-process  $gg \rightarrow ggg\Phi$ .

# Chapter 2

## Basics

---

### 2.1 Standard Model and Higgs Mechanism

The Standard Model is based on some basic principles: special relativity, locality, quantum mechanics, renormalizability, local and global symmetries. The model provides a unified framework to describe three forces of nature: the electro-weak theory, proposed by Glashow, Salam and Weinberg. It describes electromagnetic and weak interactions between lepton and quarks. The underlying group structure is composed of a direct product of two gauge symmetry groups  $SU(2)_L \otimes U(1)_Y$ , corresponding to weak left-handed isospin and hypercharge. The theory of strong interactions between colored quarks enters via Quantum Chromo-Dynamics (QCD), which is based on the non-Abelian gauge symmetry group  $SU(3)_C$ . Thus, the full group structure reads as

$$SU(3)_C \otimes SU(2)_L \otimes U(1)_Y . \quad (2.1)$$

The content of matter fields is given by three generations of chiral leptons and quarks. They are split to left-handed isospin doublets and right-handed isospin-singlets:

- Leptons:

$$L_L = \begin{pmatrix} \nu_e \\ e \end{pmatrix}_L, \quad \begin{pmatrix} \nu_\mu \\ \mu \end{pmatrix}_L, \quad \begin{pmatrix} \nu_\tau \\ \tau \end{pmatrix}_L; \quad L_R = e_R, \mu_R, \tau_R,$$

- Quarks:

$$Q_L = \begin{pmatrix} u \\ d \end{pmatrix}_L, \quad \begin{pmatrix} c \\ s \end{pmatrix}_L, \quad \begin{pmatrix} t \\ b \end{pmatrix}_L; \quad Q_R = u_R, d_R, c_R, s_R, t_R, b_R.$$

The hypercharge of fermions  $Y_f$  is defined by the Gell-Mann-Nijishima relation

$$Y_f = 2\left(Q_f - I_f^3\right), \quad (2.2)$$

with  $Q_f$  the electric charge in units of  $+e$ , and  $I_f^3$ , the third component of the weak isospin. The values of  $Y_f$  for all generations of the fermion matter fields are given by

$$Y_L = -1, \quad Y_{e_R} = -2, \quad Y_Q = \frac{1}{3}, \quad Y_{u_R} = \frac{4}{3}, \quad Y_{d_R} = -\frac{2}{3}. \quad (2.3)$$

Leptons do not carry color charge and, hence, are color-singlets under the global SU(3)-symmetry of the QCD, in contrast to quarks, which are assigned as SU(3)-triplets.

Forces between fermionic matter fields are mediated by spin-one bosons. These vector fields are derived assuming, that the Lagrangian of a fermion field is invariant under local gauge transformations for a group  $G$ . Here, of course, the group  $G$  corresponds to the three sub-groups, mentioned in Eq. (2.1). Carrier of the electromagnetic force is the massless photon  $\gamma$ , whereas the massive  $W$  and  $Z$  bosons mediate the weak force between the SU(2)-multiplets, described above. The neutral gauge boson  $Z$  interacts with all fermion fields, the charged gauge bosons  $W^\pm$ , however, induce transitions between the left-handed doublets only. The right-handed singlets remain untouched. In addition, with this different coupling behavior to left- and right-handed fermions, the experimentally observed violation of parity of the weak force is considered automatically. The strong force between quarks is mediated by eight massless gluons, which carry simultaneously color and anti-color.

The experimentally observed masses of the weak gauge bosons, leptons and quarks turn out to be problematic from the theoretical point of view. Explicit mass terms for gauge bosons,  $m^2 A^\mu A_\mu$ , destroy gauge invariance, which is a basic requirement for the renormalizability of the theory. Mass terms for leptons and quarks,  $m\bar{F}F = m(\bar{F}_L F_R + \bar{F}_R F_L)$ , are also not possible, because the product of a doublet with a singlet is not invariant under SU(2)<sub>L</sub>-isospin rotations. This problem can be circumvented, if the model is extended by a

further scalar SU(2)-doublet field  $\Phi$

$$\Phi(x) = \begin{pmatrix} \phi^+(x) \\ \phi^0(x) \end{pmatrix}, \quad (2.4)$$

with hypercharge  $Y_\Phi = 1$  and potential

$$V(\Phi) = -\mu^2(\Phi^\dagger\Phi) + \frac{\lambda}{4}(\Phi^\dagger\Phi)^2, \quad \text{with } \mu^2 > 0, \lambda > 0. \quad (2.5)$$

The minimization of  $V$  breaks the  $SU(2)_L \otimes U(1)_Y \rightarrow U(1)_Q$  spontaneously and the scalar field  $\Phi$  acquires a VEV  $v$

$$\langle\Phi\rangle = \frac{1}{\sqrt{2}} \begin{pmatrix} 0 \\ v \end{pmatrix} \quad \text{with } v = \frac{2\mu}{\sqrt{\lambda}} = \left(\sqrt{2}G_F\right)^{-1/2} \approx 246 \text{ GeV}. \quad (2.6)$$

$G_F$  denotes the Fermi-constant with the experimentally fixed value at  $G_F = 1.16637 \cdot 10^{-5}$ . The expansion of  $\Phi$  around the VEV can be written as

$$\Phi(x) = \frac{1}{\sqrt{2}} \begin{pmatrix} \theta_1(x) + \theta_2(x) \\ v + H_{SM}^0(x) + i\theta_3(x) \end{pmatrix}. \quad (2.7)$$

According to the Goldstone Theorem, the number of Goldstone bosons,  $\theta_{1,2,3}(x)$ , corresponds to the number of broken generators. Furthermore, they can be rotated away using the local  $SU(2)_Y$  symmetry (unitary gauge)

$$\Phi(x) \rightarrow \exp\left[-i\frac{\tau^a}{v}\theta^a\right]\Phi(x) = \frac{1}{\sqrt{2}} \begin{pmatrix} 0 \\ v + H_{SM}^0(x) \end{pmatrix}. \quad (2.8)$$

Masses of the gauge bosons are given by the the kinetic term

$$(D_\mu\Phi)^\dagger(D^\mu\Phi) \quad \text{with } D_\mu\Phi = \left(\partial_\mu - ig_2W_\mu^a\tau^a - ig_1\frac{Y}{2}B_\mu\right)\Phi, \quad (2.9)$$

in which  $\tau^a = \sigma^a/2$  with  $a = 1, 2, 3$  are the known Pauli-matrices.  $W_\mu^a$  correspond to the gauge bosons and  $g_2$  to the coupling constant of the  $SU(2)_L$  group.  $B_\mu$  and  $g_1$  describe the  $U(1)_Y$  gauge boson and its coupling constant. After the diagonalization procedure, one gets the following relations for the masses of the gauge bosons

$$M_Z = \sqrt{g_1^2 + g_2^2}\frac{v}{2}, \quad M_W = g_2\frac{v}{2}, \quad M_{A_\mu} = 0. \quad (2.10)$$

Since the  $SU(3)$  symmetry is not broken, there is no mass term for the gluon. Now, the Higgs-doublet  $\Phi$  allows for Yukawa-like terms

$$g_f \left[ (\bar{F}_L \cdot \Phi) F_R + \text{h.c.} \right], \quad (2.11)$$

that generate, after the spontaneous symmetry breakdown, the wanted mass-terms for fermions

$$g_f \frac{v}{\sqrt{2}} (\bar{f}_L f_R + \bar{f}_R f_L), \quad (2.12)$$

where  $f$  denotes the entry of the corresponding  $SU(2)$  doublet and singlet. Finally, the insertion of the Higgs-doublet (2.8) into the potential (2.5) gives the mass of the Higgs boson

$$M_{H_{SM}^0} = \sqrt{2}\mu = \frac{v}{\sqrt{2}}\sqrt{\lambda}. \quad (2.13)$$

## 2.2 Higgs mechanism in the MSSM

The Minimal Supersymmetric Standard Model (MSSM) is the simplest supersymmetric extension of the SM. In this connection, supersymmetry extends the Poincaré-group by new generators, that correlate bosonic and fermionic degrees of freedom. For a more introductive description see Ref. [5]. Thus, the particle spectrum of the SM gets expanded. Quarks and leptons obtain scalar partners, called squarks and sleptons. The supersymmetric partners of the gauge bosons are spin-1/2 particles, photinos, winos, zinos and gluinos. Superpartner of the Higgs boson is the higgsino. The particles of the SM and their super-partners are then combined to superfield multiplets. In contrast to the SM, the MSSM contains two Higgs-doublets

$$\Phi_1 = \begin{pmatrix} \phi_1^0 \\ \phi_1^- \end{pmatrix}, \quad Y_{\Phi_1} = -1, \quad \Phi_2 = \begin{pmatrix} \phi_2^+ \\ \phi_2^0 \end{pmatrix}, \quad Y_{\Phi_2} = 1. \quad (2.14)$$

The requirement of two doublets with opposite hypercharge is necessary to compensate the hypercharges of both higgsinos. This guarantees, that the sum of all hypercharges vanish, similar to the SM, and leads to an anomaly



free model. Yukawa couplings to both Higgs-doublets are given by the superpotential [6]

$$\begin{aligned}
W = \sum_{i,j=\text{Gen.}} & -Y_{ij}^u \hat{u}_{Ri} \hat{\Phi}_2 \cdot \hat{Q}_j + Y_{ij}^d \hat{d}_{Ri} \hat{\Phi}_1 \cdot \hat{Q}_j + Y_{ij}^l \hat{l}_{Ri} \hat{\Phi}_1 \cdot \hat{L}_j \\
& + \mu \hat{\Phi}_2 \cdot \hat{\Phi}_1 ,
\end{aligned} \tag{2.15}$$

where the hat marks the corresponding superfield multiplets and the  $Y$  denotes Yukawa couplings among lepton and quark generations. The mass parameter  $\mu$  is necessary to avoid an additional Peccei-Quinn symmetry [7]. Moreover, supersymmetry claims for the superpotential  $W$  to be a holomorphic function with respect to the superfields and, thus, forces the Higgs-doublet  $\hat{\Phi}_1$  to couple to down-type fermions and  $\hat{\Phi}_2$  to up-type fermions only. By the way, this different coupling behavior of both Higgs-doublets corresponds exactly to that of the general 2HDM Model II [8]. The scalar potential reads as

$$\begin{aligned}
V_H = & \bar{m}_1^2 (|\phi_1^0|^2 + |\phi_1^-|^2) + \bar{m}_2^2 (|\phi_2^0|^2 + |\phi_2^+|^2) - \bar{m}_3^2 (\phi_1^- \phi_2^+ - \phi_1^0 \phi_2^0 \\
& + \text{h.c.}) + \frac{g_1^2 + g_2^2}{8} (|\phi_1^0|^2 + |\phi_1^-|^2 - |\phi_2^0|^2 - |\phi_2^+|^2)^2 \\
& + \frac{g_2^2}{2} |\phi_1^{-*} \phi_1^0 + \phi_2^{0*} \phi_2^+|^2 ,
\end{aligned} \tag{2.16}$$

with the abbreviations

$$\bar{m}_1^2 = |\mu|^2 + m_{\Phi_1}^2, \quad \bar{m}_2^2 = |\mu|^2 + m_{\Phi_2}^2, \quad \bar{m}_3^2 = B\mu , \tag{2.17}$$

containing soft SUSY-breaking scalar Higgs-mass terms  $m_{\Phi_i}$  [6]. The constants  $g_2$  and  $g_1$  are the usual  $SU(2)_L \otimes U(1)_Y$  gauge couplings. The symmetry-breaking proceeds similar to the SM. Here, the neutral components of both Higgs fields acquire VEVs

$$\langle \Phi_1 \rangle = \frac{1}{\sqrt{2}} \begin{pmatrix} v_1 \\ 0 \end{pmatrix}, \quad \langle \Phi_2 \rangle = \frac{1}{\sqrt{2}} \begin{pmatrix} 0 \\ v_2 \end{pmatrix}, \tag{2.18}$$

with

$$\tan \beta = \frac{v_2}{v_1} = \frac{v \sin \beta}{v \cos \beta} \quad \text{and} \quad v^2 = v_1^2 + v_2^2 \approx 246 \text{ GeV} . \tag{2.19}$$

Phase freedom of both VEVs restricts the angle  $\beta$  to the range  $0 \leq \beta \leq \pi/2$ . The expansion of  $\Phi_{1,2}$  around the VEVs yields

$$\Phi_1 = \frac{1}{\sqrt{2}} \begin{pmatrix} v_1 + H_1^0 + iP_1^0 \\ H_1^- \end{pmatrix}, \quad \Phi_2 = \frac{1}{\sqrt{2}} \begin{pmatrix} H_2^+ \\ v_2 + H_2^0 + iP_2^0 \end{pmatrix}. \quad (2.20)$$

The mass-matrix of the components of both Higgs-fields results from the second derivatives of  $V_H$  (2.16), according to the corresponding fields at the points given in Eq. (2.18). The conservation of electric charge avoids mixing between charged and neutral Higgs fields. Consequently, there are two mass matrices, one for the charged sector and one for the neutral sector [9]. Moreover, assumed  $\mathcal{CP}$ -invariance of the Higgs sector does not mix real and imaginary components of the neutral Higgs bosons. The eight degrees of freedom correspond then to three Goldstone bosons  $G^0$ ,  $G^\pm$  and five Higgs bosons, neutral  $h$ ,  $H$ ,  $A$  and also two charged  $H^\pm$ . The light  $h$  and heavy  $H$  are  $\mathcal{CP}$ -even, whereas  $G^0$  and  $A$  are  $\mathcal{CP}$ -odd. The diagonalization of the mass-matrix is done with the following transformations

$$\begin{pmatrix} G^0 \\ A \end{pmatrix} = \begin{pmatrix} \cos \beta & \sin \beta \\ -\sin \beta & \cos \beta \end{pmatrix} \begin{pmatrix} P_1^0 \\ P_2^0 \end{pmatrix}, \quad (2.21)$$

$$\begin{pmatrix} G^\pm \\ H^\pm \end{pmatrix} = \begin{pmatrix} \cos \beta & \sin \beta \\ -\sin \beta & \cos \beta \end{pmatrix} \begin{pmatrix} H_1^\pm \\ H_2^\pm \end{pmatrix}, \quad (2.22)$$

$$\begin{pmatrix} H \\ h \end{pmatrix} = \begin{pmatrix} \cos \alpha & \sin \alpha \\ -\sin \alpha & \cos \alpha \end{pmatrix} \begin{pmatrix} H_1^0 \\ H_2^0 \end{pmatrix}, \quad (2.23)$$

with  $\beta$  given in Eq. (2.19). The angle  $\alpha$  is defined in the following way

$$\tan 2\alpha = \frac{m_h^2 + m_H^2}{m_A^2 - M_Z^2} \tan 2\beta = \frac{m_A^2 + M_Z^2}{m_A^2 - M_Z^2} \tan 2\beta, \quad (2.24)$$

in which  $\alpha$  is restricted to the interval  $-\pi/2 \leq \alpha \leq 0$  by  $0 \leq \beta \leq \pi/2$ . The tree-level physical squared masses of the two  $\mathcal{CP}$ -even Higgs bosons are

$$m_{H,h}^2 = \frac{1}{2} \left\{ m_A^2 + M_Z^2 \pm \left[ (m_A^2 + M_Z^2)^2 - 4M_Z^2 m_A^2 \cos^2 2\beta \right]^{1/2} \right\}. \quad (2.25)$$

Hence, the Higgs-mass spectrum is completely controlled at tree-level by  $m_A$  and  $\tan \beta$ . Further important tree-level relations for the remaining Higgs-

masses are [10]

$$m_{H^\pm}^2 = m_A^2 + M_W^2 > \max(M_W^2, m_A^2) , \quad (2.26)$$

$$m_h^2 + m_H^2 = m_A^2 + M_Z^2 , \quad (2.27)$$

$$m_h < \min(m_A, M_Z) |\cos 2\beta| < \min(m_A, M_Z) , \quad (2.28)$$

$$m_H > \max(m_A, M_Z) . \quad (2.29)$$

Furthermore, radiative corrections shift the tree-level masses to higher values. These corrections can be very large, because they contain couplings to top-quarks as well as to their scalar super-partners. Especially the mass of the light Higgs boson  $h$  is increased by several tens of GeV, shifting it from the  $M_Z$  value to  $m_h \lesssim 135$  GeV. The corresponding correction, which contain top-quark and -squark contribution is given by

$$\Delta m_h^2 = \frac{3}{2\pi^2 v^2} m_t^4 \log(m_{\tilde{t}}^2/m_t^2) . \quad (2.30)$$

For a more detailed description of the Higgs-sector in the MSSM see Refs. [6, 9, 10]. Couplings of Higgs bosons to fermions are, in comparison to the SM, modified by trigonometric functions containing the angles  $\alpha$  and  $\beta$ . They can be looked up in App. A. Moreover,  $WWA$ ,  $ZZA$  and  $WZH^\pm$  vertices are not present at tree-level, because they are forbidden by  $\mathcal{CP}$ -invariance.

## 2.3 Masses and mixing patterns of squarks

There are three sources of squark-mass terms in the scalar potential part of the Lagrangian density . They are given by

$$V^{\tilde{q}} = V_{\text{SOFT}}^{\tilde{q}} + V_F^{\tilde{q}} + V_D^{\tilde{q}} . \quad (2.31)$$

$V_{\text{SOFT}}^{\tilde{q}}$  contains explicit mass-terms as well as trilinear  $A$ -terms. F-term contributions arise from the superpotential  $W$  (2.15). Contributions of the D-terms are specified in Eq (2.33). The squared mass-matrix for up-type squarks can be then written as

$$\begin{pmatrix} m_{\tilde{t}_L}^2 + m_t^2 + D(\tilde{t}_L) & -m_t(A^u + \mu \cot \beta) \\ -m_t(A^u + \mu \cot \beta) & m_{\tilde{t}_R}^2 + m_t^2 + D(\tilde{t}_R) \end{pmatrix} , \quad (2.32)$$

with

$$\begin{aligned}
D(\tilde{t}_L) &= M_Z^2 \cos 2\beta \left( \frac{1}{2} - \frac{2}{3} \sin^2 \theta_W \right), \\
D(\tilde{t}_R) &= M_Z^2 \cos 2\beta \left( + \frac{2}{3} \sin^2 \theta_W \right).
\end{aligned} \tag{2.33}$$

The eigenvalues of this matrix reads as follows

$$\begin{aligned}
m_{\tilde{t}_{1,2}}^2 &= \frac{1}{2} (m_{\tilde{t}_L}^2 + m_{\tilde{t}_R}^2) + \frac{1}{4} M_Z^2 \cos 2\beta + m_t^2 \\
&\mp \left\{ \left[ \frac{1}{2} m_{\tilde{t}_L}^2 - m_{\tilde{t}_R}^2 + M_Z^2 \cos 2\beta \left( \frac{1}{4} - \frac{2}{3} \sin^2 \theta_W \right) \right]^2 \right. \\
&\quad \left. - m_t^2 (\mu \cot \beta + A^t)^2 \right\}^{\frac{1}{2}}.
\end{aligned} \tag{2.34}$$

If one assumes no flavor mixing, the top-squark mixing matrix has the following form

$$\begin{pmatrix} \tilde{t}_1 \\ \tilde{t}_2 \end{pmatrix} = \begin{pmatrix} \cos \theta_t & \sin \theta_t \\ -\sin \theta_t & \cos \theta_t \end{pmatrix} \begin{pmatrix} \tilde{t}_L \\ \tilde{t}_R \end{pmatrix}. \tag{2.35}$$

The mixing angle  $\theta_t$  can be deduced from

$$\tan \theta_t = \frac{m_{\tilde{t}_L}^2 + m_t^2 + M_Z^2 \cos 2\beta \left( \frac{1}{2} - \frac{2}{3} \sin^2 \theta_W \right) - m_{\tilde{t}_1}^2}{-m_t (A^t + \mu \cot \beta)}. \tag{2.36}$$

Taking into account that  $m_{\tilde{b}_L} = m_{\tilde{t}_L}$  via SU(2) symmetry, the derivation of the mass-matrix for down-type squarks follows the same procedure, but with corresponding definitions for charges, angles and masses (see Ref. [9]). The off-diagonal terms in the matrix of Eq. (2.32) can be particularly large for the third generation of squarks. In the case of the top-squark, these terms are proportional to the top-quark mass and yield a large mass splitting between  $\tilde{t}_1$  and  $\tilde{t}_2$ , which can make  $\tilde{t}_1$  very light.

Higgs couplings to up- and down-type squarks can be found in App. A.

## 2.4 Quantum Chromo-Dynamics

QCD is a gauge theory, based on the local non-Abelian SU(3)<sub>C</sub> group and describes interactions of the strong force between quarks, the constituents

of hadrons. The involved charge of the interaction is called color and corresponds to three degrees of freedom of the fundamental representation of the global SU(3) symmetry. The strong force is mediated by eight spin-1 bosons, the gluons, which carry color and anti-color. They are related to the conjugated representation of the SU(3) symmetry group. Due to the fact, that gluons are charged, in contrast to the photon of QED, they can interact also among each other via three- and four-gluon vertices. This property has an effect on the coupling strength  $\alpha_S$ , which is defined at a certain scale  $Q^2$  in the following way

$$\begin{aligned}\alpha_S(Q^2) &= \frac{g_S^2(Q^2)}{4\pi} \\ &= \frac{\alpha_S(\mu^2)}{1 + \alpha_S(\mu^2)/12\pi(11N_C - 2N_f) \log(Q^2/\mu^2)} .\end{aligned}\quad (2.37)$$

$N_c$  denotes the number of colors,  $N_f$  the number of fermions and  $\mu$  is a reference scale. For  $Q^2 \rightarrow \infty$  the coupling strength  $\alpha_S$  vanishes. This behavior is known as asymptotic freedom and was discovered by Wilczek, Gross and Politzer [11, 12]. Now, this feature gives the possibility to perform perturbative QCD calculations at high energies. Whereas for low energies, calculations get more involved and cannot be done perturbatively. At a scale of  $\approx 200$  MeV, called  $\Lambda_{\text{QCD}}$ ,  $\alpha_S$  even diverges.

Moreover, in experiments, no colored particles were found, but colorless bound-states. This phenomenon is called confinement and is also an effect of the gluon self-coupling. For more details about QCD see e.g. Refs.[13, 14].

The analytic expression for a hadronic cross section with two partons (quarks and gluons)  $a_1$  and  $a_2$  in initial state reads as follows

$$\begin{aligned}\sigma &= \int dx_1 dx_2 \sum_{\text{sub-proc}} f_{a_1}(x_1, \mu_F) f_{a_2}(x_2, \mu_F) \\ &\quad \times \frac{1}{4[(p_{a_1} \cdot p_{a_2}) - m_{a_1}^2 m_{a_2}^2]^{1/2}} \int d\Phi_{\text{cuts}} |\overline{\mathcal{M}}_{\text{sub-proc}}|^2 ,\end{aligned}\quad (2.38)$$

where the flux-factor  $[(p_{a_1} \cdot p_{a_2}) - m_{a_1}^2 m_{a_2}^2]^{1/2} = [2E_{a_1} 2E_{a_2} |v_{a_1} - v_{a_2}|]$  states the relative velocity of the beams. The shortcut  $|\overline{\mathcal{M}}_{\text{sub-proc}}|^2$  denotes the squared expression of the Feynman amplitude for different sub-processes,

summed over final polarizations and colors and averaged over initial polarizations and colors. The explicit expression is given by

$$|\overline{\mathcal{M}_{\text{sub-proc}}}|^2 = \frac{1}{4} \frac{1}{\#_{(\text{color})}(a_1, a_2)} \sum_{\text{color}} \sum_{\text{pol.}} |\mathcal{M}_{\text{sub-proc}}|^2. \quad (2.39)$$

The function  $\Theta_{\text{cuts}}$  describes selection cuts, which are applied on the kinematics of particles in final state. These cuts restrict the integration over the phase-space to regions, that are accessible by experiments. Furthermore, they anticipate detector capabilities and jet finding algorithms. The general expression of the Lorentz-invariant phase-space for a n-particle final-state is defined as

$$d\Phi_n(P; p_1, \dots, p_n) = \prod_{i=1}^n \left( \frac{d^3 p_i}{(2\pi)^3 2E_i} \right) (2\pi)^4 \delta^4 \left( P - \sum_i p_i \right). \quad (2.40)$$

The final result is then obtained by the twofold integration over the parton density functions (PDFs)  $f_{a_i}$ . A PDF describes the probability density to find a parton  $a_i$  inside a nucleon with a certain longitudinal momentum fraction between  $x_i$  and  $x_i + dx_i$ . The parameter  $\mu$  is called factorization scale and corresponds to the resolution, at which short- and long-distance physics is separated. If all orders of a perturbation series are taken into account, the final result for a physical observable would not depend on  $\mu$ . But, in a finite order perturbation theory physical observables involve the parameter  $\mu$ , which is then set to the characteristic scale of the underlying process.

# Chapter 3

## Higgs production processes in association with two and three jets

---

### 3.1 Introduction and motivation

In  $pp$ -collisions at the LHC several mechanisms, depicted in Fig. 3.1, contribute to the production of the Higgs boson in the SM. The dominant production mechanism, over the entire Higgs mass range and accessible at the LHC, is gluon fusion (a), which is mediated mainly by a top-quark loop. The corresponding cross section, including all top-mass effects, is also known at NLO [15, 16]. Further NNLO calculations were done only within the effective Lagrangian approximation (see App. E), where the top-mass dependence is integrated out by using the limit  $m_t \rightarrow \infty$  [17, 18]. The second largest cross section is produced via weak boson fusion (b), mediated by  $t$ -channel  $W$  or  $Z$  exchange. It contains an additional pair of hard tagging jets in the final state, arising from scattered quarks. In addition to this, the same signature can also appear in gluon fusion via  $\mathcal{O}(\alpha_S^2)$  real emission corrections [2]. They are discussed and described in detail in the following sub-chapters. QCD corrections to weak boson fusion [19, 20] are known to NLO and show the expected improvement of scale uncertainties for cross sections and different distributions. Full NLO QCD corrections to the  $Hjj$  production process via gluon fusion are only available in the effective Lagrangian approximation [21]. Since the lowest order process is loop-induced, a full NLO calculation would entail a two-loop evaluation, which is presently not feasible. In this thesis, only real emission corrections with full-mass effects are discussed in the sub-

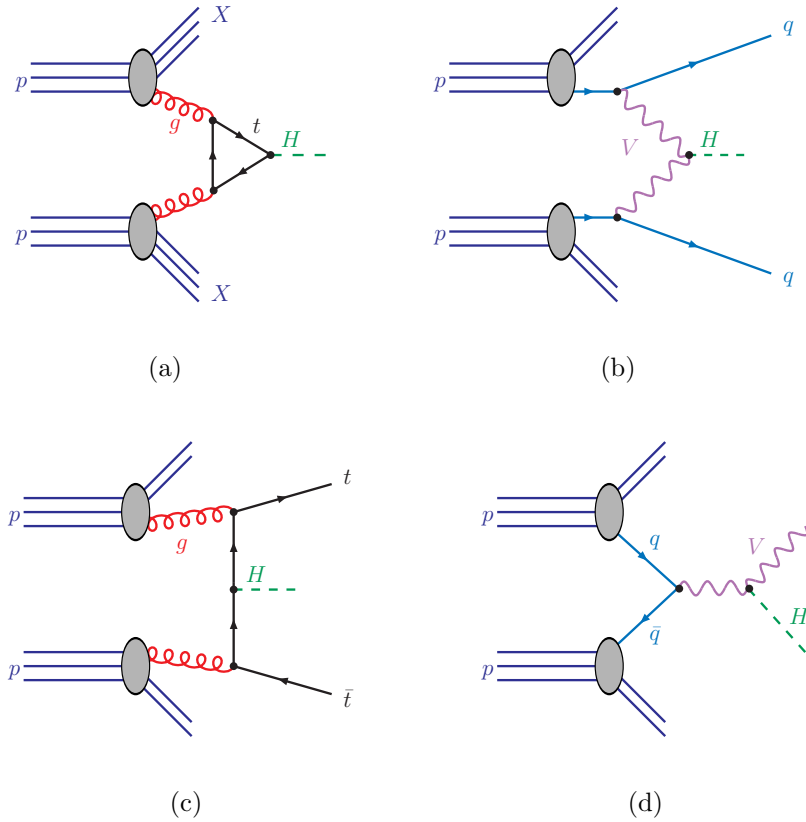


Figure 3.1: *Higgs production mechanisms at LHC: (a) Gluon fusion, (b) weak boson fusion, (c) radiation of a Higgs boson off top pair, (d) Higgs production in association with a  $W$  or  $Z$  boson.*

sequent chapters. Virtual contributions, coming from two-loop topologies, are not considered here, but pentagon- and hexagon-loops, which complicate the evaluation, especially for  $Hjjj$ . Further production mechanisms are the radiation of a Higgs boson off top pairs (c) [22, 23] and electro-weak boson associated production (d) [24, 25], where the involved boson is identified by its leptonic decay. In the MSSM gluon fusion is again the most important production channel for the Higgs bosons  $h$ ,  $H$  and  $A$ . Also Higgs-Strahlung off top and, especially, bottom quarks, which are enhanced by  $\tan\beta$ , play an important role. Higgs radiation off  $W$  or  $Z$  bosons and Higgs production via weak boson fusion is only interesting in association with the light Higgs



boson  $h$ .

The next chapter describes the calculation of Higgs production processes with two and three additional jets. In the following, additional contributions with squarks are taken into account only for the process with a two jet final state. Loop-topologies, containing gluino-vertices, are neglected, due to the fact, that these contributions are suppressed by large gluino-masses on the one hand. And on the other hand, they appear in loop-diagrams with through-going light quark lines and, hence, provide an additional suppression of the Higgs coupling to squarks. Furthermore, no ghost-fields  $c$  and  $\bar{c}$  appear in the calculation, because the colored QCD-ghosts are massless and therefore imply a vanishing coupling to the Higgs bosons.

## 3.2 Outline of the calculation

Due to a large number of contributing Feynman graphs, it is most convenient to give analytic results for the scattering amplitudes for fixed polarizations of external quarks and gluons, instead of using trace techniques to express polarization averaged squares of amplitudes in terms of relativistic invariants. The spinor algebra of those helicity amplitudes can be handled easily with the help of the formalism and methods developed in Ref. [26, 27]. Further calculation methods are based on the framework introduced in Ref. [1, 2]. The analytic expressions of amplitudes are then evaluated numerically with the gluon fusion part *GGFLO* of the program *VBFNLO* [4].

Throughout the calculation all masses of external fermions are set to zero. If not specified explicitly, all gluon momenta are treated as outgoing. Working in the chiral representation, the external (anti-) fermions can be described by a two-component Weyl-spinor of chirality  $\tau$  [27]

$$\psi(\bar{p}_i, \bar{\sigma}_i)_\tau = S_i \sqrt{2\bar{p}_i^0} \delta_{\sigma_i\tau} \chi_{\sigma_i}(\bar{p}_i) . \quad (3.1)$$

Here,  $\bar{p}_i$  denotes the physical momenta expressing the phase space and the wave functions of fermions of fixed helicity  $\bar{\sigma}_i$ , as well as  $\bar{q}_i$  for on-shell gauge bosons, whereas  $p_i$  and  $q_i$  describe momenta appearing in the momentum flow in Feynman diagrams. Both sets of momenta and helicities are related by the sign factors  $S_i$

$$p_i = S_i \bar{p}_i , \quad q_i = S_i \bar{q}_i \quad \text{and} \quad \sigma_i = S_i \bar{\sigma}_i , \quad (3.2)$$

with  $S_i = +1$  for fermions and  $S_i = -1$  for anti-fermions. Momenta  $\bar{q}_i$  of out- and ingoing gluons are controlled by the factors  $S_i = +1$  and  $S_i = -1$  respectively. This allows easy switching between different production channels. The factor  $\delta_{\sigma_i\tau}$  ensures conservation of helicity in the chiral limit and  $\chi_{\sigma_i}(\bar{p}_i)$  denotes the helicity eigenstates. The polarization vectors for on-shell gluons are available in *VBFNLO* [4] in two different representations [28], which, of course, satisfy the transversality property

$$q \cdot \epsilon(\bar{q}) = 0 \quad \text{with} \quad \epsilon^\mu(\bar{q}) = (0, \vec{\epsilon}(\bar{q})) : \quad (3.3)$$

- 1) real polarization vectors, i.e.  $\epsilon_i^*(\bar{q}_i) = \epsilon_i(\bar{q}_i)$ , with gauge boson momentum  $\bar{q}^\mu$  as basis vector:

$$\epsilon_i(\bar{q}_i, 1) = (|\vec{\bar{q}}_i| \bar{q}_{iT})^{-1} (0, \bar{q}_{ix} \bar{q}_{iz}, \bar{q}_{iy} \bar{q}_{iz}, -\bar{q}_{iT}^2), \quad (3.4)$$

$$\epsilon_i(\bar{q}_i, 2) = (\bar{q}_{iT})^{-1} (0, -\bar{q}_{iy}, \bar{q}_{ix}, 0) \quad (3.5)$$

with

$$\bar{q}_i^\mu = (\bar{E}_i, \bar{q}_{ix}, \bar{q}_{iy}, \bar{q}_{iz}), \quad \bar{E}_i = (|\vec{\bar{q}}_i|^2 + m^2)^{1/2}, \quad (3.6)$$

$$\bar{q}_{iT} = (\bar{q}_{ix}^2 + \bar{q}_{iy}^2)^{1/2}. \quad (3.7)$$

These real polarization vectors describe transverse polarized gluons.

- 2) Complex polarization vectors in the helicity basis  $\lambda = \pm$  :

$$\epsilon_i(\bar{q}_i, \lambda = \pm) = \frac{1}{\sqrt{2}} (\mp \epsilon_i(\bar{q}_i, 1) - i \epsilon_i(\bar{q}_i, 2)). \quad (3.8)$$

Furthermore, through-going fermion lines with attached gluon vertex and propagator are combined to effective quark currents,

$$J_{fi}^\mu = \delta_{\sigma_f\sigma_i} \chi_{\sigma_f}^\dagger(\bar{p}_f) (\sigma^\mu)_\tau \chi_{\sigma_i}(\bar{p}_i) \frac{1}{q_{fi}^2} = \delta_{\sigma_f\sigma_i} \langle f | (\sigma^\mu)_\tau | i \rangle \frac{1}{(p_i - p_f)^2}, \quad (3.9)$$

where  $(\sigma^\mu)_{\tau=\pm}$  are the Dirac matrices in the two-component Weyl-basis,  $|i\rangle$ ,  $\langle f|$ , abbreviations for in- and outgoing external fermions and  $\tau = \sigma_i = \sigma_f$  denotes helicity conservation. Analogously to that, one can define a gluon-current, which is composed of a three-gluon-vertex contracted with two polarization vectors of outgoing on-shell gluons with indices  $i, j$

$$J_{ij}^{G,\mu}(q_{ij}) = \frac{1}{(q_i + q_j)^2} \times \left[ 2\epsilon(q_i)^\mu q_i \cdot \epsilon(q_j) + \epsilon(q_i) \cdot \epsilon(q_j) (q_j - q_i)^\mu - 2\epsilon(q_j)^\mu q_j \cdot \epsilon(q_i) \right]. \quad (3.10)$$

The propagator term belongs to the uncontracted virtual gluon with momentum  $q_{ij} = q_i + q_j$ , which is here defined as ingoing. In addition to that, the transversality property of Eq. (3.3) was used. For the emission of an on-shell gluon close to an external quark, one can use a Bra and Ket notation similar to the quark current of Eq. (3.9), but with an additional momentum variable  $q_l$  of the corresponding polarization vector [26]

$$|q_l, i\rangle = (\not{p}_i - \not{q}_l)_{-\sigma_i} (\not{\epsilon}_l)_{\sigma_i} \chi_{\sigma_i}(\bar{p}_i) \frac{1}{(p_i - q_l)^2}, \quad (3.11)$$

$$\langle f, q_l| = \chi_{\sigma_f}^\dagger(\bar{p}_f) (\not{\epsilon}_l)_{\sigma_f} (\not{p}_f + \not{q}_l)_{-\sigma_f} \frac{1}{(p_f + q_l)^2}. \quad (3.12)$$

The central part of the calculation are different loop-topologies with fermionic and scalar particles couplings to  $\mathcal{CP}$ -even and  $\mathcal{CP}$ -odd Higgs bosons. The simplest topology is a triangle graph  $T_{\Phi,p}^{\mu_1\mu_2}(q_1, q_2, m_p)$ , where  $q_1, q_2$  denote momenta of the attached gluons. The shortcut  $\Phi$  stands for all neutral Higgs bosons,  $H_{SM}, h, H, A$  and  $m_p$  is the mass of the scalar or fermionic loop-particle. The tensor  $B_{\Phi,p}^{\mu_1\mu_2\mu_3}(q_1, q_2, q_3, m_p)$  describes box-like contributions. The analytically and numerically most complex graphs are the pentagons  $P_{\Phi,p}^{\mu_1\mu_2\mu_3\mu_4}(q_1, q_2, q_3, q_4, m_p)$  and hexagons  $H_{\Phi,p}^{\mu_1\mu_2\mu_3\mu_4\mu_5}(q_1, q_2, q_3, q_4, q_5, m_p)$ . Charge-conjugation related diagrams, where the loop momentum is running clockwise and counter-clockwise, can be counted as one by exploiting Furry's theorem [29]. This effectively reduces the number of diagrams by a factor of two. All briefly mentioned topologies differ in their tensor structure, depending on, which particle couples to the Higgs boson, as well as on the Higgs boson coupling itself:

1)  **$\mathcal{CP}$ -odd Higgs boson  $A$**

For the  $\mathcal{CP}$ -odd Higgs boson  $A$  only couplings to fermions are taken into account. Massive squark loops can be safely neglected, because these contributions sum up to zero at amplitude level [8], due to the fact, that the both attached sfermions have to be in different bases (left-right basis  $L, R$  or mixed basis 1,2, see Eq. (A.25)) to give a non-vanishing contribution. Here the index  $f = t, b$  denotes top and bottom quark loops.

2)  **$\mathcal{CP}$ -even Higgs bosons  $H_{SM}, h, H$**

The  $\mathcal{CP}$ -even Standard Model Higgs boson  $H_{SM}$  is produced only with

massive quark loops. The couplings of the light  $h$  and heavy  $H$  MSSM Higgs bosons differ by additional factors containing the mixing angle  $\alpha$  of the neutral Higgs-doublet components and the mixing angle  $\beta$  of both vacuum expectation values.

In the MSSM, the  $\mathcal{CP}$ -even Higgs bosons can also couple to squarks. However, a single triangle-tensor  $\overline{T}_{h,H,\tilde{f}}^{\mu_1\mu_2}(q_1, q_2, m_{\tilde{f}})$  is proportional to an  $\epsilon^{-1}$ -pole in dimensional regularization (DREG) and, hence, it is UV-divergent. The MSSM provides also a further vertex, which is composed of two sfermions and two gluons (see Appendix D). Now, this  $\epsilon^{-1}$ -pole cancels by addition of a two-point function  $S_{h,H,\tilde{f}}^{\mu_1\mu_2}(q_1, q_2, m_{\tilde{f}})$  (see Fig. B.3 in App. B), containing the  $\tilde{q}\tilde{q}gg$ -vertex. The new divergence free triangle tensor is given by

$$T_{h,H,\tilde{f}}^{\mu_1\mu_2}(q_1, q_2, m_{\tilde{f}}) = \overline{T}_{h,H,\tilde{f}}^{\mu_1\mu_2}(q_1, q_2, m_{\tilde{f}}) + S_{h,H,\tilde{f}}^{\mu_1\mu_2}(q_1, q_2, m_{\tilde{f}}) . \quad (3.13)$$

All contributing topologies are described in more detail in Appendix B. Furthermore, polarization vectors of on-shell gluons with a triangle-loop insertion can be expressed by effective polarization vectors,

$$e_{i\Phi}^{p,\mu_1} = \frac{\epsilon_{\mu_2}(\overline{q}_i)}{(q_i + P_\Phi)^2} T_{\Phi,p}^{\mu_1\mu_2}(q_i, q_i + P_\Phi, m_p) , \quad (3.14)$$

where  $q_i$  is the external gluon momentum, while  $P_\Phi$  denotes the momentum of the Higgs boson  $\Phi$ . All coupling constants and loop factors are conveniently absorbed into an overall factor  $F_p$ . Detailed expressions for  $F_p$  are declared in the particular two or three jet process.

### 3.3 Higgs production in association with two jets

The production of the neutral Higgs bosons  $\Phi$  in association with two jets, at order  $\alpha_s^4$ , can be carried out via the sub-processes

$$q q \rightarrow q q \Phi , \quad q Q \rightarrow q Q \Phi , \quad q g \rightarrow q g \Phi , \quad g g \rightarrow g g \Phi . \quad (3.15)$$

The first two entries denote scattering of identical and non-identical quark flavors. The two last entries describe quark-gluon and gluon-gluon scattering. Further contributions can be achieved by crossing relations using the

sign factors  $S_i$ , introduced in Eq. (3.2) and the fact, that the Lagrangian is invariant under the application of the charge-conjugation operator  $\hat{C} = \gamma^0 \gamma^2$ ,

- quark-quark scattering:

$$\begin{aligned}
\bar{q} \bar{q} &\longrightarrow \bar{q} \bar{q} \Phi \quad (\text{via } C \text{ invariance of amplitude}) , \\
q \bar{q} &\longrightarrow q \bar{q} \Phi , \\
q \bar{q} &\longrightarrow g g \Phi ,
\end{aligned} \tag{3.16}$$

- quark-gluon scattering:

$$\begin{aligned}
g q &\longrightarrow g q \Phi \quad (\text{flipped beams}) , \\
\bar{q} g &\longrightarrow \bar{q} g \Phi \quad (\text{via } C \text{ invariance of amplitude}) , \\
g \bar{q} &\longrightarrow g \bar{q} \Phi \quad (\text{via } C \text{ invariance of amplitude} + \text{flipped beams}) ,
\end{aligned} \tag{3.17}$$

- gluon-gluon scattering:

$$\begin{aligned}
g g &\longrightarrow q \bar{q} \Phi , \\
g g &\longrightarrow g g \Phi .
\end{aligned} \tag{3.18}$$

The overall factor  $F_p^{2j}$  reads as

$$F_p^{2j} = \mathcal{C}_p \frac{g_S^4}{16\pi^2} = \mathcal{C}_p \alpha_s^2 \tag{3.19}$$

The abbreviation  $\mathcal{C}_p$  stands for the Yukawa coupling to fermions and for the Higgs coupling to sfermions. Detailed informations on couplings are given in Appendix A. The index  $p = t, b, \tilde{t}_{1,2}, \tilde{b}_{1,2}$  denotes top and bottom quarks as well as stop and sbottom squarks.

### 3.3.1 $qQ \rightarrow qQ\Phi$ and $qq \rightarrow qq\Phi$

The sub-process  $q Q \rightarrow q Q \Phi$  of Eq. (3.15), depicted on the left side in Fig. 3.2, is the simplest contribution to  $\Phi + 2$  jet production, if the Higgs boson couples to fermions only. Here  $Q$  denotes a different flavor. For identical quarks, an additional diagram can be obtained by interchanging the final-state-quarks. Higgs couplings to scalar quarks yield additional

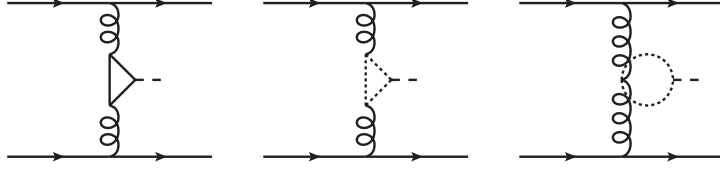


Figure 3.2: *Quark and squark contributions to  $qq \rightarrow qq\Phi$  amplitudes.*

contributions with squark-triangles. Furthermore, the MSSM provides new vertex-structures, which generate new loop-topologies, e.g. the two-point-loop, shown in the right panel of Fig. 3.2. At most, there are 6 diagrams, if both coupling types are taken into account. Following Ref. [2, 3, 30], the amplitude for different flavors and loop particles can be written as

$$\begin{aligned} \mathcal{A}^{qQ} &= \sum_p F_p^{qQ,2j} J_{21}^{\mu_1} J_{43}^{\mu_2} T_{\mu_1\mu_2}^{\Phi,p}(q_1, q_2, m_p) t_{i_2i_1}^a t_{i_4i_3}^a \\ &= \mathcal{A}_{2143}^{qQ} t_{i_2i_1}^a t_{i_4i_3}^a. \end{aligned} \quad (3.20)$$

The overall factor

$$F_p^{qQ,2j} = S_1 S_2 S_3 S_4 4\sqrt{\bar{p}_1^0 \bar{p}_2^0 \bar{p}_3^0 \bar{p}_4^0} F_p^{2j} \quad (3.21)$$

includes, in addition, normalization factors of external quark spinors (see Eq. (3.2) and (3.19)). External quark lines are expressed by the effective quark currents, introduced in Eq. (3.9). Both gluons attached to the triangle tensor  $T_{\mu_1\mu_2}^{\Phi,p}(q_1, q_2, m_p)$  are assumed as out-going and have momenta  $q_1 = p_2 - p_1$  and  $q_2 = p_4 - p_3$ . The sum of fermionic and sfermionic charge-conjugated triangle graphs  $T^{\mu_1\mu_2}$  and sfermionic two-point function  $S^{\mu_1\mu_2}$  are proportional to the single color factor  $\delta^{a_2a_3}$  (B.5). The two color factors  $\delta^{a_1a_2}$  and  $\delta^{a_3a_4}$ , coming from propagators of the virtual gluons, and the remaining color generators  $t_{i_2i_1}^{a_1}$  and  $t_{i_4i_3}^{a_4}$  of both gluons-vertices attached to the fermion currents of Eq. (3.9), yield the following simple color structure for the amplitude

$$t_{i_2i_1}^{a_1} \delta^{a_1a_2} \delta^{a_2a_3} \delta^{a_3a_4} t_{i_4i_3}^{a_4} = t_{i_2i_1}^a t_{i_4i_3}^a. \quad (3.22)$$

For identical fermions, Pauli-interference has to be considered additionally. That means, that to the amplitude of equation (3.20) a term with inter-

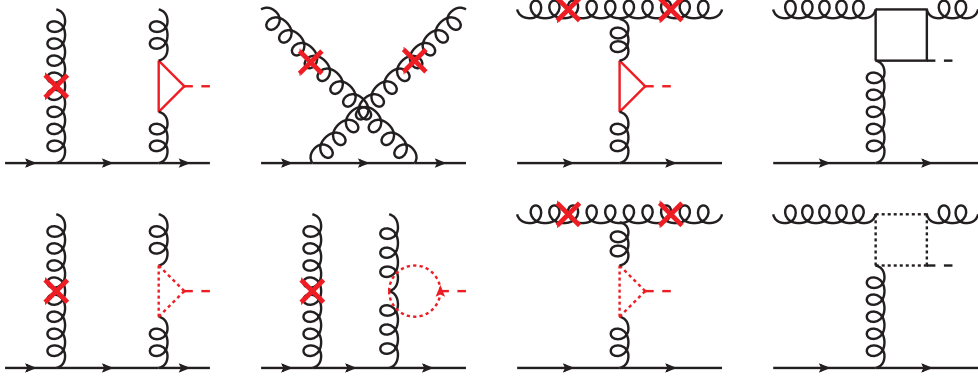


Figure 3.3: Quark and squark contributions to  $qg \rightarrow qg\Phi$  amplitudes.

changed final state quarks must be added

$$\mathcal{A}^{qq} = \mathcal{A}_{2143}^{qq} t_{i_2 i_1}^a t_{i_4 i_3}^a - \mathcal{A}_{4123}^{qq} t_{i_4 i_1}^a t_{i_2 i_3}^a . \quad (3.23)$$

Fermi-statistics provides a relative sign-factor swap for the second term. Finally, the squared amplitude, summed over initial and final particle colors, becomes

$$\begin{aligned} \sum_{\text{color}} |\mathcal{A}^{qq}|^2 &= \left( |\mathcal{A}_{2143}|^2 + |\mathcal{A}_{4123}|^2 \right) \frac{N^2 - 1}{4} + 2 \operatorname{Re} \left( \mathcal{A}_{2143} \mathcal{A}_{4123}^* \right) \\ &\times \frac{N^2 - 1}{4N} . \end{aligned} \quad (3.24)$$

Setting  $\mathcal{A}_{4123} = 0$  in Eq. (3.24), one gets the squared matrix elements for  $\mathcal{A}^{qQ}$ .

### 3.3.2 $qg \rightarrow qg\Phi$

This sub-process contains two (anti-)quarks and two gluons as external particles. The momenta of the initial and final state gluons are set to  $q_i = -\bar{q}_i$  and  $q_f = +\bar{q}_f$  respectively. In the case of fermion-loops, there are only ten different Feynman graphs, if Furry's theorem is taken into account. That are seven graphs with a triangle insertion and three box graphs with cyclic permutation of the attached gluons. They are sketched in the Fig. 3.3. The red crosses denote further positions for possible triangle-loop or scalar two-point

function insertions. In the sfermionic case, additional triangle graphs  $T_{B,\Phi,\tilde{f}}^{\mu_1\mu_2\mu_3}$  with a box-like color structure and a  $\tilde{q}\tilde{q}gg$ -vertex (see Appendix B.1.5) appear additionally to the 17 graphs composed of squark-triangles with accompanying squark two-point functions and squark-boxes. However, the new triangle contribution has a vanishing color factor and, hence, does not contribute to the sub-process (a brief proof of this statement is shown in Appendix B.1.5). The amplitude for the sub-process  $qg \rightarrow qg\Phi$  can be written in a compact form, using the notations of Chapter 3.2,

$$\begin{aligned}
\mathcal{A}^{qg} &= \mathcal{A}_{\mu_1\mu_2}^{qg} \epsilon_1^{\mu_1} \epsilon_2^{\mu_2} = \sum_p F_p^{qg,2j} \\
&\times \left\{ (t^{a_1} t^{a_2})_{i_2 i_1} \left[ \langle 2 | (\mathcal{E}_{1\Phi}^p)_{\sigma_1} | q_2, 1 \rangle + \langle 2, q_1 | (\mathcal{E}_{2\Phi}^p)_{\sigma_1} | 1 \rangle \right] \right. \\
&\quad + (t^{a_2} t^{a_1})_{i_2 i_1} \left[ \langle 2 | (\mathcal{E}_{2\Phi}^p)_{\sigma_1} | q_1, 1 \rangle + \langle 2, q_2 | (\mathcal{E}_{1\Phi}^p)_{\sigma_1} | 1 \rangle \right] \\
&\quad + [t^{a_1}, t^{a_2}]_{i_2 i_1} \left[ 2 \left( e_{1\Phi}^p \cdot \epsilon_2 J_{21} \cdot q_2 - e_{1\Phi}^p \cdot J_{21} \epsilon_2 \cdot (p_2 - p_1) \right. \right. \\
&\quad \left. \left. - e_{1\Phi}^p \cdot q_2 J_{21} \cdot \epsilon_2 \right) - 2 \left( e_{2\Phi}^p \cdot \epsilon_1 J_{21} \cdot q_1 - e_{2\Phi}^p \cdot q_1 J_{21} \cdot \epsilon_1 \right. \right. \\
&\quad \left. \left. - e_{2\Phi}^p \cdot J_{21} \epsilon_1 \cdot (p_2 - p_1) \right) + J_{12}^{G,\mu_1} J_{21}^{\mu_2} T_{\mu_1\mu_2}^{\Phi,p} (q_1 + q_2, p_2 - p_1, m_p) \right. \\
&\quad \left. - B_{\mu_1\mu_2\mu_3}^{\Phi,p} (q_1, q_2, p_2 - p_1, m_p) \epsilon_1^{\mu_1} \epsilon_1^{\mu_3} J_{21}^{\mu_3} \right] \left. \right\}. \tag{3.25}
\end{aligned}$$

Spinor normalization factors are absorbed again into the overall factor

$$F_p^{qg,2j} = -S_1 S_2 2 \sqrt{\bar{p}_1^0 \bar{p}_2^0} \delta_{\sigma_1 \sigma_2} F_p^{2j}. \tag{3.26}$$

The first four terms correspond to the Compton-like graphs with effective polarization vectors  $e_i^{p,\mu}$  (3.14). In the sfermionic case, one has to keep in mind, that the effective polarization vector is composed of two parts (see Eq. (3.13))

$$e_i^{\tilde{f},\mu_1} = \frac{\epsilon_{\mu_2}(\bar{q}_i)}{(q_i + P)^2} \left[ \bar{T}_{\Phi,\tilde{f}}^{\mu_1\mu_2}(q_i, q_i + P_\Phi, m_{\tilde{f}}) + S_{\Phi,\tilde{f}}^{\mu_1\mu_2}(q_i, q_i + P_\Phi, m_{\tilde{f}}) \right]. \tag{3.27}$$



The color factor  $(t^{a_1 t^{a_2}})_{i_2 i_1}$  results from the color contribution  $\delta^{a_2 a_3}$  of the gluon propagator of the effective polarization vector and both gluon vertices  $t_{i_2 i_1}^{a_3}$  and  $t_{i_2 i_1}^{a_1}$ . The same applies for  $(t^{a_2 t^{a_1}})_{i_2 i_1}$ . The remaining terms correspond to three graphs containing a three-gluon-vertex with either attached effective polarization vector and effective quark current or both effective currents of Eqs. (3.9) and (3.10). Box diagrams enter via the tensor  $B_{\Phi,p}^{\mu_1 \mu_2 \mu_3}(q_1, q_2, q_3, m_p)$ , which is described in more detail in Appendix B.2. These diagrams are proportional to the structure constant  $f^{abc}$  with contracted  $t_{i_2 i_1}^c$ , coming from the effective quark current of Eq.(3.9). Finally, the amplitude can be separated into two parts with independent color structures

$$\mathcal{A}^{gg} = (t^{a_1 t^{a_2}})_{i_2 i_1} \mathcal{A}_{12}^{gg} + (t^{a_2 t^{a_1}})_{i_2 i_1} \mathcal{A}_{21}^{gg} . \quad (3.28)$$

The indices 12 and 21 label amplitudes with interchanged external gluons. Thus, the resulting color-summed squared amplitude takes the form,

$$\begin{aligned} \sum_{\text{color}} |\mathcal{A}^{gg}|^2 &= \left( |\mathcal{A}_{12}^{gg}|^2 + |\mathcal{A}_{21}^{gg}|^2 \right) \frac{(N^2 - 1)^2}{4N} - 2 \operatorname{Re} \left[ \mathcal{A}_{12}^{gg} (\mathcal{A}_{21}^{gg})^* \right] \\ &\times \frac{N^2 - 1}{4N} . \end{aligned} \quad (3.29)$$

### 3.3.3 $gg \rightarrow gg\Phi$

Here, the momenta of gluons in initial and final state are set again to  $q_i = -\bar{q}_i$  and  $q_f = +\bar{q}_f$  respectively. Taking Furry's theorem into consideration, 49 fermionic diagrams contribute to that sub-process: 19 graphs with triangle insertions, 18 box contributions and 12 pentagon diagrams. In the sfermionic case, additionally to the mentioned topologies, three triangle graphs with two  $\tilde{q}\tilde{q}gg$ -vertices and 18 box diagrams with one  $\tilde{q}\tilde{q}gg$ -vertex provide further contributions. Both new topologies have a pentagon-like color structure (more in appendix B). Here, it is strategically favorable to start with the pentagons and investigate their color structure. The four attached gluons give rise to  $4! = 24$  different color traces of the form,

$$\operatorname{tr} [t^{a_i} t^{a_j} t^{a_k} t^{a_l}], \quad \text{with } i, j, k, l = 1, 2, 3, 4 \quad \text{and} \quad i \neq j \neq k \neq l , \quad (3.30)$$

from which  $(4 - 1)! = 6$  are independent only due to the invariance property of the trace under cyclic permutations. They can be combined to three independent real-valued color structures,

$$\begin{aligned}
c_1 &= \text{tr} [t^{a_1} t^{a_2} t^{a_3} t^{a_4}] + \text{tr} [t^{a_1} t^{a_4} t^{a_3} t^{a_2}] , \\
c_2 &= \text{tr} [t^{a_1} t^{a_3} t^{a_4} t^{a_2}] + \text{tr} [t^{a_1} t^{a_2} t^{a_4} t^{a_3}] , \\
c_3 &= \text{tr} [t^{a_1} t^{a_4} t^{a_2} t^{a_3}] + \text{tr} [t^{a_1} t^{a_3} t^{a_2} t^{a_4}] .
\end{aligned} \tag{3.31}$$

All  $c_i$  correspond to the sum of two pentagons with opposite loop momentum flow. Finally, to every  $c_i$ , four charge-conjugated pentagons can be assigned with cyclic permutation of external gluons. The evaluation of the color traces yields

$$\begin{aligned}
c_1 &= \frac{1}{4} \left( \frac{2}{N} \delta^{a_1 a_2} \delta^{a_3 a_4} + d^{a_1 a_2 m} d^{a_3 a_4 m} - f^{a_1 a_2 m} f^{a_3 a_4 m} \right) , \\
c_2 &= \frac{1}{4} \left( \frac{2}{N} \delta^{a_1 a_3} \delta^{a_4 a_2} + d^{a_1 a_3 m} d^{a_4 a_2 m} - f^{a_1 a_3 m} f^{a_4 a_2 m} \right) , \\
c_3 &= \frac{1}{4} \left( \frac{2}{N} \delta^{a_1 d} \delta^{a_2 a_3} + d^{a_1 a_4 m} d^{a_2 a_3 m} - f^{a_1 a_4 m} f^{a_2 a_3 m} \right) ,
\end{aligned} \tag{3.32}$$

for which some  $SU(N)$ -identities of Appendix C were used. The color structure of the remaining diagrams is proportional to two structure constants e.g.  $f^{a_1 a_2 m} f^{m a_3 a_4}$ . Furthermore, the combination of two structure constants can be expressed with help of the following identities by the color coefficients of Eq. (3.31)

$$\begin{aligned}
c_1 - c_2 &= -\frac{1}{2} f^{a_1 a_2 m} f^{a_3 d m} \implies f^{a_1 a_2 m} f^{a_3 d m} = 2(c_2 - c_1) , \\
c_3 - c_1 &= -\frac{1}{2} f^{a_1 d m} f^{a_2 a_3 m} \implies f^{a_1 d m} f^{a_2 a_3 m} = 2(c_1 - c_3) , \\
c_2 - c_3 &= -\frac{1}{2} f^{a_1 a_3 m} f^{d a_2 m} \implies f^{a_1 a_3 m} f^{d a_2 m} = 2(c_3 - c_2) .
\end{aligned} \tag{3.33}$$

The sum of all differences of the  $c_i$  satisfies the Jacobian identity,

$$\begin{aligned}
& -2 \left[ (c_1 - c_2) + (c_3 - c_1) + (c_2 - c_3) \right] \\
& = f^{a_1 a_2 m} f^{m a_3 a_4} + f^{a_1 a_4 m} f^{m a_2 a_3} + f^{a_1 a_3 m} f^{m a_4 a_2} = 0 .
\end{aligned} \tag{3.34}$$

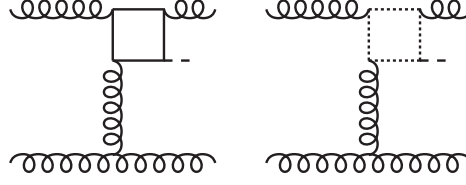


Figure 3.4: *Quark- and squark-box contributions to  $gg \rightarrow gg\Phi$  amplitudes.*

In terms of these color coefficients, the complete amplitude for  $gg \rightarrow gg\Phi$  can be decomposed into three separately gauge invariant sub-amplitudes,

$$\mathcal{A}^{gg} = \sum_{i=1}^3 c_i \mathcal{A}_i^{gg} = F_p^{2j} \sum_{i=1}^3 c_i \bar{\mathcal{A}}_{i,\mu_1\mu_2\mu_3\mu_4}^{gg} \epsilon_1^{\mu_1} \epsilon_2^{\mu_2} \epsilon_3^{\mu_3} \epsilon_4^{\mu_4}, \quad (3.35)$$

with the overall factor  $F_p^{2j}$  from Eq. (3.19). Finally, all remaining diagrams with box, triangles and two-point topologies are explained briefly:

### 1) Fermionic and sfermionic box diagrams

Box diagrams are attached to the gluon-current of Eq. (3.10), as shown in Fig. 3.4. The momentum of the virtual gluon is denoted by  $q_{ij} = q_i + q_j$ . For a gluon permutation  $(q_{12}, q_3, q_4)$  with color factor  $f^{a_1 a_2 m} f^{m a_3 a_4}$ , the partial amplitude can be written as,

$$\mathcal{A}_{12,3,4}^{\text{Box}} = 2(c_2 - c_1) B_{\Phi,p}^{\alpha\mu_2\mu_3}(q_{12}, q_3, q_4, m_p) J_{12,\alpha}^G \epsilon_{3,\mu_2} \epsilon_{4,\mu_3}. \quad (3.36)$$

There are, of course, two further contributions with permutations  $(q_3, q_4, q_{12})$  and  $(q_4, q_{12}, q_3)$  with the same color structure, which can be achieved via cyclic permutation of the attached gluons. Those are already taken into account in the definition of the box tensor in Eq. (B.28). For the remaining 15 diagrams, all color factors and momenta sets are listed here

- $(q_{13}, q_2, q_4), (q_2, q_4, q_{13}), (q_4, q_{13}, q_2) \implies f^{a_1 a_3 m} f^{m a_2 a_4} = 2(c_2 - c_3),$
- $(q_{14}, q_2, q_3), (q_2, q_3, q_{14}), (q_3, q_{14}, q_2) \implies f^{a_1 a_4 m} f^{m a_2 a_3} = 2(c_1 - c_3),$
- $(q_{23}, q_1, q_4), (q_1, q_4, q_{23}), (q_4, q_{23}, q_1) \implies f^{a_2 a_3 m} f^{m a_1 a_4} = 2(c_1 - c_3),$
- $(q_{24}, q_1, q_3), (q_1, q_3, q_{24}), (q_3, q_{24}, q_1) \implies f^{a_2 a_4 m} f^{m a_1 a_3} = 2(c_2 - c_3),$

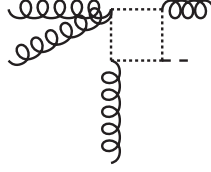


Figure 3.5: *Pentagon-like squark-box contribution to  $gg \rightarrow gg\Phi$  amplitudes.*

- $(q_{34}, q_1, q_2), (q_1, q_2, q_{34}), (q_2, q_{34}, q_1) \implies f^{a_3 a_4 m} f^{m a_1 a_2} = 2(c_2 - c_1)$  .

## 2) Sfermionic box diagrams with $\tilde{q}\tilde{q}gg$ -vertex

The box diagram, depicted in Fig. 3.5, is contracted directly with four polarization vectors of the external gluons. The  $\tilde{q}\tilde{q}gg$ -vertex provides a pentagon-like color structure, which can be expressed very easily by the color coefficients of Eq. (3.31). Hence, for a gluon permutation  $(q_{12}, q_3, q_4)$ , the partial amplitude with the box tensor of Eq. (B.48) reads as

$$\begin{aligned}
\mathcal{A}_{12,3,4}^{\text{BoxP}} &= \left( \text{tr} [t^{a_1} t^{a_2} t^{a_3} t^{a_4}] + \text{tr} [t^{a_2} t^{a_1} t^{a_3} t^{a_4}] + \text{tr} [t^{a_4} t^{a_3} t^{a_1} t^{a_2}] \right. \\
&\quad \left. + \text{tr} [t^{a_4} t^{a_3} t^{a_2} t^{a_1}] \right) B_{\text{P},\Phi,\tilde{f}}^{\mu_1 \mu_2 \mu_3 \mu_4}(q_{12}, q_3, q_4, m_{\tilde{f}}) \epsilon_{1, \mu_1} \epsilon_{2, \mu_2} \epsilon_{3, \mu_3} \epsilon_{4, \mu_4} \\
&= (c_1 + c_2) B_{\text{P},\Phi,\tilde{f}}^{\mu_1 \mu_2 \mu_3 \mu_4}(q_{12}, q_3, q_4, m_{\tilde{f}}) \epsilon_{1, \mu_1} \epsilon_{2, \mu_2} \epsilon_{3, \mu_3} \epsilon_{4, \mu_4} .
\end{aligned} \tag{3.37}$$

The definition of  $B_{\text{P},\Phi,\tilde{f}}^{\mu_1 \mu_2 \mu_3 \mu_4}(q_{12}, q_3, q_4, m_{\tilde{f}})$  contains also two additional contributions with cyclicly permuted momenta sets. The remaining 15 graphs with corresponding color factors are given by,

- $(q_{13}, q_2, q_4), (q_2, q_4, q_{13}), (q_4, q_{13}, q_2) \implies (c_2 + c_3)$  ,
- $(q_{14}, q_2, q_3), (q_2, q_3, q_{14}), (q_3, q_{14}, q_2) \implies (c_1 + c_3)$  ,
- $(q_{23}, q_1, q_4), (q_1, q_4, q_{23}), (q_4, q_{23}, q_1) \implies (c_1 + c_3)$  ,
- $(q_{24}, q_1, q_3), (q_1, q_3, q_{24}), (q_3, q_{24}, q_1) \implies (c_2 + c_3)$  ,
- $(q_{34}, q_1, q_2), (q_1, q_2, q_{34}), (q_2, q_{34}, q_1) \implies (c_1 + c_2)$  .

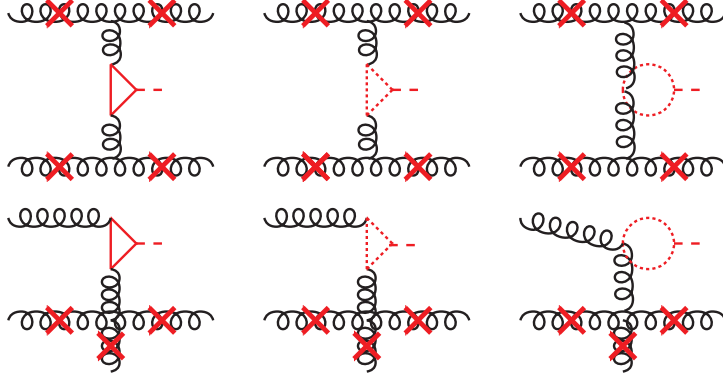


Figure 3.6: *Quark- and squark-triangle contributions to  $gg \rightarrow gg\Phi$  amplitudes.*

### 3) Fermionic and sfermionic triangle diagrams

All subsequent described contributions with triangle-loop insertions are illustrated in Fig. 3.6. The first three contributions can be built up with the general triangle tensor  $T_{\Phi,p}^{\mu_1\mu_2}(q_1, q_2, m_p)$  and two gluon currents of Eq. (3.10). For a momentum set,  $(q_{12}, q_{34})$ , the partial amplitude with color factor  $f^{a_1a_2m} f^{ma_3a_4}$  is given by,

$$\mathcal{A}_{12,34}^{\text{Tri } 1} = 2 (c_2 - c_1) T_{\mu_1\mu_2}^{\Phi,p}(q_{12}, q_{34}, m_p) J_{12}^{G,\mu_1} J_{34}^{G,\mu_2}. \quad (3.38)$$

The color factors for the remaining two gluon momenta sets are,

- $(q_{13}, q_{24}) \implies f^{a_1a_3m} f^{a_2a_4m} = 2(c_2 - c_3),$
- $(q_{14}, q_{23}) \implies f^{a_1a_4m} f^{a_2a_3m} = 2(c_1 - c_3).$

For the next 15 diagrams, the building blocks are a three-gluon vertex, the gluon current of Eq. (3.10) and an effective polarization vector of Eq. (3.14). For a gluon momenta configuration  $(q_{12}, e_{3\Phi}^p, q_4)$  with color factor  $f^{a_1a_2m} f^{ma_3a_4}$ , the partial amplitude can be written as,

$$\mathcal{A}_{12,3,4}^{\text{Tri } 2} = 2 (c_2 - c_1) \left[ e_{3\Phi}^p \cdot \epsilon_4 (q_3 + P_\Phi - q_4) \cdot J_{12}^G + e_{3\Phi}^p \cdot J_{12}^G (q_{12} - q_3 - P_\Phi) \cdot \epsilon_4 + \epsilon_4 \cdot J_{12}^G (q_{12} + q_4) \cdot e_{3\Phi}^p, q_4 \right], \quad (3.39)$$

where  $P_\Phi$  denotes the Higgs momentum. The color coefficients for the other 11 diagrams are

- $(q_{12}, q_3, e_{4\Phi}^p) \implies f^{a_1 a_2 m} f^{a_3 a_4 m} = 2(c_2 - c_1)$ ,
- $(q_{13}, e_{2\Phi}^p, q_4) \implies f^{a_1 a_3 m} f^{a_2 a_4 m} = 2(c_2 - c_3)$ ,
- $(q_{13}, q_2, e_{4\Phi}^p) \implies f^{a_1 a_3 m} f^{a_2 a_4 m} = 2(c_2 - c_3)$ ,
- $(q_{14}, e_{2\Phi}^p, q_3) \implies f^{a_1 a_4 m} f^{a_2 a_3 m} = 2(c_1 - c_3)$ ,
- $(q_{14}, q_2, e_{4\Phi}^p) \implies f^{a_1 a_4 m} f^{a_2 a_3 m} = 2(c_1 - c_3)$ ,
- $(q_{23}, e_{1\Phi}^p, q_4) \implies f^{a_2 a_3 m} f^{a_1 a_4 m} = 2(c_1 - c_3)$ ,
- $(q_{23}, q_1, e_{4\Phi}^p) \implies f^{a_2 a_3 m} f^{a_1 a_4 m} = 2(c_1 - c_3)$ ,
- $(q_{24}, e_{1\Phi}^p, q_3) \implies f^{a_2 a_4 m} f^{a_1 a_3 m} = 2(c_2 - c_3)$ ,
- $(q_{24}, q_1, e_{3\Phi}^p) \implies f^{a_2 a_4 m} f^{a_1 a_3 m} = 2(c_2 - c_3)$ ,
- $(q_{34}, e_{1\Phi}^p, q_2) \implies f^{a_3 a_4 m} f^{a_1 a_2 m} = 2(c_2 - c_1)$ ,
- $(q_{34}, q_1, e_{2\Phi}^p) \implies f^{a_3 a_4 m} f^{a_1 a_2 m} = 2(c_2 - c_1)$ .

The four-gluon (Appendix D) vertex gives rise to four additional contributions with one attached effective polarization vector. In addition, this vertex is composed of three terms, which are separately proportional to two structure constants. For a permutation  $(e_{1\Phi}^p, \epsilon_2, \epsilon_3, \epsilon_4)$ , the partial amplitude reads as follows

$$\begin{aligned}
\mathcal{A}_{1,2,3,4}^{\text{Tri } 3} = & 2(c_2 - c_1) \left[ (e_{1\Phi}^p \cdot \epsilon_3)(\epsilon_2 \cdot \epsilon_4) - (e_{1\Phi}^p \cdot \epsilon_4)(\epsilon_2 \cdot \epsilon_3) \right] \\
& + 2(c_2 - c_3) \left[ (e_{1\Phi}^p \cdot \epsilon_2)(\epsilon_3 \cdot \epsilon_4) - (e_{1\Phi}^p \cdot \epsilon_4)(\epsilon_2 \cdot \epsilon_3) \right] \\
& + 2(c_1 - c_3) \left[ (e_{1\Phi}^p \cdot \epsilon_2)(\epsilon_3 \cdot \epsilon_4) - (e_{1\Phi}^p \cdot \epsilon_3)(\epsilon_2 \cdot \epsilon_4) \right]. \quad (3.40)
\end{aligned}$$

The remaining permutations with the same color structure are

- $(\epsilon_1, e_{2\Phi}^p, \epsilon_3, \epsilon_4), \quad (\epsilon_1, \epsilon_2, e_{3\Phi}^p, \epsilon_4), \quad (\epsilon_1, \epsilon_2, \epsilon_3, e_{4\Phi}^p)$ .

#### 4) Sfermionic triangle diagrams with two $\tilde{q}\tilde{q}gg$ -vertices

Finally, the last triangle topology (B.1.6), depicted in Fig. 3.7, is contracted directly with four polarization vectors of the external gluons. The two  $\tilde{q}\tilde{q}gg$ -vertices provide a pentagon-like color structure, which can be also expressed

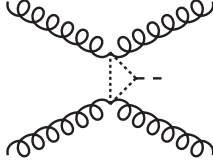


Figure 3.7: *Pentagon-like squark-triangle contributions to  $gg \rightarrow gg\Phi$  amplitudes.*

very easily by the color coefficients of Eq. (3.31). Hence, for a gluon permutation  $(q_{12}, q_{34})$  the partial amplitude with the triangle tensor of Eq. (B.1.6) is given by,

$$\begin{aligned}
\mathcal{A}_{12,34}^{\text{TriP}} &= 2 \left( \text{tr}[t^{a_1} t^{a_2} t^{a_3} t^{a_4}] + \text{tr}[t^{a_1} t^{a_2} t^{a_4} t^{a_3}] + \text{tr}[t^{a_2} t^{a_1} t^{a_3} t^{a_4}] \right. \\
&\quad \left. + \text{tr}[t^{a_2} t^{a_1} t^{a_4} t^{a_3}] \right) T_{\mu_1 \mu_2 \mu_3 \mu_4}^{\text{P}, \Phi, \tilde{f}}(q_{12}, q_{34}, m_{\tilde{f}}) \epsilon_1^{\mu_1} \epsilon_2^{\mu_2} \epsilon_3^{\mu_3} \epsilon_4^{\mu_4} \\
&= 2 (c_1 + c_2) T_{\mu_1 \mu_2 \mu_3 \mu_4}^{\text{P}, \Phi, \tilde{f}}(q_{12}, q_{34}, m_{\tilde{f}}) \epsilon_1^{\mu_1} \epsilon_2^{\mu_2} \epsilon_3^{\mu_3} \epsilon_4^{\mu_4} . \tag{3.41}
\end{aligned}$$

The other permutations are

- $(q_{13}, q_{24}) \implies 2 \left( \text{tr}[t^{a_1} t^{a_3} t^{a_2} t^{a_4}] + \text{tr}[t^{a_1} t^{a_3} t^{a_4} t^{a_2}] + \text{tr}[t^{a_3} t^{a_1} t^{a_2} t^{a_4}] \right. \\ \left. + \text{tr}[t^{a_3} t^{a_1} t^{a_4} t^{a_2}] \right) = 2 (c_2 + c_3) ,$
- $(q_{14}, q_{23}) \implies 2 \left( \text{tr}[t^{a_1} t^{a_4} t^{a_2} t^{a_3}] + \text{tr}[t^{a_1} t^{a_4} t^{a_3} t^{a_2}] + \text{tr}[t^{a_4} t^{a_1} t^{a_2} t^{a_3}] \right. \\ \left. + \text{tr}[t^{a_4} t^{a_1} t^{a_3} t^{a_2}] \right) = 2 (c_1 + c_3) .$

The sum over colored gluons of the squared amplitude becomes

$$\begin{aligned}
\sum_{\text{color}} |\mathcal{A}^{gg}|^2 &= \sum_{i,j=1}^3 \mathcal{A}_i^{gg} (\mathcal{A}_j^{gg})^* \sum_{\text{col}} c_i c_j \\
&= C_1 \sum_{i=1}^3 |\mathcal{A}_i^{gg}|^2 + C_2 \sum_{i,j=1; i \neq j}^3 \mathcal{A}_i^{gg} (\mathcal{A}_j^{gg})^* \tag{3.42}
\end{aligned}$$

with

$$\mathcal{C}_1 \equiv \sum_{\text{col}} c_i c_i = \frac{(N^2 - 1)(N^4 - 2N^2 + 6)}{8N^2}, \quad (\text{no sum. over } i), \quad (3.43)$$

$$\mathcal{C}_2 \equiv \sum_{\text{col}} c_i c_j = \frac{(N^2 - 1)(3 - N^2)}{4N^2}, \quad i \neq j. \quad (3.44)$$

### 3.4 Higgs production in association with three jets

For the production of Higgs bosons  $\Phi$  in a  $2 \rightarrow 4$  QCD process of the order  $\alpha_s^5$ , the former sub-processes are complemented by an additional gluon in the final-state with momentum  $q_f = +\bar{q}_f$ . The production of neutral Higgs bosons  $\Phi$  can then be carried out via the following sub-processes,

$$q q \rightarrow q q g \Phi, \quad q Q \rightarrow q Q g \Phi, \quad q g \rightarrow q g g \Phi, \quad g g \rightarrow g g g \Phi. \quad (3.45)$$

Further crossing related sub-processes are given by,

- quark-quark scattering:

$$\begin{aligned} \bar{q} \bar{q} &\longrightarrow \bar{q} \bar{q} g \Phi \quad (\text{via } C \text{ invariance of amplitude}), \\ q \bar{q} &\longrightarrow q \bar{q} g \Phi, \\ q \bar{q} &\longrightarrow Q \bar{Q} g \Phi, \\ q \bar{q} &\longrightarrow g g g \Phi, \end{aligned} \quad (3.46)$$

- quark-gluon scattering:

$$\begin{aligned} q g &\longrightarrow \bar{q} q q \Phi, \\ q g &\longrightarrow \bar{Q} Q q \Phi, \\ g q &\longrightarrow \bar{q} q q \Phi \quad (\text{flipped beams}), \\ g q &\longrightarrow g q g \Phi \quad (\text{flipped beams}), \\ \bar{q} g &\longrightarrow \bar{q} g g \Phi \quad (\text{via } C \text{ invariance of amplitude}), \\ g \bar{q} &\longrightarrow g \bar{q} g \Phi \quad (\text{via } C \text{ invariance of amp. + flipped beams}), \end{aligned} \quad (3.47)$$



- gluon-gluon scattering:

$$\begin{aligned}
g g &\longrightarrow q \bar{q} g \Phi , \\
g g &\longrightarrow g g g \Phi .
\end{aligned} \tag{3.48}$$

Here, the overall factor  $F_p^{3j}$ , containing all coupling constants, reads as

$$F_p^{3j} = C_p \left( \frac{g_S^2}{4\pi} \right)^{5/2} = C_p \alpha_s^5 \tag{3.49}$$

The present calculation does not include contributions with squarks. To shorten expressions for amplitudes, one can define new quark currents containing the emission of a gluon close to an external quark in the initial or final state

$$\begin{aligned}
J_{fi}^\mu(*q_l) &= \delta_{\sigma_f \sigma_i} \chi_{\sigma_f}^\dagger(\bar{p}_f) (\sigma^\mu)_\tau (\not{p}_i - \not{A}_l)_{-\sigma_i} (\not{\epsilon}_l)_{\sigma_i} \chi_{\sigma_i}(\bar{p}_i) \frac{1}{(p_i - q_l)^2} \frac{1}{q_{fi}^2} \\
&= \delta_{\sigma_f \sigma_i} \langle f | (\sigma^\mu)_\tau | q_i, l \rangle \frac{1}{(p_i - p_f + q_l)^2} ,
\end{aligned} \tag{3.50}$$

$$\begin{aligned}
J_{fi}^\mu(q_l*) &= \delta_{\sigma_f \sigma_i} \chi_{\sigma_f}^\dagger(\bar{p}_f) (\not{\epsilon}_l)_{\sigma_f} (\not{p}_f + \not{A}_l)_{-\sigma_f} \frac{1}{(p_f + q_l)^2} (\sigma^\mu)_\tau \chi_{\sigma_i}(\bar{p}_i) \frac{1}{q_{fi}^2} \\
&= \delta_{\sigma_f \sigma_i} \langle f, q_l | (\sigma^\mu)_\tau | i \rangle \frac{1}{(p_i - p_f + q_l)^2} .
\end{aligned} \tag{3.51}$$

Gluon radiation in initial or final state is denoted by a star. It tags the position of gluon emission. Further fermion currents with the effective polarization vector of Eq. (3.14) can be defined in a similar way

$$\begin{aligned}
J_{fi}^\mu(*q_l, \Phi) &= \delta_{\sigma_f \sigma_i} \chi_{\sigma_f}^\dagger(\bar{p}_f) (\sigma^\mu)_\tau (\not{p}_i + \not{A}_l + \not{P}_\Phi)_{-\sigma_i} (\not{\epsilon}_{l\Phi}^p)_{\sigma_i} \chi_{\sigma_i}(\bar{p}_i) \frac{1}{(p_i + q_l + P_\Phi)^2} \frac{1}{q_{fi}^2} \\
&= \delta_{\sigma_f \sigma_i} \langle f | (\sigma^\mu)_\tau | q_l, i, \Phi \rangle \frac{1}{(p_i - p_f + q_l + P_\Phi)^2} ,
\end{aligned} \tag{3.52}$$

$$\begin{aligned}
J_{fi}^\mu(q_l*, \Phi) &= \delta_{\sigma_f \sigma_i} \chi_{\sigma_f}^\dagger(\bar{p}_f) (\not{\epsilon}_{l\Phi}^p)_{\sigma_f} (\not{p}_f - \not{A}_l - \not{P}_\Phi)_{-\sigma_f} \frac{1}{(p_f - q_l - P_\Phi)^2} (\sigma^\mu)_\tau \chi_{\sigma_i}(\bar{p}_i) \frac{1}{q_{fi}^2} \\
&= \delta_{\sigma_f \sigma_i} \langle f, q_l, \Phi | (\sigma^\mu)_\tau | i \rangle \frac{1}{(p_i - p_f + q_l + P_\Phi)^2} .
\end{aligned} \tag{3.53}$$

This formalism also allows for further definitions of quark currents, but with two emitted gluons

$$\begin{aligned}
J_{fi}^\mu(q_l, q_m) &= \delta_{\sigma_f \sigma_i} \chi_{\sigma_f}^\dagger(\bar{p}_f) (\not{\epsilon}_l)_{\sigma_f} (\not{p}_f + \not{q}_l)_{-\sigma_f} \frac{1}{(p_f + q_l)^2} (\sigma^\mu)_\tau \\
&\times (\not{p}_i - \not{q}_m)_{-\sigma_i} (\not{\epsilon}_m)_{\sigma_i} \chi_{\sigma_i}(\bar{p}_i) \frac{1}{(p_i - q_m)^2} \frac{1}{q_{fi}^2} \\
&= \delta_{\sigma_f \sigma_i} \langle f, q_l | (\sigma^\mu)_\tau | i, q_m \rangle \frac{1}{(p_i - p_f + q_l + q_m)^2} .
\end{aligned} \tag{3.54}$$

Further currents, containing an attached Higgs boson, are

$$\begin{aligned}
J_{fi}^\mu(q_l^*, q_m, \Phi) &= \delta_{\sigma_f \sigma_i} \chi_{\sigma_f}^\dagger(\bar{p}_f) (\not{\epsilon}_{l\Phi}^p)_{\sigma_f} (\not{p}_f - \not{q}_l - P_\Phi)_{-\sigma_f} \\
&\times \frac{1}{(p_f - q_l - P_\Phi)^2} (\sigma^\mu)_\tau (\not{p}_i + \not{q}_m)_{-\sigma_i} (\not{\epsilon}_m)_{\sigma_i} \chi_{\sigma_i}(\bar{p}_i) \frac{1}{(p_i + q_m)^2} \frac{1}{q_{fi}^2} \\
&= \delta_{\sigma_f \sigma_i} \langle f, q_l, \Phi | (\sigma^\mu)_\tau | i, q_m \rangle \frac{1}{(p_i - p_f + q_l + q_m + P_\Phi)^2} ,
\end{aligned} \tag{3.55}$$

$$\begin{aligned}
J_{fi}^\mu(q_l, *q_m, \Phi) &= \delta_{\sigma_f \sigma_i} \chi_{\sigma_f}^\dagger(\bar{p}_f) (\not{\epsilon}_l)_{\sigma_f} (\not{p}_f - \not{q}_l)_{-\sigma_f} \frac{1}{(p_f - q_l)^2} (\sigma^\mu)_\tau \\
&\times (\not{p}_i + \not{q}_m + P_\Phi)_{-\sigma_i} (\not{\epsilon}_{m\Phi}^p)_{\sigma_i} \chi_{\sigma_i}(\bar{p}_i) \frac{1}{(p_i + q_m + P_\Phi)^2} \frac{1}{q_{fi}^2} \\
&= \delta_{\sigma_f \sigma_i} \langle f, q_l | (\sigma^\mu)_\tau | i, q_m, \Phi \rangle \frac{1}{(p_i - p_f + q_l + q_m + P_\Phi)^2} .
\end{aligned} \tag{3.56}$$

Finally, due to a large number of diagrams in the subsequent sub-processes, it is useful to introduce a shorthand notation for the three-gluon vertex without coupling constant

$$\text{GV}_3^{\mu_1 \mu_2 \mu_3}(k, p, q) = \left[ g^{\mu_1 \mu_2} (k - p)^{\mu_3} + g^{\mu_2 \mu_3} (p - q)^{\mu_1} + g^{\mu_3 \mu_1} (q - k)^{\mu_2} \right] , \tag{3.57}$$

with color coefficient  $f^{a_1 a_2 a_3}$ . The four-gluon vertex is composed of three parts with different color and tensor structures (App. D), which are treated by MadGraph as individual diagrams. For the illustration of partial amplitudes, the first part of the vertex is used only

$$\text{GV}_4^{\mu_1 \mu_2 \mu_3 \mu_4} = -(g^{\mu_1 \mu_3} g^{\mu_2 \mu_4} - g^{\mu_1 \mu_4} g^{\mu_2 \mu_3}) , \tag{3.58}$$

where  $f^{a_1 a_2 m} f^{m a_3 a_4}$  is the corresponding color factor.

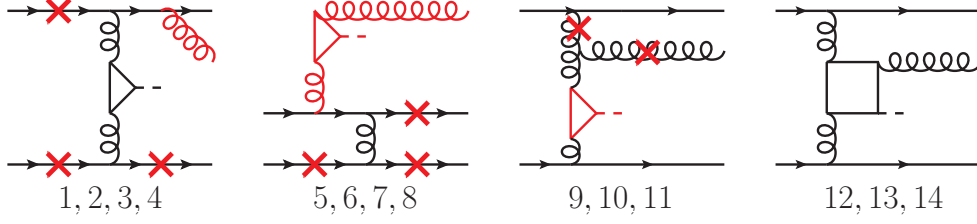


Figure 3.8: *Quark-loop contributions to  $qq \rightarrow qg\Phi$  amplitudes.*

### 3.4.1 $qQ \rightarrow qQg\Phi$ and $qq \rightarrow qqg\Phi$

The simplest contribution contains four quarks pairwise of different flavor and one gluon as external particles. In total, there are 14 diagrams, in which 11 have a triangle insertion and the remaining 3 a box topology. These diagrams are illustrated in Fig. 3.8, where different configurations are denoted by a red cross. Partial amplitudes with the emission of a gluon from a quark line from initial and final state are listed here

$$\mathcal{A}_{*21,43}^{qQ, \text{Tri } 1} = (t^{a_2} t^{a_1})_{21} t_{43}^{a_2} J_{21}^{\mu_1}(*q) J_{43}^{\mu_2} T_{\mu_1 \mu_2}^{\Phi}(p_2 - p_1 + q, p_4 - p_3, m_t), \quad (3.59)$$

$$\mathcal{A}_{21*,43}^{qQ, \text{Tri } 2} = (t^{a_1} t^{a_2})_{21} t_{43}^{a_2} J_{21}^{\mu_1}(q^*) J_{43}^{\mu_2} T_{\mu_1 \mu_2}^{\Phi}(p_2 - p_1 + q, p_4 - p_3, m_t), \quad (3.60)$$

$$\mathcal{A}_{21,43*}^{qQ, \text{Tri } 3} = t_{21}^{a_2} (t^{a_2} t^{a_1})_{43} J_{21}^{\mu_1} J_{43}^{\mu_2}(*q) T_{\mu_1 \mu_2}^{\Phi}(p_2 - p_1, p_4 - p_3 + q, m_t), \quad (3.61)$$

$$\mathcal{A}_{21,43*}^{qQ, \text{Tri } 4} = t_{21}^{a_2} (t^{a_1} t^{a_2})_{43} J_{21}^{\mu_1} J_{43}^{\mu_2}(q^*) T_{\mu_1 \mu_2}^{\Phi}(p_2 - p_1, p_4 - p_3 + q, m_t). \quad (3.62)$$

These four contributions provide the basis for the color structure of this subprocess. Hence, all subsequent partial amplitudes are distributed to that basis.

Four similar amplitudes with the same color factors can be constructed by removing the triangle insertion between both quark lines and replacing the usual polarization vector by an effective one

$$\mathcal{A}_{*21,43}^{qQ, \text{Tri } 5} = (t^{a_2} t^{a_1})_{21} t_{43}^{a_2} J_{21}(*q, \Phi) \cdot J_{43}, \quad (3.63)$$

$$\mathcal{A}_{21*,43}^{qQ, \text{Tri } 6} = (t^{a_1} t^{a_2})_{21} t_{43}^{a_2} J_{21}(q^*, \Phi) \cdot J_{43}, \quad (3.64)$$

$$\mathcal{A}_{21,*43}^{qQ,\text{Tri } 7} = t_{21}^{a_2} (t^{a_2} t^{a_1})_{43} J_{21} \cdot J_{43} (*q, \Phi) , \quad (3.65)$$

$$\mathcal{A}_{21,43*}^{qQ,\text{Tri } 8} = t_{21}^{a_2} (t^{a_1} t^{a_2})_{43} J_{21} \cdot J_{43} (q*, \Phi) . \quad (3.66)$$

The next two graphs contain a three-gluon vertex and are given by

$$\begin{aligned} \mathcal{A}_{21,43}^{qQ,\text{Tri } 9} &= t_{i_2 i_1}^{a_2} [t^{a_2} t^{a_1} - t^{a_1} t^{a_2}]_{i_2 i_1} J_{21}^{\mu_1} T_{\mu_1 \mu_2}^\Phi (p_2 - p_1, p_4 - p_3 + q, m_t) \\ &\times \left[ 2 J_{43}^{\mu_2} (p_4 - p_3) \cdot \epsilon(\bar{q}) + J_{43} \cdot \epsilon(\bar{q}) (p_3 - p_4 + \epsilon(\bar{q}))^{\mu_2} \right. \\ &\quad \left. + \epsilon(\bar{q})^{\mu_2} (p_3 - p_4 - 2q) \cdot J_{43} \right] , \end{aligned} \quad (3.67)$$

$$\begin{aligned} \mathcal{A}_{21,43}^{qQ,\text{Tri } 9} &= t_{i_2 i_1}^{a_2} [t^{a_2} t^{a_1} - t^{a_1} t^{a_2}]_{i_2 i_1} J_{21}^{\mu_1} T_{\mu_1 \mu_2}^\Phi (p_2 - p_1, p_4 - p_3 + q, m_t) \\ &\times \left[ 2 J_{43}^{\mu_2} (p_4 - p_3) \cdot \epsilon(\bar{q}) + J_{43} \cdot \epsilon(\bar{q}) (p_3 - p_4 + \epsilon(\bar{q}))^{\mu_2} \right. \\ &\quad \left. + \epsilon(\bar{q})^{\mu_2} (p_3 - p_4 - 2q) \cdot J_{43} \right] . \end{aligned} \quad (3.68)$$

The remaining contribution with a triangle insertion is composed of a three-gluon vertex, effective polarization vector of Eq. (3.14) and two quark currents, defined in Eq. (3.9)

$$\begin{aligned} \mathcal{A}_{21,43}^{qQ,\text{Tri } 11} &= t_{i_2 i_1}^{a_2} [t^{a_2} t^{a_1} - t^{a_1} t^{a_2}]_{i_2 i_1} J_{21} \cdot J_{43} (p_1 + p_4 - p_2 - p_3) \cdot e_\Phi^p \\ &\quad + J_{43} \cdot e_\Phi^p (p_3 - p_4 + q + P_\Phi) \cdot J_{21} + J_{21} \cdot e_\Phi^p (p_2 - p_1 \\ &\quad - q - P_\Phi) \cdot J_{43} . \end{aligned} \quad (3.69)$$

In addition, one can insert a box-topology into the diagram with a three-gluon vertex in three different ways. The  $3!$  permutations of the attached gluons are reduced by Furry's theorem to three graphs, which are already captured by the box tensor  $B_\Phi^{\mu_1 \mu_2 \mu_3} (q_1, q_2, q_3, m_t)$ . The partial amplitude reads as

$$\begin{aligned} \mathcal{A}_{21,43}^{qQ,\text{Box}} &= [t^{a_3} t^{a_2} - t^{a_2} t^{a_3}]_{i_2 i_1} B_\Phi^{\mu_1 \mu_2 \mu_3} (q, p_2 - p_1, p_4 - p_3, m_t) \epsilon(\bar{q})^{\mu_1} \\ &\quad \times J_{21}^{\mu_2} J_{34}^{\mu_3} . \end{aligned} \quad (3.70)$$

The color coefficient of the last four partial amplitudes is proportional to a structure constant  $f$ . It is useful to decompose it into the color basis of Eqs. (3.59-3.62)

$$f^{a_1 a_2 a_3} t_{i_2 i_1}^{a_2} t_{i_4 i_3}^{a_3} = i t_{i_2 i_1}^{a_2} [t^{a_2} t^{a_1} - t^{a_1} t^{a_2}]_{i_4 i_3} . \quad (3.71)$$

Identical quark-flavors double the amount of diagrams by interchanging final states. This provides four additional color factors,

$$(t^{a_2 t^{a_1}})_{41} t_{23}^{a_2}, \quad (t^{a_1 t^{a_2}})_{41} t_{23}^{a_2}, \quad t_{41}^{a_2} (t^{a_2 t^{a_1}})_{23}, \quad t_{41}^{a_2} (t^{a_1 t^{a_2}})_{23}. \quad (3.72)$$

One has to keep Pauli-interference in mind, that changes the sign of the corresponding diagrams. In total, there are eight different color structures, which interfere among each other. All interference terms form a symmetric  $8 \times 8$  matrix  $\mathcal{RGB}_{ij}^{qq}$ , containing products of Casimir-operators of the fundamental and adjoint representation of the  $SU(N)$  algebra. For  $N = 3$ , it is given by

$$\mathcal{RGB}_{ij}^{qq} = \frac{1}{9} \begin{pmatrix} 24 & -3 & -6 & 21 & -8 & 1 & 10 & 1 \\ -3 & 24 & 21 & -6 & 1 & 10 & 1 & -8 \\ -6 & 21 & 24 & -3 & 10 & 1 & -8 & 1 \\ 21 & -6 & -3 & 24 & 1 & -8 & 1 & 10 \\ -8 & 1 & 10 & 1 & 24 & -3 & -6 & 21 \\ 1 & 10 & 1 & -8 & -3 & 24 & 21 & -6 \\ 10 & 1 & -8 & 1 & -6 & 21 & 24 & -3 \\ 1 & -8 & 1 & 10 & 21 & -6 & -3 & 24 \end{pmatrix}. \quad (3.73)$$

The squared amplitude, summed over initial- and final-particle color, becomes

$$\sum_{\text{color}} |\mathcal{A}^{qq}|^2 = \left( F_p^{qQ,3j} \right)^2 \sum_{i,j=1}^8 \mathcal{RGB}_{ij}^{qq} \text{Re} \left[ \mathcal{A}_i (\mathcal{A}_j)^* \right], \quad (3.74)$$

with

$$F_p^{qQ,3j} = S_1 S_2 S_3 S_4 4 \sqrt{\bar{p}_1^0 \bar{p}_2^0 \bar{p}_3^0 \bar{p}_4^0} F_t^{3j}. \quad (3.75)$$

For a sub-process with different quark-flavors, only the symmetric  $4 \times 4$  part of the  $\mathcal{RGB}_{ij}^{qq}$  matrix with  $i, j = 1, \dots, 4$  should be used to calculate the squared expression of the amplitude.

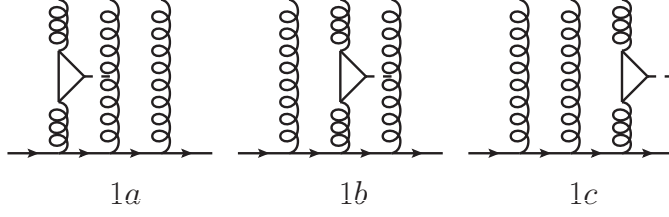


Figure 3.9: *Quark-triangle contributions to  $qg \rightarrow qgg\Phi$  amplitudes.*

### 3.4.2 $qg \rightarrow qgg\Phi$

With MadGraph [31], 84 distinct diagrams were generated for the sub-process  $qg \rightarrow qgg\Phi$  within the effective theory. The correspondence between the full and the effective theory is described in more detail in appendix E. Furthermore, the application of abbreviations introduced in previous chapters allows an indexing of different diagrams according to certain features. This procedure was already used in the Higgs + 2 jets process. It ensures a better view over the large variety and number of diagrams. In the following, expressions for partial amplitudes for a fixed permutation of external particle momenta are shown only:

#### 1) Triangle diagrams with effective polarization vector only

Fig. 3.9 shows three different possibilities to attach a triangle loop to the emitted gluons

$$\mathcal{A}_{21}^{qg, \text{Tri } 1a} = (t^{a_1} t^{a_2} t^{a_3})_{i_2 i_1} J_{21}(q_3^*, q_1, \Phi) \cdot \epsilon_2, \quad (3.76)$$

$$\mathcal{A}_{21}^{qg, \text{Tri } 1b} = (t^{a_1} t^{a_2} t^{a_3})_{i_2 i_1} J_{21}(q_3, q_1) \cdot e_{2\Phi}^p, \quad (3.77)$$

$$\mathcal{A}_{21}^{qg, \text{Tri } 1c} = (t^{a_1} t^{a_2} t^{a_3})_{i_2 i_1} J_{21}(q_3, q_1^*, \Phi) \cdot \epsilon_2. \quad (3.78)$$

There are in total 18 diagrams:  $3! = 6$  different permutations of the attached gluons and three possibilities of Higgs emission. The remaining color factors are

$$\begin{aligned} & (t^{a_3} t^{a_1} t^{a_2})_{i_2 i_1}, \quad (t^{a_1} t^{a_3} t^{a_2})_{i_2 i_1}, \quad (t^{a_2} t^{a_1} t^{a_3})_{i_2 i_1}, \\ & (t^{a_2} t^{a_3} t^{a_1})_{i_2 i_1}, \quad (t^{a_3} t^{a_2} t^{a_1})_{i_2 i_1}. \end{aligned} \quad (3.79)$$

These six color structures provide the color basis for that sub-process.

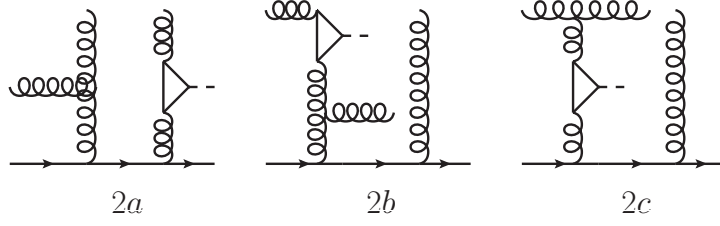


Figure 3.10: *Quark-triangle contributions to  $qg \rightarrow qgg\Phi$  amplitudes.*

## 2) Triangle diagrams with one three-gluon vertex

There are 24 different contributions, containing an effective polarization vector or a triangle loop with off-shell gluons. Three possibilities, shown in Fig. 3.10, are available to construct the partial amplitudes with given resources

$$\mathcal{A}^{qg, \text{Tri } 2a} = i f^{a_2 a_1 m} (t^m t^{a_3})_{21} J_{21}(*q_3, \Phi) \cdot J_{12}^G (q_1 + q_2)^2, \quad (3.80)$$

$$\begin{aligned} \mathcal{A}^{qg, \text{Tri } 2b} &= i f^{a_2 a_1 m} (t^m t^{a_3})_{21} J_{21}(*q_3) \cdot J_{12}^G(q_1^*, q_2, \Phi) \\ &\times (q_1 + q_2 + P_\Phi)^2, \end{aligned} \quad (3.81)$$

$$\begin{aligned} \mathcal{A}^{qg, \text{Tri } 2c} &= i f^{a_2 a_1 m} (t^m t^{a_3})_{21} T_\Phi^{\mu_1 \mu_2}(p_2 - p_1 + q_3, q_1 + q_2, m_t) \\ &\times J_{21}^{\mu_1}(*q_3) J_{12}^G. \end{aligned} \quad (3.82)$$

All appearing color factors can be reduced to the basis, given by Eqs. (3.76-3.79)

$$i f^{a_2 a_1 m} (t^m t^{a_3})_{i_2 i_1} = (t^{a_2} t^{a_1} t^{a_3} - t^{a_1} t^{a_2} t^{a_3})_{i_2 i_1}, \quad (3.83)$$

$$i f^{a_3 a_1 m} (t^m t^{a_2})_{i_2 i_1} = (t^{a_3} t^{a_1} t^{a_2} - t^{a_1} t^{a_3} t^{a_2})_{i_2 i_1}, \quad (3.84)$$

$$i f^{a_2 a_3 m} (t^m t^{a_1})_{i_2 i_1} = (t^{a_2} t^{a_3} t^{a_1} - t^{a_3} t^{a_2} t^{a_1})_{i_2 i_1}, \quad (3.85)$$

$$i f^{a_2 a_1 m} (t^{a_3} t^m)_{i_2 i_1} = (t^{a_3} t^{a_2} t^{a_1} - t^{a_3} t^{a_1} t^{a_2})_{i_2 i_1}, \quad (3.86)$$

$$i f^{a_3 a_1 m} (t^{a_2} t^m)_{i_2 i_1} = (t^{a_2} t^{a_3} t^{a_1} - t^{a_2} t^{a_1} t^{a_3})_{i_2 i_1}, \quad (3.87)$$

$$i f^{a_2 a_3 m} (t^{a_1} t^m)_{i_2 i_1} = (t^{a_1} t^{a_2} t^{a_3} - t^{a_1} t^{a_2} t^{a_3})_{i_2 i_1}. \quad (3.88)$$

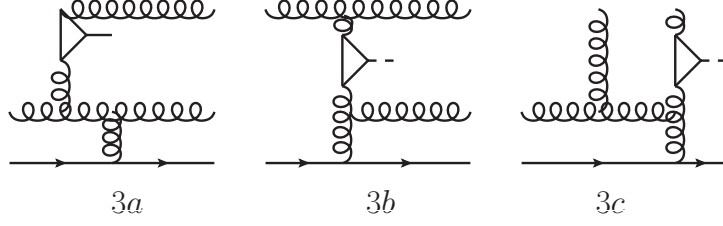


Figure 3.11: *Quark-triangle contributions to  $gg \rightarrow qg\Phi$  amplitudes.*

**3) Triangle diagrams with two three-gluon vertices** A total of 15 diagrams with a triangle insertion connected to two three-gluon vertices makes contributions: 9 with effective polarization vector and 6 with a triangle tensor attached to two virtual gluons. Construction possibilities for partial amplitudes, depicted in Fig. 3.11, are given by,

$$\begin{aligned} \mathcal{A}^{qg, \text{Tri } 3a} &= f^{a_2 a_1 m} f^{a_3 m n} t_{i_2 i_1}^n \text{GV}_3^{\mu_1 \mu_2 \mu_3}(-q_3, -q_{12} - P_\Phi, p_1 - p_2) \\ &\times \epsilon_{3, \mu_1} J_{12, \mu_2}^G(q_1, q_2^*, \Phi) J_{21, \mu_3} , \end{aligned} \quad (3.89)$$

$$\begin{aligned} \mathcal{A}^{qg, \text{Tri } 3b} &= f^{a_2 a_1 m} f^{a_3 m n} t_{i_2 i_1}^n \text{GV}_3^{\mu_2 \mu_3 \mu_4}(-q_3, p_2 - p_1 + q_3, p_2 - p_1) \\ &\times T_{\mu_1 \mu_2}^\Phi(q_{12}, p_2 - p_1 + q_3, m_t) J_{12}^{G, \mu_1} J_{21, \mu_3} \epsilon_{\mu_4, 3} \\ &\times \frac{1}{(p_2 - p_1 + q_3)^2} , \end{aligned} \quad (3.90)$$

$$\begin{aligned} \mathcal{A}^{qg, \text{Tri } 3c} &= f^{a_2 a_1 m} f^{a_3 m n} t_{i_2 i_1}^n \text{GV}_3^{\mu_1 \mu_2 \mu_3}(-q_3 - P_\Phi, -q_{12}, p_1 - p_2) \\ &\times e_{p, \mu_1}^{3, \Phi} J_{12, \mu_2}^G J_{21, \mu_3} . \end{aligned} \quad (3.91)$$

Here, only three different color factors appear in the calculation, which can be reduced to the color basis using the identity of Eq. (C.10) in the following way

$$f^{a_2 a_1 m} f^{a_3 m n} t_{i_2 i_1}^n = (-t^{a_2} t^{a_1} t^{a_3} + t^{a_1} t^{a_2} t^{a_3} + t^{a_3} t^{a_2} t^{a_1} - t^{a_3} t^{a_1} t^{a_2})_{i_2 i_1} , \quad (3.92)$$

$$f^{a_3 a_1 m} f^{a_2 m n} t_{i_2 i_1}^n = (-t^{a_3} t^{a_1} t^{a_2} + t^{a_1} t^{a_3} t^{a_2} + t^{a_2} t^{a_3} t^{a_1} - t^{a_2} t^{a_1} t^{a_3})_{i_2 i_1} , \quad (3.93)$$

$$f^{a_2 a_3 m} f^{a_1 n} t_{i_2 i_1}^n = (-t^{a_2} t^{a_3} t^{a_1} + t^{a_3} t^{a_2} t^{a_1} + t^{a_1} t^{a_2} t^{a_3} - t^{a_1} t^{a_3} t^{a_2})_{i_2 i_1} . \quad (3.94)$$



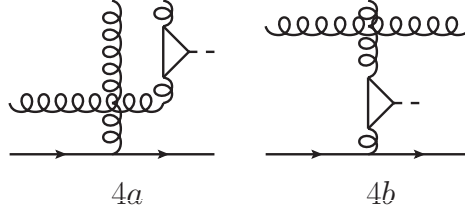


Figure 3.12: *Quark-triangle contributions to  $qq \rightarrow qgg\Phi$  amplitudes.*

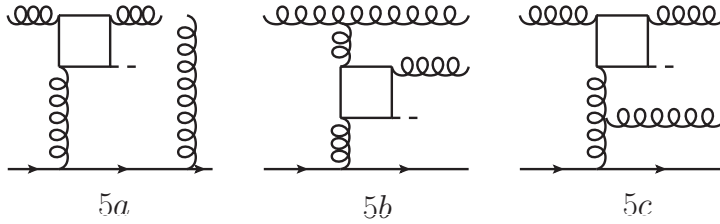


Figure 3.13: *Quark-box contributions to  $qq \rightarrow qgg\Phi$  amplitudes.*

#### 4) Triangle diagrams with four gluon vertex

MadGraph [31] generates 12 graphs, which correspond to 4 four-gluon vertices. The partial amplitudes, shown in Fig. 3.12, reads as

$$\mathcal{A}^{qq, \text{Tri } 4a} = f^{a_1 a_2 m} f^{m a_3 n} t_{i_2 i_1}^n \text{GV}_{4, \mu_1 \mu_2 \mu_3 \mu_4} \epsilon_3^{\mu_1, p} \epsilon_2^{\mu_2} \epsilon_3^{\mu_3} J_{21}^{\mu_4}, \quad (3.95)$$

$$\begin{aligned} \mathcal{A}^{qq, \text{Tri } 4b} &= f^{a_1 a_2 m} f^{m a_3 n} t_{i_2 i_1}^n \text{GV}_{4, \mu_1 \mu_2 \mu_3 \mu_4} \epsilon_1^{\mu_1} \epsilon_2^{\mu_2} \epsilon_3^{\mu_3} \\ &\times T_{\Phi}^{\mu_4 \mu_5}(q_{123}, p_2 - p_1, m_t) J_{21, \mu_5}. \end{aligned} \quad (3.96)$$

The color structure is the same as in Eqs. (3.92 -3.94), except for a relative sign, due to different permutations of the involved gluons.

#### 5) Box diagrams

Partial amplitudes with a box tensor, depicted in Fig. 3.13, can be constructed in the following ways

$$\begin{aligned} \mathcal{A}^{qq, \text{Box } 5a} &= i f^{a_2 a_1 m} (t^m t^{a_3})_{i_2 i_1} B_{\mu_1 \mu_2 \mu_3}^{\Phi}(q_2, q_1, p_2 - p_1 + q_3, m_t) \\ &\times \epsilon_2^{\mu_1} \epsilon_1^{\mu_2} J_{21}^{\mu_3}(q_3^*), \end{aligned} \quad (3.97)$$

$$\mathcal{A}^{qq, \text{Box } 5b} = f^{a_2 a_1 m} f^{a_3 m n} t_{i_2 i_1}^n B_{\mu_1 \mu_2 \mu_3}^{\Phi}(q_{12}, q_3, p_2 - p_1, m_t)$$

$$\times J_{32}^{G, \mu_1} \epsilon_1^{\mu_2} J_{21}^{\mu_3} , \quad (3.98)$$

$$\begin{aligned} \mathcal{A}^{gg, \text{Box } 5c} &= f^{a_2 a_1 m} f^{a_3 m n} t_{i_2 i_1}^n \text{GV}_{3, \mu_3 \mu_4 \mu_5} B_{\mu_1 \mu_2 \mu_3}^\Phi(q_2, q_1, p_2 - p_1 + q_3, m_t) \\ &\times \epsilon_1^{\mu_2} \epsilon_2^{\mu_1} \epsilon_1^{\mu_4} J_{21}^{\mu_5} . \end{aligned} \quad (3.99)$$

The decomposition of the color factors in terms of the basis elements was already shown in Eqs. (3.83 -3.88) and (3.92 -3.94).

## 6) Pentagon diagrams

In the effective theory there is only one pentagon, that corresponds to a four-gluon vertex with an additional Higgs boson emission. Furthermore, it features the same tensor and color structure of a four-gluon vertex. The full loop theory provides 12 pentagon diagrams, if Furry's theorem is taken into account. The color structure does not correspond to a four-gluon vertex and therefore has to be treated separately

$$\begin{aligned} \bullet \text{ perm.: } &\left\{ (a_1, a_2, a_3, d), (a_2, a_3, d, a_1), (a_3, d, a_1, a_2), (d, a_1, a_2, a_3) \right. \\ &\left. (a_1, d, a_3, a_2), (d, a_3, a_2, a_1), (a_3, a_2, a_1, d), (a_2, a_1, d, a_3) \right\} \\ c_1 t_{i_2 i_1}^{a_4} &= -\frac{1}{2N} d^{a_1 a_2 a_3} \delta_{i_2 i_1} + \frac{1}{2} (t^{a_1} t^{a_2} t^{a_3} + t^{a_3} t^{a_2} t^{a_1})_{i_2 i_1} , \end{aligned} \quad (3.100)$$

$$\begin{aligned} \bullet \text{ perm.: } &\left\{ (a_1, a_3, d, a_2), (a_3, d, a_2, a_1), (d, a_2, a_1, a_3), (a_2, a_1, a_3, d) \right. \\ &\left. (a_1, a_2, d, a_3), (a_2, d, a_3, a_1), (d, a_3, a_1, a_2), (a_3, a_1, a_2, d) \right\} \\ c_2 t_{i_2 i_1}^{a_4} &= -\frac{1}{2N} d^{a_1 a_2 a_3} \delta_{i_2 i_1} + \frac{1}{2} (t^{a_3} t^{a_1} t^{a_2} + t^{a_2} t^{a_1} t^{a_3})_{i_2 i_1} , \end{aligned} \quad (3.101)$$

$$\begin{aligned} \bullet \text{ perm.: } &\left\{ (a_1, d, a_2, a_3), (d, a_2, a_3, a_1), (a_2, a_3, a_1, d), (a_3, a_1, d, a_2) \right. \\ &\left. (a_1, a_3, a_2, d), (a_3, a_2, d, a_1), (a_2, d, a_1, a_3), (d, a_1, a_3, a_2) \right\} \\ c_3 t_{i_2 i_1}^{a_4} &= -\frac{1}{2N} d^{a_1 a_2 a_3} \delta_{i_2 i_1} + \frac{1}{2} (t^{a_2} t^{a_3} t^{a_1} + t^{a_1} t^{a_3} t^{a_2})_{i_2 i_1} , \end{aligned} \quad (3.102)$$

where the  $c_i$  of Eq. (3.32) and  $\text{SU}(N)$ -identities of Appendix C were used. The color generator  $t_{i_2 i_1}^{a_4}$  comes from the attached quark current of Eq. (3.9) and is contracted with the free index  $a_4$  inside the  $c_i$ . An example of such a diagram is shown in Fig. 3.14. In comparison to the effective theory, the

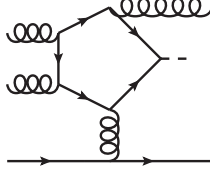


Figure 3.14: *Quark-pentagon contributions to  $gg \rightarrow qgg\Phi$  amplitudes.*

existence of the total symmetric structure constant  $d^{a_1 a_2 a_3}$  extends the color space by an additional dimension. Using the basis (3.76-3.79) at first, one can build up a symmetric  $6 \times 6$  matrix  $\mathcal{RGB}_{ij}^{qq}$ , which contains again  $SU(N)$  Casimir invariants

$$\mathcal{RGB}_{ij}^{qq} = \frac{1}{9} \begin{pmatrix} 64 & 1 & -8 & -8 & 1 & 10 \\ 1 & 64 & -8 & 10 & 1 & -8 \\ -8 & -8 & 64 & 1 & 10 & 1 \\ -8 & 10 & 1 & 64 & -8 & 1 \\ 1 & 1 & 10 & -8 & 64 & -8 \\ 10 & -8 & 1 & 1 & -8 & 64 \end{pmatrix}. \quad (3.103)$$

The squared expression and interference term of the total symmetric structure constant  $d$  with the color basis read as

$$\begin{aligned} C_1 &= \left( -\frac{1}{2N} d^{a_1 a_2 a_3} \delta_{i_2 i_1} \right)^2 \stackrel{N=3}{=} \frac{10}{36}, \\ C_2 &= -\frac{1}{2N} d^{a_1 a_2 a_3} \delta_{i_2 i_1} \left[ (t^{a_i} t^{a_j} t^{a_k})_{i_2 i_1} \right]^\dagger \stackrel{N=3}{=} \frac{10}{72}, \\ & i, j, k = 1, 2, 3 \quad \text{and} \quad i \neq j \neq k. \end{aligned} \quad (3.104)$$

For the loop-induced theory, the squared amplitude, summed over initial- and final-particle color, becomes

$$\sum_{\text{color}} |\mathcal{A}^{qq}|^2 = \left( F_p^{qq,3j} \right)^2 \left\{ \sum_{i,j=1}^6 \mathcal{RGB}_{ij}^{qq} \text{Re} \left[ \mathcal{A}_i (\mathcal{A}_j)^* \right] + C_1 |\mathcal{A}^{\text{pen}}|^2 \right.$$

$$+ 2 C_2 \sum_{i=1}^6 \text{Re} \left[ \mathcal{A}_i \left( \mathcal{A}^{\text{pen}} \right)^* \right] \Bigg\} , \quad (3.105)$$

with

$$F_p^{gg,3j} = -S_1 S_2 2 \sqrt{\bar{p}_1^0 \bar{p}_2^0} \delta_{\sigma_1 \sigma_2} F_p^{3j} . \quad (3.106)$$

The shorthand  $(\mathcal{A}^{\text{pen}})$  denotes the sum of the 12 pentagon contributions. To switch to the effective theory, one has to set both color coefficients  $C_i = 0$  and take notice of the different color structure of the effective pentagons.

### 3.4.3 $gg \rightarrow ggg\Phi$

Using MadGraph [31], 380 diagrams were generated in the effective limit approach. The full theory provides further hexagon-like topologies additionally to the already complicated pentagons. This circumstances make that process numerically very challenging. Due to the large number of diagrams and the length of the result, expressions for the amplitudes are not written here explicitly. It is strategically favorable to start with the hexagons and investigate their color structure. The five external gluons give rise to  $5! = 120$  hexagons. They are proportional to 120 different color traces of the form

$$\begin{aligned} \text{tr} [t^{a_i} t^{a_j} t^{a_k} t^{a_l} t^{a_m}] \quad \text{with} \quad i, j, k, l, m = 1, \dots, 5 \\ \text{and} \quad i \neq j \neq k \neq l \neq m , \end{aligned} \quad (3.107)$$

in which  $(5 - 1)! = 24$  are independent, only due to the invariance property of the trace under cyclic permutations. They are given explicitly by

$$\begin{aligned} (1) \text{tr} [t^{a_1} t^{a_2} t^{a_3} t^{a_4} t^{a_5}], (2) \text{tr} [t^{a_1} t^{a_2} t^{a_3} t^{a_5} t^{a_4}], (3) \text{tr} [t^{a_1} t^{a_2} t^{a_4} t^{a_5} t^{a_3}], \\ (4) \text{tr} [t^{a_1} t^{a_2} t^{a_5} t^{a_4} t^{a_3}], (5) \text{tr} [t^{a_1} t^{a_3} t^{a_4} t^{a_5} t^{a_2}], (6) \text{tr} [t^{a_1} t^{a_3} t^{a_5} t^{a_4} t^{a_2}], \\ (7) \text{tr} [t^{a_1} t^{a_4} t^{a_5} t^{a_3} t^{a_2}], (8) \text{tr} [t^{a_1} t^{a_5} t^{a_4} t^{a_3} t^{a_2}], (9) \text{tr} [t^{a_1} t^{a_3} t^{a_4} t^{a_2} t^{a_5}], \\ (10) \text{tr} [t^{a_1} t^{a_3} t^{a_2} t^{a_5} t^{a_4}], (11) \text{tr} [t^{a_1} t^{a_3} t^{a_3} t^{a_2} t^{a_4}], (12) \text{tr} [t^{a_1} t^{a_4} t^{a_2} t^{a_5} t^{a_3}], \\ (13) \text{tr} [t^{a_1} t^{a_4} t^{a_5} t^{a_2} t^{a_3}], (14) \text{tr} [t^{a_1} t^{a_5} t^{a_2} t^{a_4} t^{a_3}], (15) \text{tr} [t^{a_1} t^{a_3} t^{a_2} t^{a_4} t^{a_5}], \\ (16) \text{tr} [t^{a_1} t^{a_5} t^{a_4} t^{a_2} t^{a_3}], (17) \text{tr} [t^{a_1} t^{a_2} t^{a_4} t^{a_3} t^{a_5}], (18) \text{tr} [t^{a_1} t^{a_2} t^{a_5} t^{a_3} t^{a_4}], \\ (19) \text{tr} [t^{a_1} t^{a_4} t^{a_3} t^{a_5} t^{a_2}], (20) \text{tr} [t^{a_1} t^{a_5} t^{a_3} t^{a_4} t^{a_2}], (21) \text{tr} [t^{a_1} t^{a_4} t^{a_3} t^{a_2} t^{a_5}], \\ (22) \text{tr} [t^{a_1} t^{a_5} t^{a_2} t^{a_3} t^{a_4}], (23) \text{tr} [t^{a_1} t^{a_4} t^{a_2} t^{a_3} t^{a_5}], (24) \text{tr} [t^{a_1} t^{a_5} t^{a_3} t^{a_2} t^{a_4}] . \end{aligned} \quad (3.108)$$

These 24 traces provide the color basis for the sub-process. The number of hexagons can be now reduced via Furry's theorem [29] from 120 to 60. All charge-conjugated hexagons are then distributed to 12 differences of two opposite color traces, which are built up from the color basis (3.108). In the previous sub-process, all pentagons were attached to the quark current of Eq. (3.9), which is here replaced by the gluon current (3.10). This replacement gives rise to 120 contributions with pentagon insertions. Using the color coefficients (3.31) and the commutator relation  $[t^{a_1}, t^{a_2}] = if^{a_1 a_2 a_3} t^{a_3}$ , one arrives at 10 basic momenta configurations for the pentagon graphs. The first momenta configuration  $\{1, 2, 3, [4, 5]\}$  with gluon current  $J_{45}^G$  yields

$$c_1 f^{ma_4 a_5} = -i \left( \text{tr} [t^{a_1} t^{a_2} t^{a_3} t^{a_4} t^{a_5}] \text{tr} - \text{tr} [t^{a_1} t^{a_2} t^{a_3} t^{a_5} t^{a_4}] \right. \\ \left. + \text{tr} [t^{a_1} t^{a_4} t^{a_5} t^{a_3} t^{a_2}] - \text{tr} [t^{a_1} t^{a_5} t^{a_4} t^{a_3} t^{a_2}] \right), \quad (3.109)$$

$$c_2 f^{ma_4 a_5} = -i \left( \text{tr} [t^{a_1} t^{a_3} t^{a_4} t^{a_5} t^{a_2}] - \text{tr} [t^{a_1} t^{a_3} t^{a_5} t^{a_4} t^{a_2}] \right. \\ \left. + \text{tr} [t^{a_1} t^{a_2} t^{a_4} t^{a_5} t^{a_3}] - \text{tr} [t^{a_1} t^{a_2} t^{a_5} t^{a_4} t^{a_3}] \right), \quad (3.110)$$

$$c_3 f^{ma_4 a_5} = -i \left( \text{tr} [t^{a_1} t^{a_4} t^{a_5} t^{a_2} t^{a_3}] - \text{tr} [t^{a_1} t^{a_5} t^{a_4} t^{a_2} t^{a_3}] \right. \\ \left. + \text{tr} [t^{a_1} t^{a_3} t^{a_2} t^{a_4} t^{a_5}] - \text{tr} [t^{a_1} t^{a_3} t^{a_2} t^{a_5} t^{a_4}] \right). \quad (3.111)$$

The structure constants  $f$  are contracted via the index  $m$  with the free index  $a_4$ , replaced by  $m$  inside the  $c_i$ . One has to keep in mind, that every  $c_i$  is proportional to a sum of four charge-conjugated pentagons with cyclicly permuted gluons. The remaining permutations are listed in Appendix F.1. Graphs with triangle and box insertions are all proportional to a color factor composed of three structure constants  $f$ . It can be decomposed in terms of the color basis in the following way using the  $SU(N)$  identities of Appendix C

$$f^{a_1 a_2 m} f^{m a_3 n} f^{n a_4 a_5} \\ = 2i \left( -\text{tr} [t^{a_1} t^{a_2} t^{a_4} t^{a_5} t^{a_3}] + \text{tr} [t^{a_1} t^{a_2} t^{a_5} t^{a_4} t^{a_3}] - \text{tr} [t^{a_1} t^{a_2} t^{a_3} t^{a_4} t^{a_5}] \right. \\ \left. + \text{tr} [t^{a_1} t^{a_2} t^{a_3} t^{a_5} t^{a_4}] - \text{tr} [t^{a_2} t^{a_1} t^{a_4} t^{a_5} t^{a_3}] + \text{tr} [t^{a_2} t^{a_1} t^{a_5} t^{a_4} t^{a_3}] \right. \\ \left. - \text{tr} [t^{a_2} t^{a_1} t^{a_3} t^{a_4} t^{a_5}] + \text{tr} [t^{a_2} t^{a_1} t^{a_3} t^{a_5} t^{a_4}] \right). \quad (3.112)$$

All remaining Feynman graphs, containing a triangle- or a box-loop, are substantially similar to those shown in the former sub-process, but with quark-currents replaced by the corresponding gluon-currents. The rewriting rules of the Appendix E for triangle- and box-diagrams provide a simple switch to the full theory. Even the pentagons can be implemented in a quite easy way, because their color structure (see Eq. (3.109) and App. F.1) can be reduced directly to the color basis of Eq. (3.108). Finally a  $24 \times 24$  symmetric color matrix  $\mathcal{RGB}_{ij}^{gg}$ , built up from the color basis, mixes all partial amplitudes and yields the squared expression of the sum of all partial amplitudes

$$\sum_{\text{color}} |\mathcal{A}^{qq}|^2 = \left(F_p^{3j}\right)^2 \sum_{i,j=1}^{24} \mathcal{RGB}_{ij}^{gg} \text{Re} \left[ \mathcal{A}_i (\mathcal{A}_j)^* \right]. \quad (3.113)$$

The entries of the matrix  $\mathcal{RGB}_{ij}^{gg}$  can be extracted directly from the corresponding sub-process, generated by *MadGraph* [31].

# Chapter 4

## Numerical implementation and checks

---

Analytic expressions for the amplitudes of the previous chapters were implemented in the Fortran program *VBFNLO* [4]. The tensor reduction of the loop contributions up to boxes is performed via Passarino-Veltman reduction [32, 33], while for the pentagons the Denner-Dittmaier algorithm [34, 35] is used, which avoids the inversion of small Gram determinants emerging in planar configurations of the Higgs and the two final state partons. The program was numerically tested in several ways. Besides usual gauge- and Lorentz-invariance tests, the different topologies were also checked separately. The contraction of a fermionic triangle-tensor  $T_{\Phi,f}^{\mu_1\mu_2}(q_1, q_2, m_f)$  with gluon momentum  $q_i^\mu$  vanishes in the case of the  $\mathcal{CP}$ -odd Higgs-boson, due to total antisymmetry of the Levi-Civita symbol and in the  $\mathcal{CP}$ -even case, since both form factors  $F_L$  and  $F_T$ , defined in Eqs. (B.8, B.9), are transversal. Hence, the Ward-identity for triangle loops is given by

$$q_1^{\mu_1} T_{\mu_1\mu_2}^{\Phi,f}(q_1, q_2, m_f) = q_2^{\mu_1} T_{\mu_1\mu_2}^{\Phi,f}(q_1, q_2, m_f) = 0 . \quad (4.1)$$

Contracting with external gluon momenta, the tensor expressions of fermionic boxes, pentagons and hexagons reduce to differences of triangles, boxes and pentagons respectively. With the tensor integrals as defined in the Appendix B, the Ward-identities for the boxes read

$$q_1^{\mu_1} B_{\mu_1\mu_2\mu_3}^{\Phi,f}(q_1, q_2, q_3, m_f) = T_{\mu_2\mu_3}^{\Phi,f}(q_{12}, q_3, m_f) - T_{\mu_2\mu_3}^{\Phi,f}(q_2, q_3, m_f) , \quad (4.2)$$

$$q_2^{\mu_2} B_{\mu_1\mu_2\mu_3}^{\Phi,f}(q_1, q_2, q_3, m_f) = T_{\mu_1\mu_3}^{\Phi,f}(q_1, q_{23}, m_f) - T_{\mu_1\mu_3}^{\Phi,f}(q_{12}, q_3, m_f) , \quad (4.3)$$

$$q_3^{\mu_3} B_{\mu_1\mu_2\mu_3}^{\Phi,f}(q_1, q_2, q_3, m_f) = T_{\mu_1\mu_2}^{\Phi,f}(q_1, q_2, m_f) - T_{\mu_1\mu_2}^{\Phi,f}(q_1, q_{23}, m_f) , \quad (4.4)$$

where the abbreviation  $q_{ij} = q_i + q_j$  has been used. Similarly, for the pentagons one finds

$$\begin{aligned} q_1^{\mu_1} P_{\mu_1\mu_2\mu_3\mu_4}^{\Phi,f}(q_1, q_2, q_3, q_4, m_f) \\ = B_{\mu_2\mu_3\mu_4}^{\Phi,f}(q_{12}, q_3, q_4, m_f) - B_{\mu_2\mu_3\mu_4}^{\Phi,f}(q_2, q_3, q_4, m_f), \end{aligned} \quad (4.5)$$

$$\begin{aligned} q_2^{\mu_2} P_{\mu_1\mu_2\mu_3\mu_4}^{\Phi,f}(q_1, q_2, q_3, q_4, m_f) \\ = B_{\mu_1\mu_3\mu_4}^{\Phi,f}(q_1, q_{23}, q_4, m_f) - B_{\mu_1\mu_3\mu_4}^{\Phi,f}(q_{12}, q_3, q_4, m_f), \end{aligned} \quad (4.6)$$

$$\begin{aligned} q_3^{\mu_3} P_{\mu_1\mu_2\mu_3\mu_4}^{\Phi,f}(q_1, q_2, q_3, q_4, m_f) \\ = B_{\mu_1\mu_2\mu_4}^{\Phi,f}(q_1, q_2, q_{34}, m_f) - B_{\mu_1\mu_2\mu_4}^{\Phi,f}(q_1, q_{23}, q_4, m_f), \end{aligned} \quad (4.7)$$

$$\begin{aligned} q_4^{\mu_4} P_{\mu_1\mu_2\mu_3\mu_4}^{\Phi,f}(q_1, q_2, q_3, q_4, m_f) \\ = B_{\mu_1\mu_2\mu_3}^{\Phi,f}(q_1, q_2, q_3, m_f) - B_{\mu_1\mu_2\mu_3}^{\Phi,f}(q_1, q_2, q_{34}, m_f). \end{aligned} \quad (4.8)$$

In the exactly same manner, one can continue with this procedure for the hexagons [36]. These identities were tested numerically and they, typically, are satisfied at least at the  $10^{-9}$  level, when using Denner-Dittmaier reduction for the tensor integrals. With decreasing number of external legs the accuracy of these identities improves.

In addition, one can perform a QED-check for the pentagons. Replacing gluons by photons and considering the process  $\gamma\gamma \rightarrow \gamma\gamma\Phi$ , diagrams with three- and four-gluon-vertices vanish, because these structures are not available in an Abelian theory. The amplitude is simply given by the sum of all pentagon graphs, without color factors. When contracting with an external gauge boson momentum, one obtains zero, since boxes are not allowed for photons, by Furry's theorem. The amplitudes pass this test as well.

Squared expressions of amplitudes with squark-contributions and the Higgs couplings to up-type and down-type squarks were checked numerically for a selection of randomly generated phase space points against the *FeynArts*, *FormCalc* [37, 38, 39] package and agreed at least at  $10^{-6}$  level. Also full cross sections of individual sub-processes in the  $\Phi jj$  production coincided within the integration error, which was below 1%.

To check the full scattering amplitudes, one can make use of the heavy-top effective Lagrangian, which is explained in more detail in App. E. As  $m_t$  becomes large, the results calculated with full fermion loops must approach the approximate ones, derived from the effective Lagrangian. This check was



performed with  $m_t = 5000$  GeV, and cross sections of the two jet processes converge towards the effective limit as expected.

The implementation of scattering amplitudes of the  $\Phi jjj$  production into the framework of *VBFNLO* was checked against MadGraph [31] within the effective limit by comparing amplitudes at individual phase space points. The comparisons for the Higgs-bosons  $H_{\text{SM}}$  and  $A$  agreed at the  $10^{-16}$  level. For large top-quark mass values,  $m_t = 5000$  GeV, the full loop contributions were checked only for sub-processes containing quark and gluons as external particles (see Eqs. (3.46) and (3.47)). As expected, the convergence towards the effective limit could also be confirmed numerically for a selection of randomly generated phase space points and fully integrated cross sections.



# Chapter 5

## Applications to LHC physics

---

### 5.1 Introduction

The numerical analysis of the  $\Phi + 2$  and  $\Phi + 3$  jet cross section was performed with the gluon fusion part *GGFLO* of the parton level Monte Carlo program *VBFNLO* [4], using the CTEQ6L1 [40] set for parton-distribution functions. In order to prevent soft or collinear divergencies in the cross sections, a minimal set of acceptance cuts has to be introduced [1]

$$p_{Tj} > 20 \text{ GeV}, \quad |\eta_j| < 4.5, \quad R_{jj} > 0.6, \quad (5.1)$$

where  $p_{Tj}$  is the transverse momentum of a final state parton and  $R_{jj}$  describes the separation of the two partons in the pseudo-rapidity  $\eta$  versus azimuthal-angle plane

$$R_{jj} = \sqrt{\Delta\eta_{jj}^2 + \phi_{jj}^2}, \quad (5.2)$$

with  $\Delta\eta_{jj} = |\eta_{j1} - \eta_{j2}|$  and  $\phi_{jj} = \phi_{j1} - \phi_{j2}$ . These cuts anticipate LHC detector capabilities and jet finding algorithms and will be called "inclusive cuts" (IC). For weak-boson fusion (WBF) studies, gluon-fusion induced processes can be suppressed by the use of an additional set of selection cuts (WBFC) [2]

$$\Delta\eta_{jj} = |\eta_{j1} - \eta_{j2}| > 4.2, \quad \eta_{j1} \cdot \eta_{j2} < 0, \quad m_{jj} > 600 \text{ GeV}. \quad (5.3)$$

The WBFC allow only well separated tagging jets, lying in opposite detector hemispheres and having large dijet invariant mass. Furthermore, a one-loop running of  $\alpha_s$  was performed with a fixed value at the  $M_Z$  scale, that is  $\alpha_s(M_Z) = 0.13$ . If not specified explicitly, for the top-quark mass the

updated value of  $m_t = 171.3$  GeV [41] is used in Yukawa couplings as well as in loops with virtual top-quarks. In the case of bottom-loops, a running Yukawa coupling is taken into account with the Higgs-mass as reference scale. Within the Higgs-mass range of 100-600 GeV, the bottom-quark mass is 33-42 % smaller than, the pole mass of 4.79 GeV [41] used in the loop propagators. The evolution of  $m_b$  up to a reference scale  $\mu$  can be expressed as

$$\overline{m}_b(\mu) = \overline{m}_b(m_b) \frac{c[\alpha_s(\mu)/\pi]}{c[\alpha_s(m_b)/\pi]}. \quad (5.4)$$

with  $\overline{m}_b(m_b) = 4.2$  GeV, as derived from the relation between pole mass and MS-bar mass. For the coefficient function  $c$  the five flavor approximation [16] is given by

$$c(x) = \left(\frac{23}{6}x\right)^{\frac{12}{23}} [1 + 1.175x + 1.501x^2 + 0.1725x^3]. \quad (5.5)$$

Unless specified otherwise, the factorization scales for two and three jet processes are set to

$$\mu_f^{2j} = \sqrt{p_{T1} p_{T2}} \quad \text{and} \quad \mu_f^{3j} = (p_{T1} p_{T2} p_{T3})^{1/3}, \quad (5.6)$$

while the renormalization scales are fixed by setting [1, 42]

$$\alpha_s^4(\mu_R) = \alpha_s(p_{T1})\alpha_s(p_{T2})\alpha_s^2(m_\Phi) \quad \text{and} \quad (5.7)$$

$$\alpha_s^5(\mu_R) = \alpha_s(p_{T1})\alpha_s(p_{T2})\alpha_s(p_{T3})\alpha_s^2(m_\Phi). \quad (5.8)$$

## 5.2 Production of the $\mathcal{CP}$ -odd Higgs boson $A$ in association with two jets

The production of the  $\mathcal{CP}$ -odd Higgs boson  $A$  in association with two jets at order  $\alpha_s^4$ , proceeds in analogy to the  $\mathcal{CP}$ -even Higgs boson  $H_{SM}$  of the SM [2, 3]. The Higgs boson  $A$  is produced via massive quark loops, for which only the third quark generation is taken into account. Here, for the top-quark mass the value of  $m_t = 172.6$  GeV is used. Furthermore, massive squark loops can be safely neglected, because these contributions sum up to zero at amplitude level (see (A.25)).

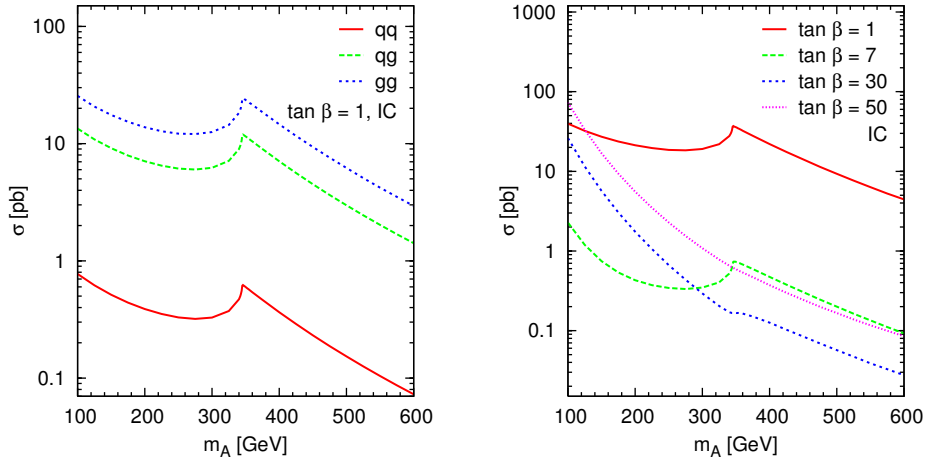


Figure 5.1:  $A + 2$  jet cross sections as a function of the Higgs boson mass. Left panel: individual contributions to the gluon-fusion process ( $gg$ ,  $qg$  and  $qq$  amplitudes) for  $\tan\beta = 1$ . Right panel: cross sections of the complete  $A + 2$  jet process for different  $\tan\beta$ . All processes include interferences of top- and bottom-quark loops. For both panels the inclusive cuts (IC) of Eq. (5.1) are applied.

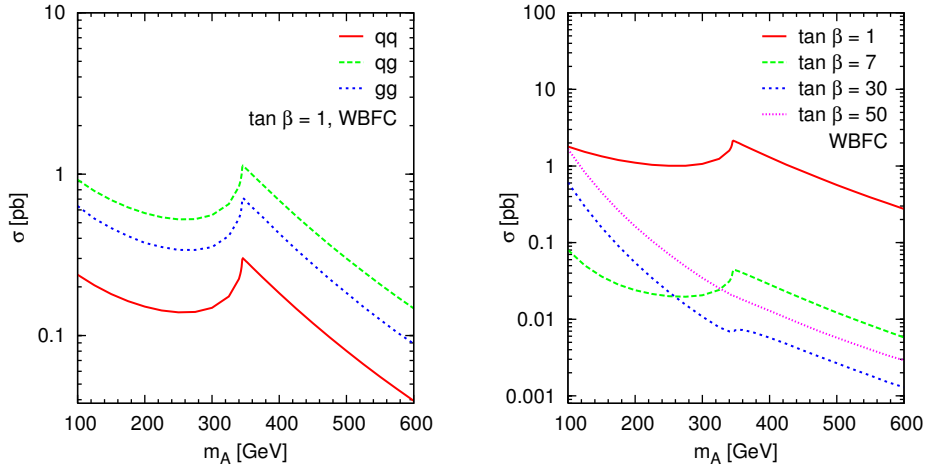


Figure 5.2:  $A + 2$  jet cross sections as functions of the Higgs boson mass but with applied WBFC set (5.3).

Expected cross sections at the LHC are shown in Fig. 5.1, as a function of the Higgs boson mass  $m_A$  within the minimal cuts of Eq. (5.1). The left

panel in Fig. 5.1 shows different cross sections of the individual contributions ( $gg$ ,  $qg$  and  $qq$  amplitudes) to the gluon fusion process with  $\tan\beta = 1$ . Cross sections for processes containing external gluons are much bigger than those induced by quark-quark contributions. The reason is an increase of the gluon-pdf at small  $x$  leading to soft events in the initial state. The mass dependence of the cross section of the complete gluon-fusion process for different  $\tan\beta$  and with top- and bottom-quark interference is given in the right panel of Fig. 5.1. For small  $\tan\beta$ , the cross section induced by a top-quark loop dominates compared to the cross section with bottom-quark loop, which is naturally suppressed by the small Yukawa coupling. The minimal cross section is obtained for  $\tan\beta \approx 7$  due to  $\mathcal{C}_t^A \approx \mathcal{C}_b^A$  (see Eq. (A.7) and (A.8)). In case of large  $\tan\beta$ , the bottom-quark contributions dominate. However, they show a much more rapid decrease of the cross section with rising  $m_A$ , since the suppression scale of loops is now set by the heavy Higgs boson mass instead of the quark mass. The striking peak arises due to threshold enhancement at  $m_H \approx 2 m_t$ , whereas for the bottom-quark loop dominated process no peak appears within this mass range. To avoid singular increase of the cross section, the threshold enhancement was smeared out by integrating over the expected Breit-Wigner peak of the Higgs. For this purpose, the width was determined by adding partial widths for  $A \rightarrow \{gg, \tau^+\tau^-, b\bar{b}, t\bar{t}\}$ . In comparison to Fig. 5.1, subprocesses with external gluons, shown in Fig. 5.2, are strongly suppressed by the WBFC set, because events with jets in the central region are cut away due to the requirement of large dijet invariant mass. Hence the over-all cross section decreases as expected.

The left side of Fig. 5.3 shows the  $\tan\beta$  dependence of the cross section for different Higgs-masses. Here, the minimum moves with increasing Higgs-mass to higher values of  $\tan\beta$ . On the one hand this behavior is correlated with the steeper fall-off of the bottom-loop dominated contributions to the cross section for large  $\tan\beta$  with increasing Higgs mass. And on the other hand, it is simply the fact, that couplings to up-type quarks are weakened and to down-type quarks enhanced by  $\tan\beta$  respectively. The presence of the  $\gamma_5$ -matrix in the analytic expression for the fermion loops leads, of course, to a new tensor structure (see Appendix B) and to a normalization of the loops, that gives rise to a  $(3/2)^2 = 2.25$  bigger cross section compared to the Standard Model [1], if  $\tan\beta = 1$ , as given in Fig. 5.3. Up to Higgs-masses

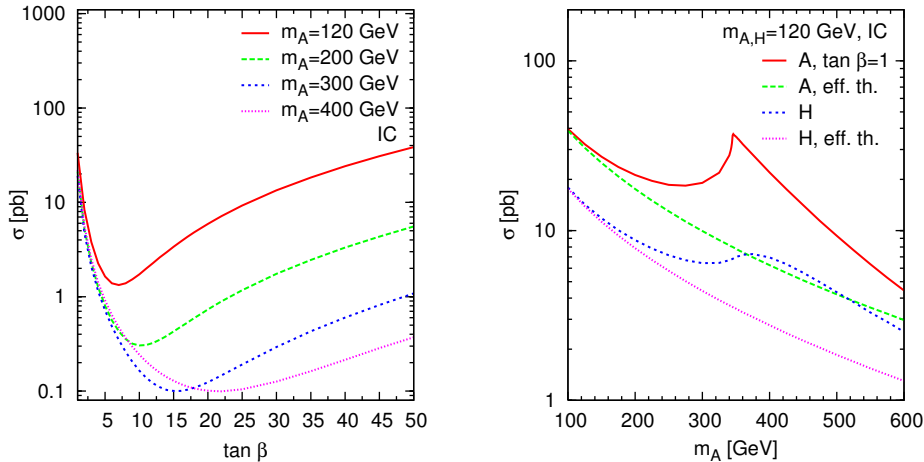


Figure 5.3: Cross section as a function of  $\tan\beta$  for different Higgs masses (left panel) and comparison of cross sections of the  $\mathcal{CP}$ -odd and  $\mathcal{CP}$ -even Higgs coupling in both loop-induced and effective theory (right panel). Here, the inclusive cuts (IC) of Eq. (5.1) were applied.

of 160 GeV and for small transverse momenta  $p_{Tj} \lesssim m_t$ , the effective Lagrangian approximation gives correct results and can be used as a numerically fast alternative for phenomenological studies. The effective Lagrangians for the  $\mathcal{CP}$ -even and  $\mathcal{CP}$ -odd Higgs bosons are described in more detail in Appendix E. Furthermore, the enhancement at threshold is more smoother in the case of the  $\mathcal{CP}$ -even Higgs boson due to the additional contributing partial widths of decays to  $W$  and  $Z$  gauge bosons. For the  $\mathcal{CP}$ -odd case, those decay modes are forbidden at tree-level and, thus, have not been considered. Effects of bottom-loop dominated  $Ajj$  production become also noticeable on the transverse momentum distributions of the accompanying jets. They are clearly visible in Figs. 5.4 and 5.5, where the transverse-momentum distributions of the softer and the harder of the two jets are shown for pseudo-scalar Higgs masses  $m_A = 120, 200$  and  $400$  GeV and  $\tan\beta = 1, 7, 30$ . For  $p_{Tj} > m_b$ , the large scale of the kinematics invariants leads to an additional suppression of the bottom induced sub-amplitudes compared to the heavy quark effective theory. Furthermore, with increasing  $\tan\beta$  both distributions fall more steeply, which means, that both tagging jets get softer. Above  $\tan\beta \approx 30$  this evolution stagnates.

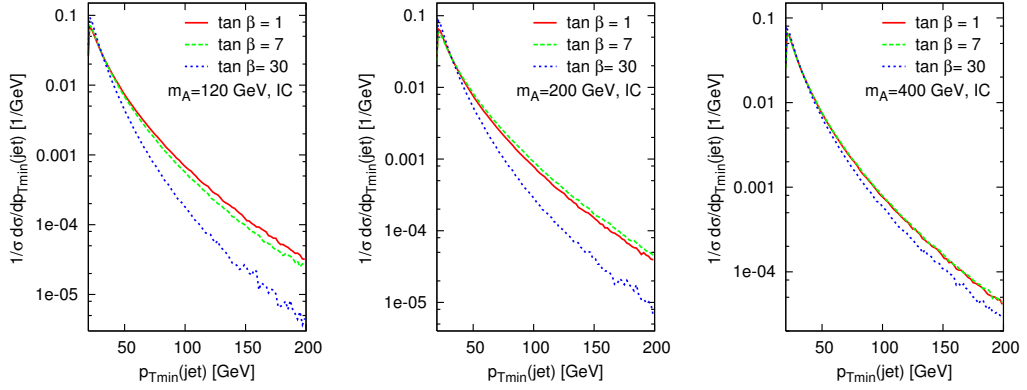


Figure 5.4: Normalized transverse-momentum distributions of the softer jet in  $Ajj$  production at the LHC, for different  $\tan\beta$  and Higgs-mass values. The inclusive selection cuts of Eq. (5.1) are applied.

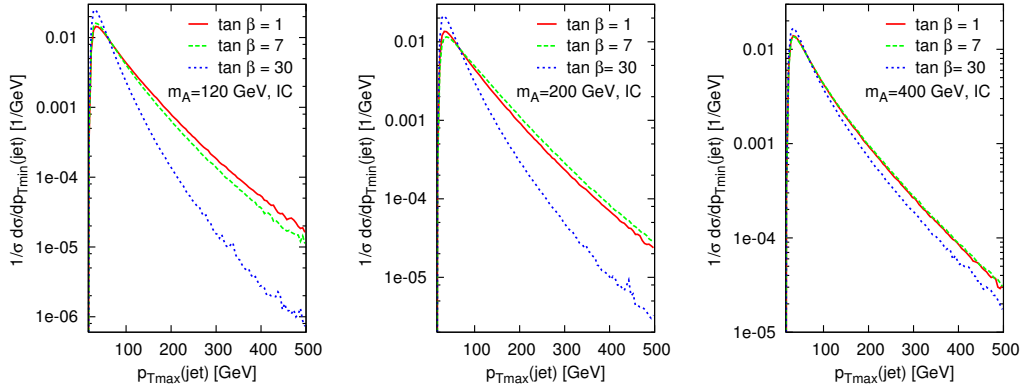


Figure 5.5: Normalized transverse-momentum distributions of the harder jet in  $Ajj$  production at the LHC, for different  $\tan\beta$  and Higgs-mass values. The inclusive selection cuts of Eq. (5.1) are applied.

The azimuthal angle distribution between the more forward and more backward of the two tagging jets provides information about the  $\mathcal{CP}$ -property of the Higgs coupling. Here, for the  $\mathcal{CP}$ -odd case the maxima of the distribution are located at  $\phi_{jj} \approx \pm 90$  degrees in contrast to the  $\mathcal{CP}$ -even coupling. A direct comparison is shown in the left panel of Fig. 5.7. The calculation



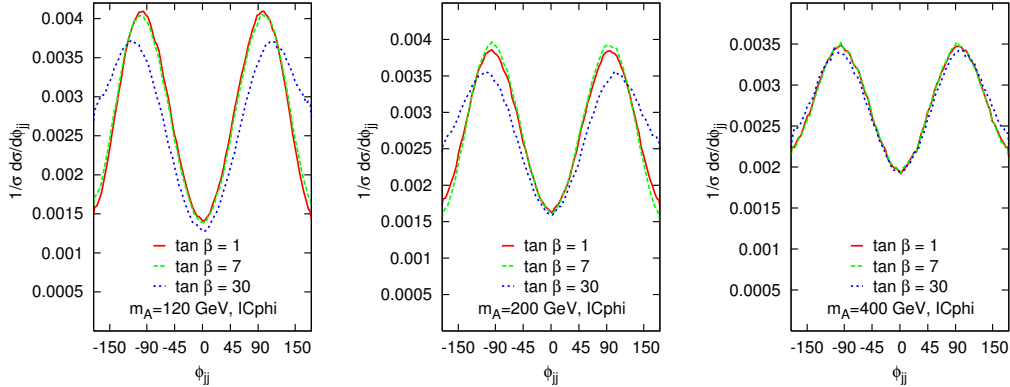


Figure 5.6: *Azimuthal-angle distributions between the two final jets of the  $\mathcal{CP}$ -odd Higgs boson for different Higgs-masses and  $\tan\beta$  values. Here, the ICphi set of Eq. (5.9) is used.*

was carried out with a modified inclusive cuts set (ICphi) [43]:

$$p_{Tj} > 30 \text{ GeV}, \quad |\eta_j| < 4.5, \quad R_{jj} > 0.6; \quad \Delta\eta_{jj} = 3. \quad (5.9)$$

The additional  $\Delta\eta_{jj}$  cut is necessary to get that distinct shape for the  $\phi_{jj}$ -distribution, which is shown in figures 5.6 and 5.7. For a relatively light pseudo-scalar Higgs boson and large  $\tan\beta$ , the softer transverse momentum distribution of the Higgs leads to kinematical distortions of the  $\phi_{jj}$  distribution: at  $\phi_{jj} \approx 0$  the Higgs recoils against two jets and hence must have  $p_{TH} > 60 \text{ GeV}$ , and this high  $p_T$ -scale leads to an additional suppression as compared to the  $\phi_{jj} \approx \pm 180$  degree case where transverse momentum balancing of the jets does allow  $p_{T,\Phi} = 0$ .

### 5.3 Production of a $\mathcal{CP}$ violating Higgs boson $\Phi$ in association with two jets

The azimuthal angle distribution for the  $\mathcal{CP}$ -even and  $\mathcal{CP}$ -odd Higgs bosons were investigated at first in the context of effective theories [44]. As mentioned already in the previous chapter, both distributions are clearly distinguishable by the position of the extreme values. Furthermore, it is interesting to investigate models with  $\mathcal{CP}$ -violating Higgs sector and see the impact of

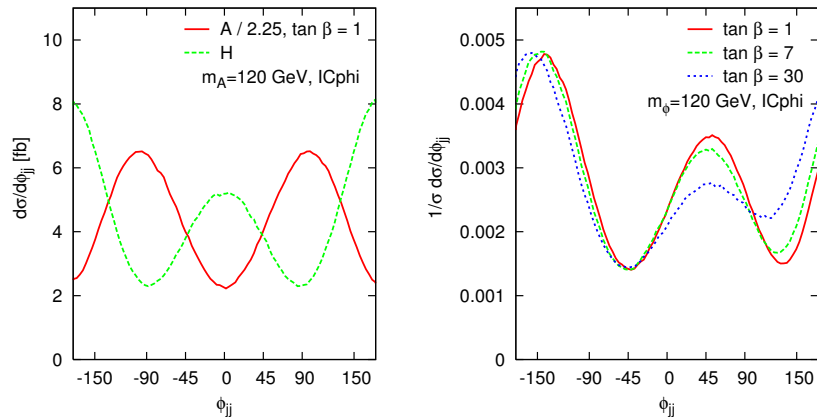


Figure 5.7: *The azimuthal-angle distribution of the  $\mathcal{CP}$ -odd and  $\mathcal{CP}$ -even coupling (left panel). Interference pattern within a toy model with  $\mathcal{CP}$ -violating Higgs-sector for different  $\tan \beta$  (right panel). The  $\mathcal{CP}$ -odd coupling was adjusted to the  $\mathcal{CP}$ -even one by a factor of  $2/3$ . Here, the ICphi set (5.9) was used.*

$\mathcal{CP}$ -effects on the azimuthal angle distribution. Such effects can appear e.g. in the cMSSM, where complex phases and loop effects cause mixing of scalar and pseudo-scalar Higgs bosons to new  $\mathcal{CP}$ -eigenstates. But these analyses are quite involved and lie beyond the scope of this work. Unfortunately the original azimuthal angle variable, defined by

$$\cos \phi_{jj} = \frac{\vec{p}_{Tj_1} \cdot \vec{p}_{Tj_2}}{|\vec{p}_{Tj_1}| |\vec{p}_{Tj_2}|}, \quad (5.10)$$

is not sensitive to these effects and would give a flat distribution corresponding to that one of the electro-weak boson fusion [45]. A redefinition of the azimuthal angle variable was introduced in Refs. [43, 46]. To mimic  $\mathcal{CP}$  violation in the Higgs sector, one can combine simply the  $\mathcal{CP}$ -even and  $\mathcal{CP}$ -odd Yukawa couplings together

$$\mathcal{Y}_\Phi = \frac{y_q m_q}{v} (iC_H + C_A \gamma_5) \quad \text{with} \quad y_u = \cot \beta, y_d = \tan \beta \quad (5.11)$$

and investigate the impact on the azimuthal angle distribution. The scaling factor  $y_q$  allows to change the strength of the new coupling to up-type and down-type quarks with  $\tan \beta$ , similar to the case of the  $A$  boson. The parameters  $C_A$  and  $C_H$  denote the magnitudes of the  $\mathcal{CP}$ -odd and  $\mathcal{CP}$ -even coupling

respectively. Depending on the value of these parameters, the azimuthal-angle distribution moves between these curves and characterizes the grade of  $\mathcal{CP}$ -violation. An example, which also includes interference effects between bottom- and top-quark loops, is shown for different  $\tan\beta$  in the right panel of Fig. 5.7. The value of  $C_A$  was fixed at  $C_A = 2/3$  to yield equal strengths for both Higgs-couplings. However, there are additional distortions of the azimuthal angle distributions, which can again be explained by kinematical effects due to transverse momentum balancing of the two jets and the Higgs boson.

## 5.4 Production of the $\mathcal{CP}$ -even Higgs bosons $h$ and $H$ in association with two jets with additional squark contributions

Numerical investigation of the  $\mathcal{CP}$ -even  $H_{\text{SM}}$  within the SM was already performed in Ref. [2]. For the contributing subprocesses, only contributions mediated by top-quark loops were taken into account. Loops with bottom-quarks were neglected, because of the missing enhancement of the Yukawa coupling by further model parameters, like  $\tan\beta$ , e.g. in a general 2HDM or the MSSM. As already mentioned, the two Higgs-doublet structure of the MSSM provides two  $\mathcal{CP}$ -even Higgs bosons with different masses, but with the same tensor structure corresponding to that of the SM Higgs boson  $H_{\text{SM}}$ . However, their Yukawa couplings to up-type and down-type quarks are modified by additional factors containing the mixing angle  $\alpha$  of the neutral components of both Higgs-doublets and the angle  $\beta$  coming from the ratio of the two vacuum expectation values  $v_1$  and  $v_2$ . This means, that contributions mediated by bottom-quark loops can gain sizeable enhancement. Furthermore, all massive supersymmetric partners of the SM particles can couple to the Higgs bosons and, hence, give further contributions. The new couplings involve additional model parameters, like the trilinear couplings  $A^t$ ,  $A^b$  and supersymmetric Higgs-mass parameter  $\mu$ , whose values are restricted by given experimental exclusion limits [41]. Here, in this analysis only contributions with squarks of the third generation are taken into account. This third generation of squarks is somewhat special, due to the

non-negligible masses of their fermion partners. The off-diagonal L-R mixing terms (see chapter 2.3) in the squark mass matrix are large, because of their proportionality to  $m_b$  or  $m_t$ . They provide a large splitting, especially in the stop case. The bottom and top squarks manifest themselves physically as the mass eigenstates  $\tilde{b}_{1,2}$  and  $\tilde{t}_{1,2}$ . This makes  $\tilde{t}_1$  the lightest squark and hence interesting for the analysis. The calculation of squark mixing angles  $\theta_{\tilde{q}}$  is explained briefly in chapter 2.3. A further property of supersymmetry is, that contributions with SM-like particles are canceled by contributions containing supersymmetric partners, which carry opposite sign factors. This effect is investigated below in more detail for the light Higgs boson  $h$  and heavy Higgs boson  $H$ . The evaluation was done using the following values as input parameters:

$A^t$ [GeV]	$A^b$ [GeV]	$\mu$ [GeV]	$m_A$ [GeV]
1000	1500	150	200

Based on the statement, that the top squark is possibly the lightest squark, the  $\tilde{t}_1$ -mass was chosen as the scan parameter for the analysis. All other masses of the remaining top and bottom squarks were calculated with the *FeynArts*, *FormCalc* [37, 38, 39] package using the input parameters mentioned above. Depending on the values for the squark masses and the parameter  $\tan\beta$ , loop corrected masses for the Higgs bosons  $h$  and  $H$  were calculated with the help of *FeynHiggs* [47, 48, 49, 50]. The masses of both Higgs bosons alter very slightly, although the contributions mediated by squark-loops change continuously during the scanning procedure. They are shown in Fig. 5.8. Hence, only marginal changes of the cross section are expected over the whole scanning range. The mass  $m_h \approx 102$  GeV is excluded by experiment and is used only for the purpose of illustration. The final evaluation was done with the gluon fusion part *GGFLO* of the *VBFNLO* program. Expected cross sections for the production of the light and the heavy Higgs bosons are shown in Fig. 5.9 as a function of the  $\tilde{t}_1$ -mass for different values of  $\tan\beta$  within the minimal cuts of Eq. (5.1).

For the light Higgs boson  $h$ , one can see very clearly the expected impact of the contributions mediated by squark-loops (left panel of Fig. 5.9). In the range between 180-400 GeV the cross section is strongly suppressed as a

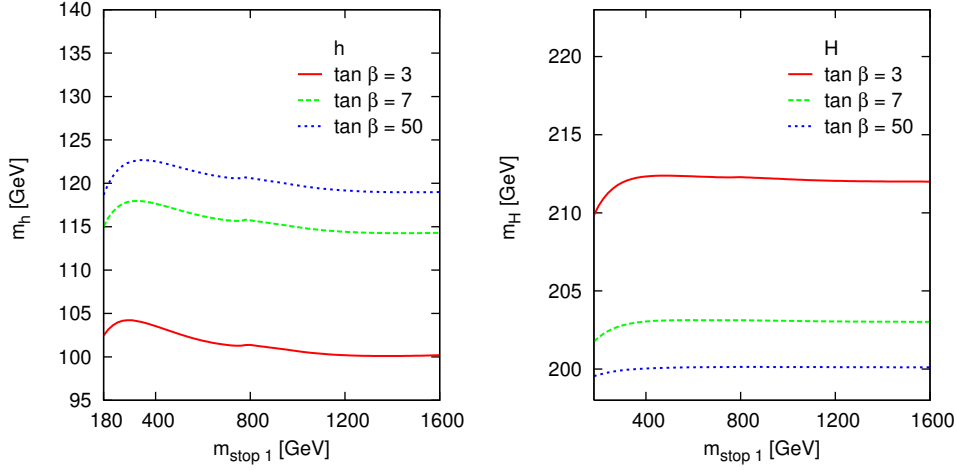


Figure 5.8: Loop-corrected Higgs masses of  $h$  and  $H$  as a function of the  $\tilde{t}_1$ -mass for different values of  $\tan\beta$ .

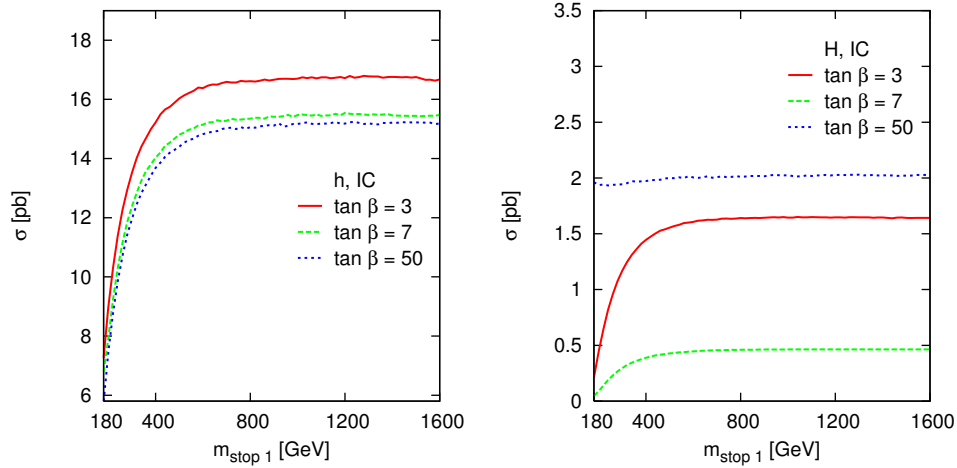


Figure 5.9: Full cross section with  $t$  and  $b$  quark as well as  $\tilde{t}_{1,2}$  and  $\tilde{b}_{1,2}$  squark contributions as a function of  $\tilde{t}_1$ -mass for different values of  $\tan\beta$  and Higgs-masses shown in Fig. 5.8. For both panels the inclusive cuts (IC) of Eq. (5.1) were applied.

result of strong cancellations between SM-like particle and SUSY-like particles. For masses beyond 600 GeV, the scalar loops decouple or rather become negligible and the evolution of the cross section stagnates with contributions

mediated only by top- and bottom-quarks. To get a feeling for the influence of  $\tan\beta$  on the Yukawa and scalar couplings, the cross sections of individual loop-contributions and the full result including interference effects of all amplitudes are shown in the upper table 5.1 for a  $\tilde{t}_1$ -mass of 180 GeV, which corresponds to the first parameter set of Fig. 5.9:

$\sigma(h)$ [fb]							
$\tan\beta$	$t$	$b$	$\tilde{t}_1$	$\tilde{t}_2$	$\tilde{b}_1$	$\tilde{b}_2$	$\Sigma+\text{int.}$
3	16058,2	20,8	2717,5	89,7	0.5	$2,9 \cdot 10^{-2}$	7263.2
7	15135,1	17,1	2964,6	84,4	0.5	$1,0 \cdot 10^{-3}$	6242.1
50	15092,2	16,4	3236,9	84,0	1,9	1,2	5746.4
$\sigma(H)$ [fb]							
3	1585,8	5,4	919,3	13,8	0,3	0,9	213.2
7	385,7	36,5	413,0	4,8	1,9	2,5	46.7
50	8,3	1980,7	140,5	1.0	117,7	229,3	1963.5

Table 5.1: *Cross sections of the light Higgs  $h$  (top) and heavy Higgs  $H$  (bottom) ordered by individual contributions with different loop-masses and values of  $\tan\beta$ . Total cross sections contain interference effects of all amplitudes. The inclusive selection cuts of Eq. (5.1) were applied.*

With increasing  $\tan\beta$ , only contributions induced by  $\tilde{b}_2$ -loop gain an appreciable enhancement. Furthermore, loops with  $\tilde{t}_1$  provide the biggest contribution in the squark-sector up to high values of  $\tan\beta$ , because of their relative small mass. However, the influence of  $\tan\beta$  is quite slight. Also the contribution of  $\tilde{t}_2$  remains almost constant and yields a small cross section, which is an effect of the bigger loop-mass. Amplitudes with top- and bottom quarks hardly get modifications, because the ratio of the trigonometric functions depending on  $\alpha$  and  $\beta$  inside the Yukawa couplings (see App. A.1)

stay, roughly speaking, in equilibrium, a sign of  $h$  decoupling at large  $m_A$ . Similar evolution of the cross sections for the heavy Higgs boson  $H$  is found in the right panel of Fig. 5.9, except for high values of  $\tan\beta$ . Generally, the cross section for the  $Hjj$  production turns out to be smaller in comparison to the light Higgs boson  $h$ . Namely it gets additional suppression due to the bigger mass. The cross sections show an equal behavior for masses beyond 600 GeV, where contributions with squarks get strongly suppressed independently of  $\tan\beta$  by rising squark-masses in the loop-propagators. To get a better understanding of the behavior of the cross section for  $\tan\beta = 50$ , values of  $\sigma$  for the first parameter set corresponding to the  $\tilde{t}_1$ -mass of 180 GeV and for different  $\tan\beta$  are shown in the lower table 5.1. Here, contributions with top-quarks are strongly suppressed in contrast to contribution mediated by bottom-quark loops for raising values of  $\tan\beta$ . This behavior is similar to that of the  $\mathcal{CP}$ -odd Higgs boson  $A$ . The same happens for up-type and down-type squarks. For high values of  $\tan\beta$ , amplitudes with bottom-loops dominate, however, contributions induced by all squark-loops are still too small to compensate the contribution given by the quark-loops.

The result is an almost flat distribution over the whole  $\tilde{t}_1$ -mass range. By the way, full cross sections show also a distinct minimum for  $\tan\beta = 7$ .

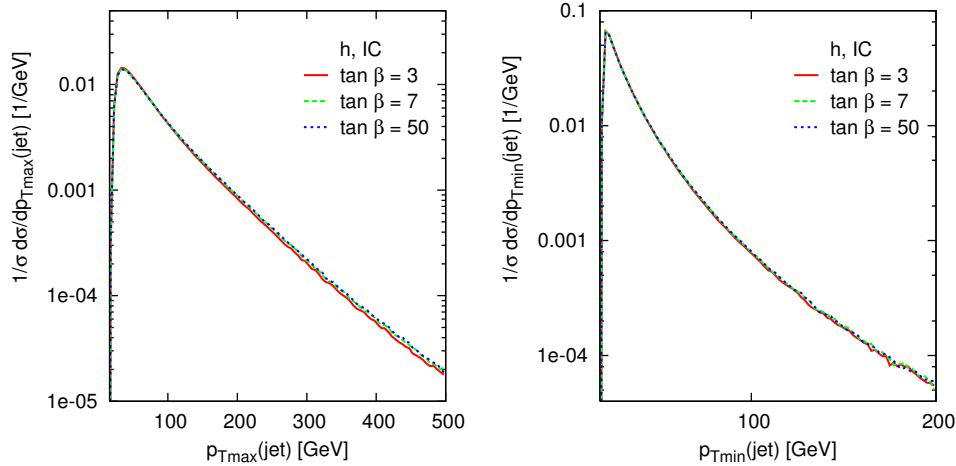


Figure 5.10: Normalized transverse-momentum distributions of the harder and softer jet in  $h,jj$  production at the LHC, for different  $\tan\beta$  and Higgs-masses shown in Fig. 5.8.

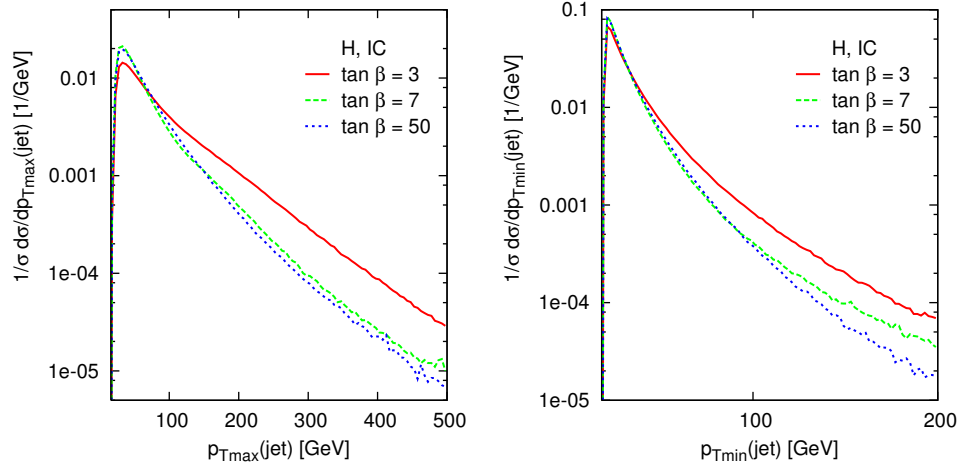


Figure 5.11: *Normalized transverse-momentum distributions of the harder and softer jet in  $Hjj$  production at the LHC, for different  $\tan\beta$  and Higgs-masses shown in Fig. 5.8.*

The reasons for this minimum are already small contributions provided by quark-loops and further suppression by amplitudes with squark-loops. Complementary to the table 5.1, distributions for the transverse momenta of the accompanying jets and azimuthal angle are shown in Figs. 5.10, 5.11 and Fig. 5.12 respectively. The almost equal shapes for the production of the light Higgs boson  $h$  with fermionic and sfermionic contributions for different  $\tan\beta$  confirm the fact, that there is no significant influence of the parameter  $\tan\beta$ . On the contrary, the heavy Higgs boson  $H$  is much more sensitive to  $\tan\beta$  and shows a similar behavior as the  $\mathcal{CP}$ -odd Higgs boson  $A$ . With increasing values of  $\tan\beta$ , the transverse momentum distribution of the softer and the harder of the two jets fall more steeply. Furthermore, the softer transverse momentum distributions of  $H$  leads also to kinematical distortion of the azimuthal angle distribution, which is here very clearly visible at  $\phi_{jj} \approx \pm 90$ . One has to keep in mind, that contributions of sfermionic loops provide an additional suppression of the cross section, which becomes noticeable on the behavior of the  $\phi_{jj}$ -distribution for  $\tan\beta = 7$  in comparison to the Higgs boson  $A$ .



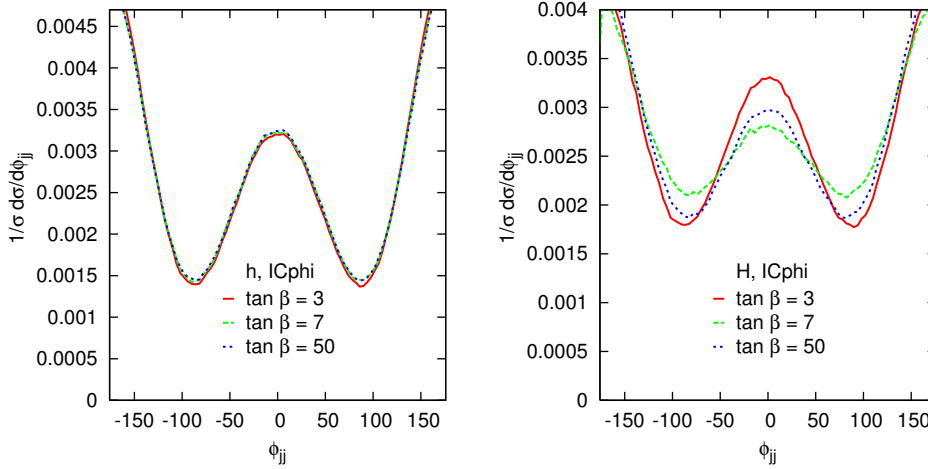


Figure 5.12: *Azimuthal-angle distributions between the two final jets of the  $\mathcal{CP}$ -even Higgs bosons  $h$  and  $H$  for different  $\tan\beta$  and Higgs-masses shown in Fig. 5.8. Here the ICphi set is used.*

## 5.5 Production of the Higgs bosons $\Phi$ in association with three jets

As already discussed in the previous chapters, the azimuthal angle correlation  $\phi_{jj}$  between the accompanying jets is a sensitive measure of the tensor structure for the Higgs couplings to electro-weak bosons or gluons. Especially in the case of Higgs boson production via gluon fusion, characteristic shapes of the  $\phi_{jj}$ -distribution for  $\mathcal{CP}$ -even and  $\mathcal{CP}$ -odd Higgs couplings, shown in Fig. 5.7, allow to discriminate between the SM or extensions e.g. the MSSM. A further aspect of interest is the modification of the azimuthal angle correlation by the emission of additional gluons. Former investigations with showering and hadronisation provided a strong de-correlation between the tagging jets in Higgs +2 jet production [51]. The de-correlation effects, however, were disproportionately illustrated due to approximations in the parton-shower. More recent analyses [52, 53] show, that after separation of hard radiation and showering effects with subsequent hadronisation, the  $\phi_{jj}$ -correlation survives with minimal modifications. Similar results were obtained by a parton level calculation with NLO corrections [21] to the  $Hjj$  process in the framework of the effective Lagrangian.

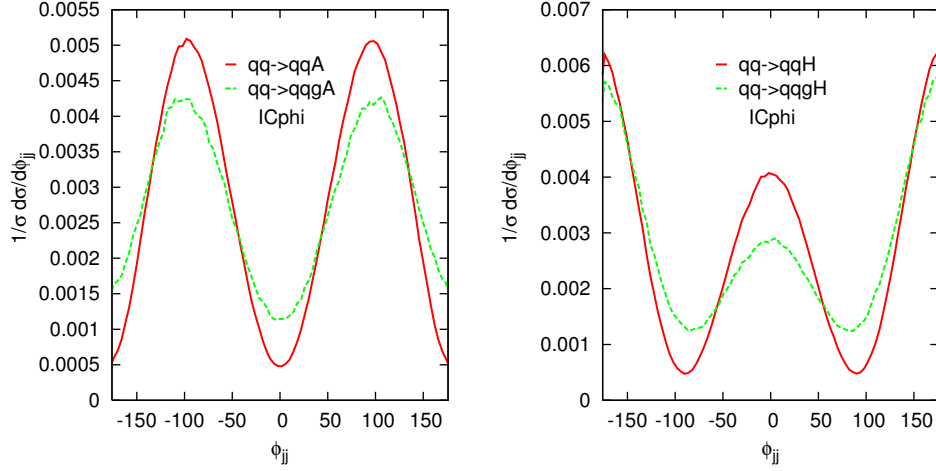


Figure 5.13: *Normalized azimuthal-angle distributions for the production of the  $\mathcal{CP}$ -odd and  $\mathcal{CP}$ -even Higgs bosons in the sub-processes  $qq \rightarrow qq\Phi$ ,  $qq \rightarrow qqg\Phi$  and crossing related sub-processes. The ICphi set of Eq. (5.9) is used.*

The calculation and implementation of the process  $\Phi jjj$  with full massive loops, introduced in chapter 3.4, allows also among other things, the investigation of de-correlation effects beyond present frameworks, which only use the effective Lagrangian approach.

As a primal result, the azimuthal-angle distributions of the processes  $qq \rightarrow qq\Phi$  and  $qq \rightarrow qqg\Phi$  with  $\Phi = H_{\text{SM}}, A$  are shown in Fig. 5.13 for the modified inclusive cuts of Eq. (5.9). Furthermore, crossing related sub-processes were also taken into account (see also Eq. (3.46)). All processes contain top-quark triangle loops and the three jet process even additional Feynman diagrams with box-loop insertions. In order to simplify matters, the value of  $\tan \beta = 1$  is taken in the coupling of the  $\mathcal{CP}$ -odd Higgs boson  $A$ .

Both  $\phi_{jj}$  distributions confirm de-correlation effects, when the process  $\Phi jj$  is extended by a further jet. One can see, that the dips at  $\phi_{jj} \approx 0$  for the  $\mathcal{CP}$ -odd  $A$  and  $\phi_{jj} \approx \pm\pi/2$  for the  $\mathcal{CP}$ -even  $H_{\text{SM}}$  are shallower than in the corresponding process with two jets. But these first results have to be handled with care, because they show contributions, which only represent a small fraction of the total process. The additional sub-processes  $qq \rightarrow qqg\Phi$ ,  $gg \rightarrow ggg\Phi$  and crossing related sub-processes, that are expected to give the

main contributions, however, could not be taken into account. The amplitudes of these contributions contain pentagons and even hexagons and make the numerical analysis quite involved. Due to the extended phase-space in the three jet process, and hence, increased amount of possible invariants entering the tensor reduction, numerical instabilities appeared at the level of five-point functions from rank two up to four. They deformed different distributions, which are the subjects of this investigation, and made the analysis impossible. A further analysis of the involved phase-space regions is necessary to have a better control over the numerical evolution of the five-point functions, that are also important as input for the six-point functions. Also further comparisons with the two-jet processes have to be performed, because the numerical evaluation of these processes caused no problems, although all versions of five-point functions up to rank four were applied. The produced results were already shown in the analysis chapters for the Higgs production processes with two jets, using at least  $2^{24}$  randomly generated phase-space points.



# Chapter 6

## Conclusions

---

Searching for the Higgs boson within the framework of the Standard Model and its supersymmetric extensions is one of the main tasks of the LHC. The two main sources of Higgs plus two jet events are weak-boson fusion and gluon fusion. Hence, a precise description of both processes is needed, in order to separate them from each other. This thesis presents the calculation of scattering amplitudes for the production of neutral Higgs bosons within the MSSM via gluon fusion with a two and three jet final state. The scattering amplitudes for these processes are induced by triangle-, box-, pentagon- and hexagon-loop diagrams at leading order. In this connection analytical expressions of loop-topologies were evaluated for scalar and fermionic particles as well as for  $\mathcal{CP}$ -odd and  $\mathcal{CP}$ -even Higgs couplings. The tensor reduction for triangle- and box-loops was performed via Passarino-Veltman reduction, while for the pentagons and hexagons the Denner-Dittmaier algorithm was applied to obtain numerically stable results. In the first part of Chapter 3, a detailed description of the analytical expressions of  $\phi jj$  scattering amplitudes for sub-processes  $qq \rightarrow qq\phi$ ,  $qg \rightarrow qq\phi$ ,  $gg \rightarrow gg\phi$  and crossing related sub-processes was presented. The second part of Chapter 3 described in a detailed way the calculation of scattering amplitudes for a Higgs plus three-jet final state. Chapter 4 was devoted to a brief description of analytical and numerical consistency checks of the calculation and implementation into the Monte Carlo program *VBFNLO*. In Chapter 5 fully integrated cross sections of the  $Ajj$  production with interference effects between top- and bottom-loops were compared for different values of  $\tan\beta$  and masses  $m_A$  of the  $\mathcal{CP}$ -odd Higgs boson. Furthermore, it was shown, that small quark masses in the bottom-loops provide a softening effect on the transverse momentum distribution of the accompanying jets, which cannot be described

within the framework of the effective Lagrangian. Distortion effects were also observed in the azimuthal angle correlation of both jets in the bottom-loop dominated  $Ajj$  production. Moreover, a pronounced difference between  $Ajj$  and  $Hjj$  production in the azimuthal angle distribution between the two jets could also be observed. This effect provides the possibility to determine the  $\mathcal{CP}$ -properties of the produced Higgs boson at the LHC. In addition to that, effects of  $\mathcal{CP}$ -violating couplings were simulated, which allow to investigate scenarios with a  $\mathcal{CP}$ -violating Higgs sector. Furthermore, interference effects of contributions containing squark- and quark-loops in the production of the  $\mathcal{CP}$ -even Higgs bosons  $h$  and  $H$  plus two jets were investigated. Performed scans for a set of MSSM-parameters confirmed the expected cancellations between the sfermionic and fermionic contributions, which resulted in a strong reduction of the integrated cross sections. Based thereupon, effects of different values of  $\tan\beta$ , especially for the heavy Higgs boson  $H$ , on azimuthal angle and transverse momentum distributions could be illustrated. Finally, preliminary results of the  $\phi jjj$  implementation were presented for a small set of sub-processes. Here, de-correlation effects of the two-jet azimuthal angle distribution were presented, which were an effect of the third jet produced by the additional gluon in the final state.

# Appendix A

## Higgs vertices to fermions and sfermions

---

### A.1 Higgs couplings to fermions

The Lagrangian for Higgs-fermion Yukawa interactions has the following form

$$\mathcal{L}_Y = \sum_{\phi=h,H,A} \sum_{f=u,d} \mathcal{C}_f^\phi \bar{F}_f F_f \phi, \quad (\text{A.1})$$

in which the corresponding factors  $\mathcal{C}_f^\phi$  are given by

**[ $H_{SM}, \mathcal{CP}$ -even]** :

$$\mathcal{C}_{u,d}^{\text{SM}} = i \frac{m_f}{v} \quad (\text{A.2})$$

**[ $h, \mathcal{CP}$ -even, u-type]** :

$$\mathcal{C}_u^h = i \frac{m_u \cos \alpha}{v \sin \beta} \quad (\text{A.3})$$

**[ $h, \mathcal{CP}$ -even, d-type]** :

$$\mathcal{C}_d^h = -i \frac{m_d \sin \alpha}{v \cos \beta} \quad (\text{A.4})$$

**[ $H, \mathcal{CP}$ -even, u-type]** :

$$\mathcal{C}_u^H = i \frac{m_u \sin \alpha}{v \sin \beta} \quad (\text{A.5})$$

[**H**, **CP**-even, **d-type**] :

$$\mathcal{C}_d^H = -i \frac{m_d \cos \alpha}{v \cos \beta} \quad (\text{A.6})$$

[**A**, **CP**-odd, **u-type**] :

$$\mathcal{C}_u^A = -\frac{m_u}{v} \cot \beta \gamma_5 \quad (\text{A.7})$$

[**A**, **CP**-odd, **d-type**] :

$$\mathcal{C}_d^A = -\frac{m_d}{v} \tan \beta \gamma_5 \quad (\text{A.8})$$



## A.2 Higgs couplings to sfermions

General expressions for the couplings of neutral Higgs bosons to squarks can be looked up in Ref. [10]. Assuming no flavor mixing, these expressions were evaluated using parameters of the MSSM. Furthermore, abbreviations are introduced for expressions containing the mixing angle  $\alpha$  between the neutral components of both Higgs doublets,  $\beta$  coming from the ratio of the two vacuum expectations values, the electro-weak mixing angle  $\theta_W$  and squark mixing angles  $\theta_{\tilde{f}}$ :

$$\begin{aligned} s_{\{\alpha,\beta\}} &= \sin\{\alpha,\beta\} , & c_{\{\alpha,\beta\}} &= \cos\{\alpha,\beta\} , & t_W &= \tan \theta_W , \\ s_{\alpha+\beta} &= \sin(\alpha + \beta) , & c_{\alpha+\beta} &= \cos(\alpha + \beta) , \\ s_{\theta_{\tilde{f}}} &= \sin \theta_{\tilde{f}} , & c_{\theta_{\tilde{f}}} &= \cos \theta_{\tilde{f}} . \end{aligned}$$

The Lagrangian for Higgs-sfermion interactions can be written as

$$\mathcal{L}_{\phi \tilde{f}} = \sum_{\phi=h,H,A} \sum_{\tilde{f}=\tilde{u}_i,\tilde{d}_j} \mathcal{C}_{\tilde{f}_i}^{\phi} \phi \tilde{f}_i^* \tilde{f}_i ,$$

in which the corresponding factors  $\mathcal{C}_{\tilde{f}_i}^{\phi}$  are given by

**[h, CP-even, u-type, 1] :**

$$\begin{aligned} \mathcal{C}_{\tilde{u}_1}^h &= \frac{2}{v s_{\beta}} \left[ \left( c_{\theta_{\tilde{u}}} s_{\theta_{\tilde{u}}} m_u A^u - m_u^2 \right) c_{\alpha} - m_u \mu c_{\theta_{\tilde{u}}} s_{\theta_{\tilde{u}}} s_{\alpha} \right] \\ &+ \frac{M_W^2}{v} \left[ c_{\theta_{\tilde{u}}}^2 \left( 1 - \frac{1}{3} t_W^2 \right) + \frac{4}{3} s_{\theta_{\tilde{u}}}^2 t_W^2 \right] s_{\alpha+\beta} \end{aligned} \quad (\text{A.9})$$

**[h, CP-even, u-type, 2] :**

$$\begin{aligned} \mathcal{C}_{\tilde{u}_2}^h &= -\frac{2}{v s_{\beta}} \left[ \left( c_{\theta_{\tilde{u}}} s_{\theta_{\tilde{u}}} \tilde{m}_u A^u + m_u^2 \right) c_{\alpha} - m_u \mu c_{\theta_{\tilde{u}}} s_{\theta_{\tilde{u}}} s_{\alpha} \right] \\ &+ \frac{M_W^2}{v} \left[ s_{\theta_{\tilde{u}}}^2 \left( 1 - \frac{1}{3} t_W^2 \right) + \frac{4}{3} c_{\theta_{\tilde{u}}}^2 t_W^2 \right] s_{\alpha+\beta} \end{aligned} \quad (\text{A.10})$$

**[h, CP-even, u-type, L] :**

$$\mathcal{C}_{\tilde{u}_L}^h = \frac{2}{v s_{\beta}} m_u^2 c_{\alpha} + \frac{M_W^2}{v} \left( 1 - \frac{1}{3} t_W^2 \right) s_{\alpha+\beta} \quad (\text{A.11})$$

$[\mathbf{h}, \mathcal{CP}\text{-even, u-type, R}] :$

$$\mathcal{C}_{\bar{u}_R}^h = \frac{2}{vs_\beta} m_u^2 c_\alpha + \frac{M_W^2}{v} \frac{4}{3} t_W^2 s_{\alpha+\beta} \quad (\text{A.12})$$

$[\mathbf{H}, \mathcal{CP}\text{-even, u-type, 1}] :$

$$\begin{aligned} \mathcal{C}_{\bar{u}_1}^H &= \frac{2}{vs_\beta} \left[ \left( c_{\theta_{\bar{u}}} s_{\theta_{\bar{u}}} m_u A^u - m_u^2 \right) s_\alpha + m_u \mu c_{\theta_{\bar{u}}} s_{\theta_{\bar{u}}} c_\alpha \right] \\ &\quad - \frac{M_W^2}{v} \left[ c_{\theta_{\bar{u}}}^2 \left( 1 - \frac{1}{3} t_W^2 \right) + \frac{4}{3} s_{\theta_{\bar{u}}}^2 t_W^2 \right] c_{\alpha+\beta} \end{aligned} \quad (\text{A.13})$$

$[\mathbf{H}, \mathcal{CP}\text{-even, u-type, 2}] :$

$$\begin{aligned} \mathcal{C}_{\bar{u}_2}^H &= -\frac{2}{vs_\beta} \left[ \left( c_{\theta_{\bar{u}}} s_{\theta_{\bar{u}}} m_u A^u + m_u^2 \right) s_\alpha + m_u \mu c_{\theta_{\bar{u}}} s_{\theta_{\bar{u}}} c_\alpha \right] \\ &\quad - \frac{M_W^2}{v} \left[ s_{\theta_{\bar{u}}}^2 \left( 1 - \frac{1}{3} t_W^2 \right) + \frac{4}{3} c_{\theta_{\bar{u}}}^2 t_W^2 \right] c_{\alpha+\beta} \end{aligned} \quad (\text{A.14})$$

$[\mathbf{H}, \mathcal{CP}\text{-even, u-type, L}] :$

$$\mathcal{C}_{\bar{u}_L}^H = -\frac{2}{vs_\beta} m_u^2 s_\alpha - \frac{M_W^2}{v} \left( 1 - \frac{1}{3} t_W^2 \right) c_{\alpha+\beta} \quad (\text{A.15})$$

$[\mathbf{H}, \mathcal{CP}\text{-even, u-type, R}] :$

$$\mathcal{C}_{\bar{u}_R}^H = -\frac{2}{vs_\beta} m_u^2 s_\alpha - \frac{M_W^2}{v} \frac{4}{3} t_W^2 c_{\alpha+\beta} \quad (\text{A.16})$$

$[\mathbf{h}, \mathcal{CP}\text{-even, d-type, 1}] :$

$$\begin{aligned} \mathcal{C}_{\bar{d}_1}^h &= -\frac{2}{vc_\beta} \left[ \left( c_{\theta_{\bar{d}}} s_{\theta_{\bar{d}}} m_d A^d - m_d^2 \right) s_\alpha - m_d \mu c_{\theta_{\bar{d}}} s_{\theta_{\bar{d}}} c_\alpha \right] \\ &\quad - \frac{M_W^2}{v} \left[ c_{\theta_{\bar{d}}}^2 \left( 1 + \frac{1}{3} t_W^2 \right) + \frac{2}{3} s_{\theta_{\bar{d}}}^2 t_W^2 \right] s_{\alpha+\beta} \end{aligned} \quad (\text{A.17})$$

$[\mathbf{h}, \mathcal{CP}\text{-even, d-type, 2}] :$

$$\begin{aligned} \mathcal{C}_{\bar{d}_2}^h &= \frac{2}{vc_\beta} \left[ \left( c_{\theta_{\bar{d}}} s_{\theta_{\bar{d}}} m_d A^d + m_d^2 \right) s_\alpha - m_d \mu c_{\theta_{\bar{d}}} s_{\theta_{\bar{d}}} c_\alpha \right] \\ &\quad - \frac{M_W^2}{v} \left[ s_{\theta_{\bar{d}}}^2 \left( 1 + \frac{1}{3} t_W^2 \right) + \frac{2}{3} c_{\theta_{\bar{d}}}^2 t_W^2 \right] s_{\alpha+\beta} \end{aligned} \quad (\text{A.18})$$

**[h, CP-even, d-type, L] :**

$$\mathcal{C}_{\tilde{d}_L}^h = \frac{2}{vc_\beta} m_d^2 s_\alpha - \frac{M_W^2}{v} \left(1 + \frac{1}{3} t_W^2\right) s_{\alpha+\beta} \quad (\text{A.19})$$

**[h, CP-even, d-type, R] :**

$$\mathcal{C}_{\tilde{d}_R}^h = \frac{2}{vc_\beta} m_d^2 s_\alpha - \frac{M_W^2}{v} \frac{2}{3} t_W^2 s_{\alpha+\beta} \quad (\text{A.20})$$

**[H, CP-even, d-type, 1] :**

$$\begin{aligned} \mathcal{C}_{\tilde{d}_1}^H &= \frac{2}{vc_\beta} \left[ \left( c_{\theta_{\tilde{d}}} s_{\theta_{\tilde{d}}} m_d A^d - m_d^2 \right) c_\alpha + m_d \mu c_{\theta_{\tilde{d}}} s_{\theta_{\tilde{d}}} s_\alpha \right] \\ &+ \frac{M_W^2}{v} \left[ c_{\theta_{\tilde{d}}}^2 \left(1 + \frac{1}{3} t_W^2\right) + \frac{2}{3} s_{\theta_{\tilde{d}}}^2 t_W^2 \right] c_{\alpha+\beta} \end{aligned} \quad (\text{A.21})$$

**[H, CP-even, d-type, 2] :**

$$\begin{aligned} \mathcal{C}_{\tilde{d}_2}^H &= -\frac{2}{vc_\beta} \left[ \left( c_{\theta_{\tilde{d}}} s_{\theta_{\tilde{d}}} m_d A^d + m_d^2 \right) c_\alpha + m_d \mu c_{\theta_{\tilde{d}}} s_{\theta_{\tilde{d}}} s_\alpha \right] \\ &+ \frac{M_W^2}{v} \left[ s_{\theta_{\tilde{d}}}^2 \left(1 + \frac{1}{3} t_W^2\right) + \frac{2}{3} c_{\theta_{\tilde{d}}}^2 t_W^2 \right] c_{\alpha+\beta} \end{aligned} \quad (\text{A.22})$$

**[H, CP-even, d-type, L] :**

$$\mathcal{C}_{\tilde{d}_L}^H = -\frac{2}{vc_\beta} m_d^2 c_\alpha + \frac{M_W^2}{v} \left(1 + \frac{1}{3} t_W^2\right) c_{\alpha+\beta} \quad (\text{A.23})$$

**[H, CP-even, d-type, R] :**

$$\mathcal{C}_{\tilde{d}_R}^H = -\frac{2}{vc_\beta} m_d^2 c_\alpha + \frac{M_W^2}{v} \frac{2}{3} t_W^2 c_{\alpha+\beta} \quad (\text{A.24})$$

**[A, CP-odd, squarks] :**

$$(\text{A.25})$$

All calculated topologies restrict the coupling squarks to reside either in one of the L,R or 1,2 bases. The property of this coupling implies, that all contributions to the cross section for the CP-odd Higgs boson A, containing loop topologies with squarks, are zero at amplitude level. For more details see the Appendix A.8 p. 399 of Ref. [8].



# Appendix B

## Loop tensors

---

### B.1 Three-point functions (Triangles)

#### B.1.1 Fermion-triangle with Higgs vertex

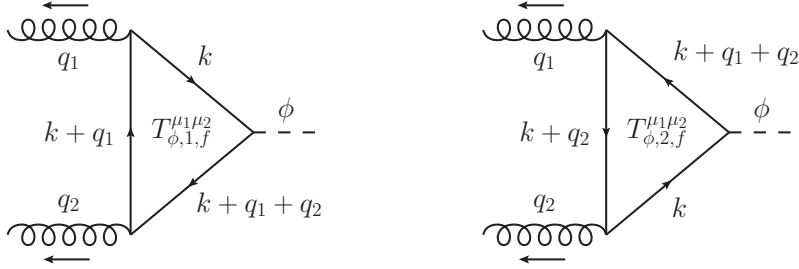


Figure B.1: *Three-point functions connected by charge-conjugation.*

The generic three-point functions for fermionic triangle graphs with Higgs vertex and opposite loop momentum, depicted in Fig. B.1, have the following expressions,

$$T_{\Phi,1,f}^{\mu_1 \mu_2}(q_1, q_2, m_f) = \int \frac{d^4 k}{i\pi^2} \text{tr} \left[ \frac{\not{k} + m_f}{k^2 - m_f^2} \gamma^{\mu_1} \frac{\not{k} + \not{q}_1 + m_f}{(k + q_1)^2 - m_f^2} \gamma^{\mu_2} \right. \\ \left. \times \frac{\not{k} + \not{q}_2 + m_f}{(k + q_2)^2 - m_f^2} \mathcal{V}_\Phi \right], \quad (\text{B.1})$$

$$T_{\Phi,2,f}^{\mu_1 \mu_2}(q_1, q_2, m_f) = \int \frac{d^4 k}{i\pi^2} \text{tr} \left[ \frac{\not{k} + m_f}{k^2 - m_f^2} \gamma^{\mu_2} \frac{\not{k} + \not{q}_2 + m_f}{(k + q_2)^2 - m_f^2} \gamma^{\mu_1} \right]$$

$$\times \frac{\mathcal{K} + q_{12} + m_f}{(k + q_{12})^2 - m_f^2} \mathcal{V}_\Phi \Big] , \quad (\text{B.2})$$

where  $q_1, q_2$  are outgoing gluon momenta and  $q_{12} = q_1 + q_2$ . The factor  $\mathcal{V}_\Phi$  denotes the  $\mathcal{CP}$  property of the Higgs coupling:  $\mathcal{V}_A = \gamma^5$  for  $\mathcal{CP}$ -odd and  $\mathcal{V}_{H_{SM}, h, H} = \mathbf{1}$  for  $\mathcal{CP}$ -even Higgs boson. Using the charge conjugation matrix  $\hat{C}$ ,

$$\hat{C}\gamma_\mu\hat{C}^{-1} = -\gamma_\mu^T, \quad \hat{C}\gamma_5\hat{C}^{-1} = \gamma_5^T \text{ with } \hat{C} = \gamma^0\gamma^2, \quad \hat{C}^2 = \mathbf{1} \quad (\text{B.3})$$

and the property of the trace  $\text{tr}[(\gamma^{\mu_1})^T(\gamma^{\mu_2})^T \dots] = \text{tr}[\dots \gamma^{\mu_2}\gamma^{\mu_1}]$ , one can derive (Furry's theorem [29])

$$T_{\Phi,1,f}^{\mu_1\mu_2}(q_1, q_2, m_f) = T_{\Phi,2,f}^{\mu_1\mu_2}(q_1, q_2, m_f) \equiv T_{\Phi,f}^{\mu_1\mu_2}(q_1, q_2, m_f) . \quad (\text{B.4})$$

Hence, the relative sign of charge-conjugated graphs changes with the number of fermion-gluon vertices. From this it follows for the color structure

$$\begin{aligned} & \text{tr}[t^{a_1}t^{a_2}]T_{\Phi,1,f}^{\mu_1\mu_2}(q_1, q_2, m_f) + \text{tr}[t^{a_2}t^{a_1}]T_{\Phi,2,f}^{\mu_1\mu_2}(q_1, q_2, m_f) \\ & = \delta^{a_1a_2}T_{\Phi,f}^{\mu_1\mu_2}(q_1, q_2, m_f) , \end{aligned} \quad (\text{B.5})$$

in which the identity  $\text{tr}[t^{a_1}t^{a_2}] = \frac{1}{2}\delta^{a_1a_2}$  was used.

### B.1.2 Fermion-triangle with $\mathcal{CP}$ -odd Higgs vertex

The evaluation of the Dirac trace with  $\mathcal{V}_A = \gamma^5$  yields

$$T_{A,f}^{\mu_1\mu_2}(q_1, q_2, m_f) = 4 m_f^2 \varepsilon^{\mu_1\mu_2q_1q_2} C_0(q_1, q_2, m_f) . \quad (\text{B.6})$$

Here,  $C_0$  denotes the scalar three-point function and  $\varepsilon^{\mu_1\mu_2q_1q_2}$  is the total anti-symmetric tensor (Levi-Civita symbol) contracted with attached gluon momenta  $q_1$  and  $q_2$ . The tensor  $T_{A,f}^{\mu_1\mu_2}(q_1, q_2, m_f)$  is UV-finite. Hence, no difficulties arise with definition of the  $\gamma_5$  Dirac-matrix in  $d$  dimensions.

### B.1.3 Fermion-triangle with $\mathcal{CP}$ -even Higgs vertex

The Relations of Eqs. (B.3), (B.4) and (B.5) hold also here, but with  $\gamma^5$  replaced by  $\mathbb{1}_4$ . The calculation of the Dirac trace leads to [2]

$$\begin{aligned}
T_{H_{SM},h,H,f}^{\mu_1\mu_2}(q_1, q_2, m_f) &= 4 m_f^2 \left[ F_T(q_1^2, q_2^2, (q_1 + q_2)^2) (q_1 \cdot q_2 g^{\mu_1\mu_2} \right. \\
&\quad \left. - q_1^{\mu_1} q_2^{\mu_2}) + F_L(q_1^2, q_2^2, (q_1 + q_2)^2) (q_1^2 q_2^2 g^{\mu_1\mu_2} - q_1^2 q_2^{\mu_1} q_2^{\mu_2} \right. \\
&\quad \left. - q_2^2 q_1^{\mu_1} q_1^{\mu_2} + q_1 \cdot q_2 q_1^{\mu_1} q_2^{\mu_2}) \right], \tag{B.7}
\end{aligned}$$

with the form factors

$$\begin{aligned}
F_L(q_1^2, q_2^2, (q_1 + q_2)^2, m_f) &= -\frac{1}{2 \det \mathcal{Q}_2} \left\{ \right. \\
&\quad \times \left[ 2 - \frac{3q_1^2 q_2 \cdot (q_1 + q_2)}{\det \mathcal{Q}_2} \right] \left( B_0(q_1, m_f) - B_0(q_1 + q_2, m_f) \right) \\
&\quad + \left[ 2 - \frac{3q_1^2 q_2 \cdot (q_1 + q_2)}{\det \mathcal{Q}_2} \right] \left( B_0(q_2, m_f) - B_0(q_1 + q_2, m_f) \right) \\
&\quad - \left[ 4m_f + q_1^2 + q_2^2 + (q_1 + q_2)^2 - \frac{3q_1^2 q_2^2 \cdot (q_1 + q_2)^2}{\det \mathcal{Q}_2} \right] \\
&\quad \left. \times C_0(q_1, q_2, m_f) - 2 \right\}, \tag{B.8}
\end{aligned}$$

$$\begin{aligned}
F_T(q_1^2, q_2^2, (q_1 + q_2)^2, m_f) &= -\frac{1}{2 \det \mathcal{Q}_2} \left\{ (q_1 + q_2)^2 [B_0(q_1, m_f) \right. \\
&\quad \left. + B_0(q_2, m_f) - 2 B_0(q_1 + q_2, m_f) - 2 q_1 \cdot q_2 C_0(q_1, q_2, m_f)] \right. \\
&\quad \left. + (q_1^2 - q_2^2) (B_0(q_1, m_f) - B_0(q_2, m_f)) \right\} - q_1 \cdot q_2 F_L. \tag{B.9}
\end{aligned}$$

Here,  $\det \mathcal{Q}_2 = q_1^2 q_2^2 - (q_1 \cdot q_2)^2$  stands for the Gram determinant. The shortcuts  $B_0$  and  $C_0$  denote scalar two- and three-point functions. Emerging  $\epsilon^{-1}$ -poles from the  $B_0$ -functions cancel each other at intermediate steps, so that the tensor  $T_{H_{SM},h,H,f}^{\mu_1\mu_2}(q_1, q_2, m_f)$  remains UV-finite. For more details see Ref. [2].

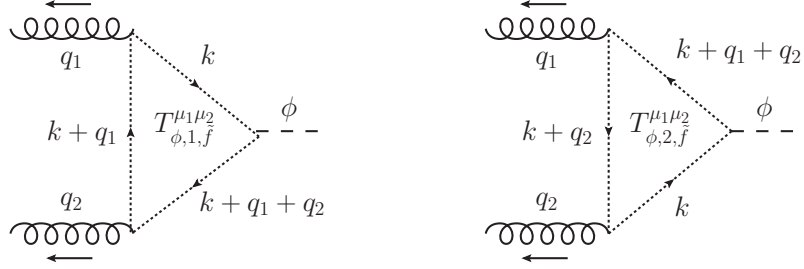


Figure B.2: *Triangle-loops with opposite fermion flow*

### B.1.4 Sfermion-triangle with $\mathcal{CP}$ -even Higgs vertex

The generic three-point functions for sfermionic triangle graphs with  $\mathcal{CP}$ -even Higgs vertex and opposite loop momentum, shown in Fig. B.2, have the following expressions

$$\begin{aligned} \overline{T}_{\Phi,1,\tilde{f}}^{\mu_1\mu_2}(q_1, q_2, m_{\tilde{f}}) &= \int \frac{d^4k}{i\pi^2} \frac{[2k + q_1]^{\mu_1} [2(k + q_1) + q_2]^{\mu_2}}{[k^2 - m_{\tilde{f}}^2] [(k + q_1)^2 - m_{\tilde{f}}^2] [(k + q_1 + q_2)^2 - m_{\tilde{f}}^2]}, \quad (\text{B.10}) \end{aligned}$$

$$\begin{aligned} \overline{T}_{\Phi,2,\tilde{f}}^{\mu_1\mu_2}(q_1, q_2, m_{\tilde{f}}) &= \int \frac{d^4k}{i\pi^2} \frac{[2k + q_2]^{\mu_2} [2(k + q_2) + q_1]^{\mu_1}}{[k^2 - m_{\tilde{f}}^2] [(k + q_2)^2 - m_{\tilde{f}}^2] [(k + q_2 + q_1)^2 - m_{\tilde{f}}^2]}. \quad (\text{B.11}) \end{aligned}$$

The  $\tilde{q}\tilde{q}A$ -vertex (Eq. (A.24)) gives only a contribution, if both squarks do not reside in the same basis ( $L/R$  or  $1/2$ ). Hence, for the case depicted in Fig. B.2, all contribution sum to zero at amplitude level.

Both tensors can be related via a shift of the loop momentum  $k \rightarrow -k - q_1 - q_2$ , so that the relation of Eq. (B.4) also holds for scalar loops

$$\overline{T}_{\Phi,1,\tilde{f}}^{\mu_1\mu_2}(q_1, q_2, m_{\tilde{f}}) = \overline{T}_{\Phi,2,\tilde{f}}^{\mu_1\mu_2}(q_1, q_2, m_{\tilde{f}}) \equiv \overline{T}_{\Phi,\tilde{f}}^{\mu_1\mu_2}(q_1, q_2, m_{\tilde{f}}). \quad (\text{B.12})$$



The evaluation of the numerator leads to

$$\begin{aligned}
& \overline{T}_{\Phi, \tilde{f}}^{\mu_1 \mu_2}(q_1, q_2, m_{\tilde{f}}) \\
&= \int \frac{d^4 k}{i\pi^2} \frac{4 k^{\mu_1} k^{\mu_2} + 2 q_1^{\mu_1} k^{\mu_2} + 2 k^{\mu_1} (2 q_1^{\mu_2} + q_2^{\mu_2}) + q_1^{\mu_1} (2 q_1^{\mu_2} + q_2^{\mu_2})}{\left[ k^2 - m_{\tilde{f}}^2 \right] \left[ (k + q_1)^2 - m_{\tilde{f}}^2 \right] \left[ (k + q_{12})^2 - m_{\tilde{f}}^2 \right]} \\
&= 4 C^{\mu_1 \mu_2}(q_1, q_2, m_{\tilde{f}}) + 2 q_1^{\mu_1} C^{\mu_2}(q_1, q_2, m_{\tilde{f}}) + 2 C^{\mu_1}(q_1, q_2, m_{\tilde{f}}) (2 q_1^{\mu_2} \\
&\quad + q_2^{\mu_2}) + q_1^{\mu_1} (2 q_1^{\mu_2} + q_2^{\mu_2}) C_0(q_1, q_2, m_{\tilde{f}}) \\
&= 2 q_2^{\mu_1} \left[ q_2^{\mu_2} (C_{12} + 2 C_{22}) + 2 q_1^{\mu_2} (C_{12} + C_{23}) \right] + q_1^{\mu_1} \left\{ 2 q_1^{\mu_2} (C_0 + 3 C_{11} \right. \\
&\quad \left. + 2 C_{21}) + q_2^{\mu_2} [C_0 + 2 (C_{11} + C_{12} + 2 C_{23})] \right\} - 4 g^{\mu_1 \mu_2} C_{24} . \quad (\text{B.13})
\end{aligned}$$

The coefficients  $C_{ij}$  originate from the Passarino-Veltman tensor reduction procedure [32, 33]. However, the  $C^{\mu_1 \mu_2}$  function contains an  $\epsilon^{-1}$ -pole in dimensional regularization and hence, it is UV-divergent. This  $\epsilon^{-1}$ -pole cancel by addition of a two-point function  $S_{h, H, \tilde{f}}^{\mu_1 \mu_2}(q_1, q_2, m_{\tilde{f}})$  with a  $\tilde{q}\tilde{q}gg$ -vertex (see Fig. B.3).

This graph has a simple analytic expression

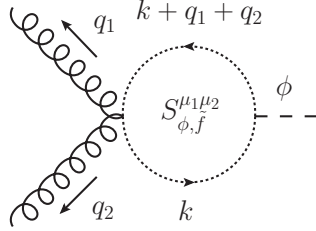


Figure B.3: *Scalar two-point function with a  $\tilde{q}\tilde{q}gg$ -vertex.*

$$\begin{aligned}
S_{h, H, \tilde{f}}^{\mu_1 \mu_2}(q_1, q_2, m_{\tilde{f}}) &= \int \frac{d^4 k}{i\pi^2} \frac{g_{\mu_1 \mu_2}}{\left[ k^2 - m_{\tilde{f}}^2 \right] \left[ (k + q_1 + q_2)^2 - m_{\tilde{f}}^2 \right]} \\
&= g^{\mu_1 \mu_2} B_0(q_{12}, m_{\tilde{f}}) \quad (\text{B.14})
\end{aligned}$$

The  $\epsilon^{-1}$ -pole coming from  $B_0$  cancels the corresponding poles originating from both sfermion triangles. Furthermore, the proportionality of the  $\tilde{q}\tilde{q}gg$ -vertex to the color factor  $\{t^{a_1}, t^{a_2}\}$  matches perfectly with Eq. (B.5), so that

all three graphs can be summed up to a divergence free contribution

$$T_{h,H,\tilde{f}}^{\mu_1\mu_2}(q_1, q_2, m_{\tilde{f}}) = \overline{T}_{h,H,\tilde{f}}^{\mu_1\mu_2}(q_1, q_2, m_{\tilde{f}}) + S_{h,H,\tilde{f}}^{\mu_1\mu_2}(q_1, q_2, m_{\tilde{f}}) . \quad (\text{B.15})$$

### B.1.5 Sfermion-triangle with $\mathcal{CP}$ -even Higgs vertex and $\tilde{q}\tilde{q}gg$ -vertex

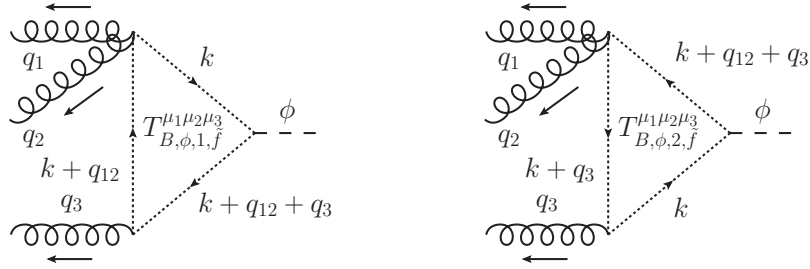


Figure B.4: Triangle-loops with opposite fermion flow and  $\tilde{q}\tilde{q}gg$ -vertex

The  $\tilde{q}\tilde{q}gg$ -vertex (D.5) allows also for triangle-graphs with three attached gluons. They are depicted in Fig. B.4. The integrals can be written in this way

$$\begin{aligned} & T_{B,\Phi,1,\tilde{f}}^{\mu_1\mu_2\mu_3}(q_{12}, q_3, m_{\tilde{f}}) \\ &= \int \frac{d^4k}{i\pi^2} \frac{g^{\mu_1\mu_2} [2(k+q_{12})+q_3]^{\mu_3}}{[k^2 - m_{\tilde{f}}^2] [(k+q_{12})^2 - m_{\tilde{f}}^2] [(k+q_{123})^2 - m_{\tilde{f}}^2]} \\ &= 2 g^{\mu_1\mu_2} C^{\mu_3}(q_{12}, q_3, m_{\tilde{f}}) + g^{\mu_1\mu_2} (2 q_{12}^{\mu_3} + q_3^{\mu_3}) C_0(q_{12}, q_3, m_{\tilde{f}}) , \quad (\text{B.16}) \end{aligned}$$

$$\begin{aligned} & T_{B,\Phi,2,\tilde{f}}^{\mu_1\mu_2\mu_3}(q_{12}, q_3, m_{\tilde{f}}) \\ &= \int \frac{d^4k}{i\pi^2} \frac{g^{\mu_1\mu_2} [2k+q_3]^{\mu_3}}{[k^2 - m_{\tilde{f}}^2] [(k+q_3)^2 - m_{\tilde{f}}^2] [(k+q_{123})^2 - m_{\tilde{f}}^2]} \\ &= 2 g^{\mu_1\mu_2} C^{\mu_3}(q_{12}, q_3, m_{\tilde{f}}) + g^{\mu_1\mu_2} q_3^{\mu_3} C_0(q_{12}, q_3, m_{\tilde{f}}) . \quad (\text{B.17}) \end{aligned}$$

Again, with a simple shift of the loop momentum  $k \rightarrow -k - q_{12} - q_3$  one gets

$$T_{B,\Phi,1,\tilde{f}}^{\mu_1\mu_2\mu_3} = -T_{B,\Phi,2,\tilde{f}}^{\mu_1\mu_2\mu_3} \equiv T_{B,\Phi,\tilde{f}}^{\mu_1\mu_2\mu_3} . \quad (\text{B.18})$$

Although it is a triangle-loop, it has a box-like color structure (see Eq. (B.26))

$$\left\{ \text{tr} \left[ \{t^{a_1}, t^{a_2}\} t^{a_3} \right] - \text{tr} \left[ t^{a_3} \{t^{a_1}, t^{a_2}\} \right] \right\} T_{\text{B},\Phi,\tilde{f}}^{\mu_1\mu_2\mu_3} = \left\{ \text{tr} [t^{a_1} t^{a_2} t^{a_3}] \right. \\ \left. + \text{tr} [t^{a_2} t^{a_1} t^{a_3}] - \text{tr} [t^{a_3} t^{a_1} t^{a_2}] - \text{tr} [t^{a_3} t^{a_2} t^{a_1}] \right\} T_{\text{B},\Phi,\tilde{f}}^{\mu_1\mu_2\mu_3} = 0, \quad (\text{B.19})$$

in which the cyclic invariance of the trace was used. Hence, these graphs give no contribution.

### B.1.6 Sfermion-triangle with $\mathcal{CP}$ -even Higgs vertex and two $\tilde{q}\tilde{q}gg$ -vertices

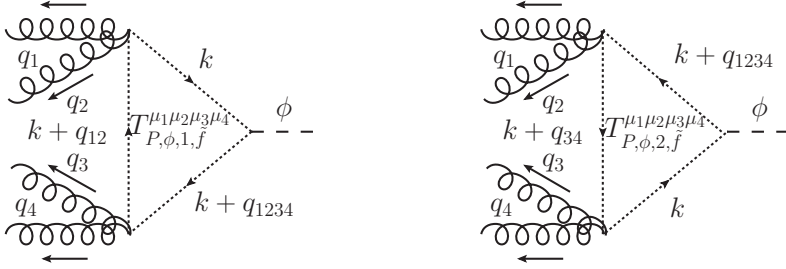


Figure B.5: *Sfermionic triangle-loops with opposite fermion flow and pentagon-like color structure*

The two  $\tilde{q}\tilde{q}gg$ -vertices allow also for triangle-graphs with four attached gluons (see Fig. B.5)

$$T_{\text{P},\Phi,\tilde{f}}^{\mu_1\mu_2\mu_3\mu_4}(q_{12}, q_{34}, m_{\tilde{f}}) \\ = \int \frac{d^4k}{i\pi^2} \frac{g^{\mu_1\mu_2} g^{\mu_3\mu_4}}{\left[ k^2 - m_{\tilde{f}}^2 \right] \left[ (k + q_{12})^2 - m_{\tilde{f}}^2 \right] \left[ (k + q_{1234})^2 - m_{\tilde{f}}^2 \right]} \quad (\text{B.20})$$

This topology is invariant under reversion of the momentum flow. Moreover, it has a pentagon-like color structure. For the sum of two graphs with

opposite loop momentum, the color factor reads as follows

$$\begin{aligned}
& \left( \text{tr} \left[ \{t^{a_1}, t^{a_2}\} \{t^{a_3}, t^{a_4}\} \right] + \text{tr} \left[ \{t^{a_3}, t^{a_4}\} \{t^{a_1}, t^{a_2}\} \right] \right) \\
& \times T_{\text{P}, \Phi, \tilde{f}}^{\mu_1 \mu_2 \mu_3 \mu_4} (q_{12}, q_{34}, m_{\tilde{f}}) = 2 \left( \text{tr} [t^{a_1} t^{a_2} t^{a_3} t^{a_4}] + \text{tr} [t^{a_1} t^{a_2} t^{a_4} t^{a_3}] \right. \\
& \left. + \text{tr} [t^{a_2} t^{a_1} t^{a_3} t^{a_4}] + \text{tr} [t^{a_2} t^{a_1} t^{a_4} t^{a_3}] \right) T_{\text{P}, \Phi, \tilde{f}}^{\mu_1 \mu_2 \mu_3 \mu_4} (q_{12}, q_{34}, m_{\tilde{f}}) , \quad (\text{B.21})
\end{aligned}$$

with

$$T_{\text{P}, \Phi, \tilde{f}}^{\mu_1 \mu_2 \mu_3 \mu_4} (q_{12}, q_{34}, m_{\tilde{f}}) = g^{\mu_1 \mu_2} g^{\mu_3 \mu_4} C_0(q_{12}, q_{34}, m_{\tilde{f}}) . \quad (\text{B.22})$$

## B.2 Four-point functions (Boxes)

### B.2.1 Fermion-box with Higgs vertex

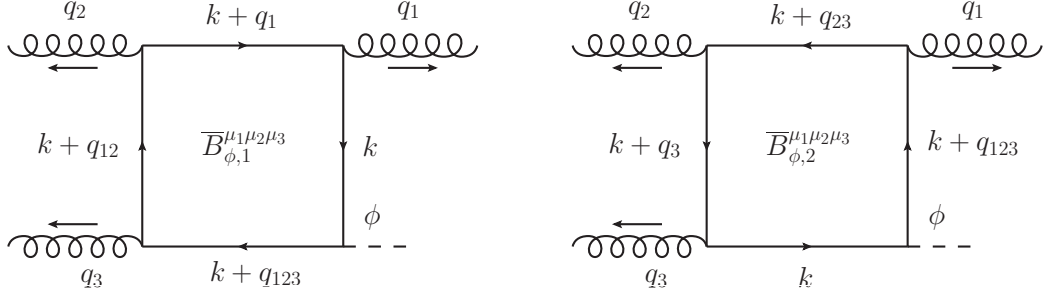


Figure B.6: *Four-point functions connected by charge-conjugation.*

Four-point functions for the production of the Higgs boson  $\Phi$  connected via charge-conjugation have the following analytical expressions

$$\begin{aligned}
\overline{B}_{\Phi,1,f}^{\mu_1 \mu_2 \mu_3} (q_1, q_2, q_3, m_f) &= \int \frac{d^4 k}{i\pi^2} \text{tr} \left[ \frac{\not{k} + m_f}{k^2 - m_f^2} \gamma^{\mu_1} \frac{\not{k} + \not{q}_1 + m_f}{(k + q_1)^2 - m_f^2} \right. \\
&\times \left. \gamma^{\mu_2} \frac{\not{k} + \not{q}_{12} + m_f}{(k + q_{12})^2 - m_f^2} \gamma^{\mu_3} \frac{\not{k} + \not{q}_{123} + m_f}{(k + q_{123})^2 - m_f^2} \mathcal{V}_\Phi \right] , \quad (\text{B.23})
\end{aligned}$$

$$\begin{aligned} \overline{B}_{\Phi,2,f}^{\mu_1\mu_2\mu_3}(q_1, q_2, q_3, m_f) &= \int \frac{d^4k}{i\pi^2} \text{tr} \left[ \frac{\not{k} + m_f}{k^2 - m_f^2} \gamma^{\mu_3} \frac{\not{k} + \not{q}_3 + m_f}{(k + q_3)^2 - m_f^2} \right. \\ &\quad \left. \times \gamma^{\mu_2} \frac{\not{k} + \not{q}_{23} + m_f}{(k + q_{23})^2 - m_f^2} \gamma^{\mu_1} \frac{\not{k} + \not{q}_{123} + m_f}{(k + q_{123})^2 - m_f^2} \mathcal{V}_\Phi \right], \end{aligned} \quad (\text{B.24})$$

where  $q_1, q_2$  and  $q_3$  are outgoing momenta,  $q_{ij} = q_i + q_j$  and  $q_{ijk} = q_i + q_j + q_k$ . From charge conjugation one gets

$$\begin{aligned} \overline{B}_{\Phi,1,f}^{\mu_1\mu_2\mu_3}(q_1, q_2, q_3, m_f) &= -\overline{B}_{\Phi,2,f}^{\mu_1\mu_2\mu_3}(q_1, q_2, q_3, m_f) \\ &\equiv \overline{B}_{\Phi,f}^{\mu_1\mu_2\mu_3}(q_1, q_2, q_3, m_f). \end{aligned} \quad (\text{B.25})$$

Further two permutations can be achieved by cyclic permutation of (1, 2, 3). The color structure for the sum of the two diagrams is

$$\begin{aligned} &\text{tr}(t^{a_1} t^{a_2} t^{a_3}) \overline{B}_{\Phi,1,f}^{\mu_1\mu_2\mu_3}(q_1, q_2, q_3, m_f) + \text{tr}(t^{a_3} t^{a_2} t^{a_1}) \overline{B}_{\Phi,2,f}^{\mu_1\mu_2\mu_3}(q_1, q_2, q_3, m_f) \\ &= \left[ \text{tr}(t^{a_1} t^{a_2} t^{a_3}) - \text{tr}(t^{a_3} t^{a_2} t^{a_1}) \right] \overline{B}_{\Phi,f}^{\mu_1\mu_2\mu_3}(q_1, q_2, q_3, m_f) \\ &= \frac{i}{2} f^{a_1 a_2 a_3} \overline{B}_{\Phi,f}^{\mu_1\mu_2\mu_3}(q_1, q_2, q_3, m_f), \end{aligned} \quad (\text{B.26})$$

in which the following identity was used

$$\text{tr}(t^{a_1} t^{a_2} t^{a_3}) = \frac{1}{4} (d^{a_1 a_2 a_3} + i f^{a_1 a_2 a_3}). \quad (\text{B.27})$$

Altogether the sum over the six permutations of boxes is then proportional to the single factor  $f^{a_1 a_2 a_3}$ . In the Fortran program *VBFNLO* all permutations of boxes are combined to one box factor

$$\begin{aligned} B_{\Phi,f}^{\mu_1\mu_2\mu_3}(q_1, q_2, q_3, m_f) &= \frac{1}{2} \left[ \overline{B}_{\Phi,f}^{\mu_1\mu_2\mu_3}(q_1, q_2, q_3, m_f) \right. \\ &\quad \left. + \overline{B}_{\Phi,f}^{\mu_2\mu_3\mu_1}(q_2, q_3, q_1, m_f) + \overline{B}_{\Phi,f}^{\mu_3\mu_1\mu_2}(q_3, q_1, q_2, m_f) \right], \end{aligned} \quad (\text{B.28})$$

which is totally antisymmetric in the gluon indices  $(q_i, \mu_i)$ ,  $i = 1, 2, 3$ .

## B.2.2 Fermion-box with $\mathcal{CP}$ -odd Higgs vertex

The evaluation of the Dirac-trace for the permutation (1, 2, 3) of attached gluons with  $\mathcal{V}_A$  leads to

$$\begin{aligned}
\overline{B}_{A,f}^{\mu_1\mu_2\mu_3}(q_1, q_2, q_3, m_f) = 4 m_f^2 \left\{ \right. \\
& \left[ \varepsilon^{\mu_3 q_1 q_2 q_3} g^{\mu_1 \mu_2} - \varepsilon^{\mu_2 q_1 q_2 q_3} g^{\mu_1 \mu_3} + \varepsilon^{\mu_2 \mu_3 q_2 q_3} q_1^{\mu_1} - \varepsilon^{\mu_2 \mu_3 q_1 q_3} q_2^{\mu_1} \right. \\
& + \varepsilon^{\mu_2 \mu_3 q_1 q_2} q_3^{\mu_1} + \varepsilon^{\mu_1 q_1 q_2 q_3} g^{\mu_2 \mu_3} + \varepsilon^{\mu_1 \mu_3 q_2 q_3} q_1^{\mu_2} - \varepsilon^{\mu_1 \mu_3 q_1 q_2} q_3^{\mu_2} \\
& - \varepsilon^{\mu_1 \mu_2 q_2 q_3} q_1^{\mu_3} + \varepsilon^{\mu_1 \mu_2 q_1 q_3} q_2^{\mu_3} + \varepsilon^{\mu_1 \mu_2 \mu_3 q_3} g^{\mu_1 \mu_2} - \varepsilon^{\mu_1 \mu_2 \mu_3 q_2} g^{\mu_1 \mu_3} \\
& + \varepsilon^{\mu_1 \mu_2 \mu_3 q_1} g^{\mu_2 \mu_3} + \varepsilon^{\mu_1 \mu_3 q_1 q_3} (2 q_1^{\mu_2} + q_2^{\mu_2}) + \varepsilon^{\mu_1 \mu_2 q_1 q_2} [2 (q_1^{\mu_3} \\
& + q_2^{\mu_3}) + q_3^{\mu_3}] \left. \right] D_0(q_1, q_2, q_3, m_f) \\
& - \varepsilon^{\mu_1 \mu_2 \mu_3 q_3} C_0(q_1 + q_2, q_3, m_f) - \varepsilon^{\mu_1 \mu_2 \mu_3 q_1} C_0(q_1, q_2 + q_3, m_f) \\
& + 2 \varepsilon^{\mu_2 \mu_3 q_2 q_3} D^{\mu_1}(q_1, q_2, q_3, m_f) + 2 \varepsilon^{\mu_1 \mu_3 q_1 q_3} D^{\mu_2}(q_1, q_2, q_3, m_f) \\
& \left. + 2 \varepsilon^{\mu_1 \mu_2 q_1 q_2} D^{\mu_3}(q_1, q_2, q_3, m_f) \right\}. \tag{B.29}
\end{aligned}$$

The  $D_0$  and  $D_\mu$  are four-point functions. Whereas the former denotes a scalar function, the latter can be expressed by the usual Passarino-Veltman decomposition [32] as

$$D^\mu(q_1, q_2, q_3, m_f) = q_1^\mu D_{11} + q_2^\mu D_{12} + q_3^\mu D_{13}. \tag{B.30}$$

Note that after contraction with polarization vectors  $\epsilon_1^{\mu_1}$ ,  $\epsilon_2^{\mu_2}$  and quark current  $J_{21}^{\mu_3}$  (3.9), the expression (B.29) still contains terms with factors  $(\epsilon_1 \cdot q_1)$ ,  $(\epsilon_2 \cdot q_2)$ ,  $(J_{21} \cdot q_3)$  even though they vanish, since gluon polarization vectors  $\epsilon_i^\mu$  and momenta  $q_i^\mu$  are perpendicular to each other and the quark current  $J_{21}$  is conserved. However, these terms are important for numerical gauge checks, where the corresponding gluon polarization vector is replaced by its momentum. In this connection, the virtual gluon has a non-zero  $q_i^2$ , and hence, these terms give finite contributions.

### B.2.3 Fermion-box with $\mathcal{CP}$ -even Higgs vertex

Following Ref. [2], the four-point function with  $\mathcal{CP}$ -even Higgs vertex can be expressed in terms of few independent tensor structures

$$\begin{aligned}
B_{H_{SM},h,H,f}^{\mu_1\mu_2\mu_3}(q_1, q_2, q_3, m_f) = & 4 m_f^2 \left\{ g^{\mu_1\mu_2} q_1^{\mu_3} B_a(q_1, q_2, q_3) \right. \\
& + g^{\mu_2\mu_3} q_2^{\mu_1} B_a(q_2, q_3, q_1) + g^{\mu_3\mu_1} q_3^{\mu_2} B_a(q_3, q_1, q_2) \\
& - g^{\mu_2\mu_1} q_2^{\mu_3} B_a(q_2, q_1, q_3) - g^{\mu_1\mu_3} q_1^{\mu_2} B_a(q_1, q_3, q_2) \\
& - g^{\mu_3\mu_2} q_3^{\mu_1} B_a(q_3, q_2, q_1) + q_3^{\mu_1} q_3^{\mu_2} q_1^{\mu_3} B_b(q_1, q_2, q_3) \\
& + q_2^{\mu_1} q_1^{\mu_2} q_1^{\mu_3} B_b(q_2, q_3, q_1) + q_2^{\mu_1} q_3^{\mu_2} q_2^{\mu_3} B_b(q_3, q_1, q_2) \\
& - q_3^{\mu_1} q_3^{\mu_2} q_2^{\mu_3} B_b(q_2, q_1, q_3) - q_2^{\mu_1} q_1^{\mu_2} q_2^{\mu_3} B_b(q_1, q_3, q_2) \\
& - q_3^{\mu_1} q_1^{\mu_2} q_1^{\mu_3} B_b(q_3, q_2, q_1) + q_2^{\mu_1} q_3^{\mu_2} q_1^{\mu_3} B_c(q_1, q_2, q_3) \\
& \left. - q_3^{\mu_1} q_1^{\mu_2} q_2^{\mu_3} B_c(q_2, q_1, q_3) \right\}, \tag{B.31}
\end{aligned}$$

with scalar functions

$$\begin{aligned}
B_a(q_1, q_2, q_3) = & \frac{1}{2} q_2 \cdot q_3 \left[ D_0(q_1, q_2, q_3) + D_0(q_2, q_3, q_1) + D_0(q_3, q_1, q_2) \right] \\
& - q_1 \cdot q_2 \left[ D_{13}(q_2, q_3, q_1) + D_{12}(q_3, q_1, q_2) - D_{13}(q_3, q_2, q_1) \right] \\
& - 4 \left[ D_{313}(q_2, q_3, q_1) + D_{312}(q_3, q_1, q_2) - D_{313}(q_3, q_2, q_1) \right] \\
& - C_0(q_1, q_2 + q_3), \tag{B.32}
\end{aligned}$$

$$\begin{aligned}
B_b(q_1, q_2, q_3) = & D_{13}(q_1, q_2, q_3) + D_{12}(q_2, q_3, q_1) - D_{13}(q_2, q_1, q_3) \\
& + 4 \left[ D_{37}(q_1, q_2, q_3) + D_{23}(q_1, q_2, q_3) + D_{38}(q_2, q_3, q_1) \right. \\
& \left. + D_{26}(q_2, q_3, q_1) - D_{39}(q_2, q_1, q_3) - D_{23}(q_2, q_1, q_3) \right], \tag{B.33}
\end{aligned}$$

$$\begin{aligned}
B_c(q_1, q_2, q_3) = & -\frac{1}{2} \left[ D_0(q_1, q_2, q_3) + D_0(q_2, q_3, q_1) + D_0(q_3, q_1, q_2) \right] \\
& + 4 \left[ D_{26}(q_1, q_2, q_3) + D_{26}(q_2, q_3, q_1) + D_{26}(q_3, q_1, q_2) \right. \\
& \left. + D_{310}(q_1, q_2, q_3) + D_{310}(q_2, q_3, q_1) + D_{310}(q_3, q_1, q_2) \right]. \tag{B.34}
\end{aligned}$$

The coefficients  $D_{ij}$  and  $D_{ijk}$  originate from the Passarino-Veltman tensor decomposition of  $D^\mu$ ,  $D^{\mu_1\mu_2}$  and  $D^{\mu_1\mu_2\mu_3}$  respectively. For more details see Ref. [2].

## B.2.4 Sfermion-box with $\mathcal{CP}$ -even Higgs vertex

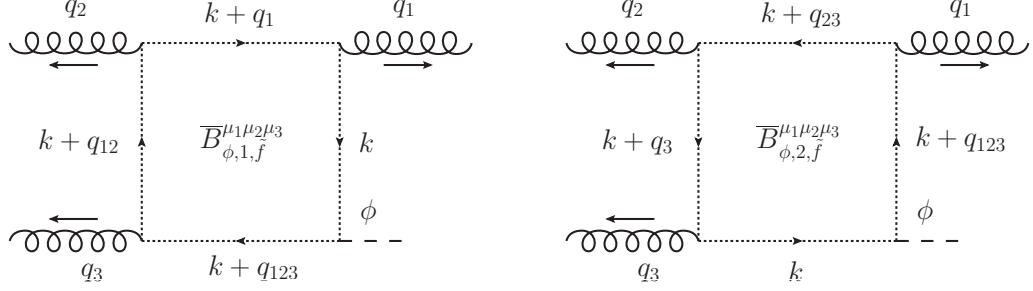


Figure B.7: *Sfermionic box-loops with opposite fermion flow*

The generic four-point functions for sfermionic box graphs with  $\mathcal{CP}$ -even Higgs vertex and opposite loop momentum, shown in Fig. B.7, have the following expressions

$$\begin{aligned} \overline{B}_{\Phi,1,\tilde{f}}^{\mu_1\mu_2\mu_3}(q_1, q_2, q_3, m_{\tilde{f}}) &= \int \frac{d^4k}{i\pi^2} \frac{[2k + q_1]^{\mu_1} [2(k + q_1) + q_2]^{\mu_2}}{[k^2 - m_{\tilde{f}}^2] [(k + q_1)^2 - m_{\tilde{f}}^2]} \\ &\quad \times \frac{[2(k + q_{12}) + q_3]^{\mu_3}}{[(k + q_{12})^2 - m_{\tilde{f}}^2] [(k + q_{123})^2 - m_{\tilde{f}}^2]}, \end{aligned} \quad (\text{B.35})$$

$$\begin{aligned} \overline{B}_{\Phi,2,\tilde{f}}^{\mu_1\mu_2\mu_3}(q_1, q_2, q_3, m_{\tilde{f}}) &= \int \frac{d^4k}{i\pi^2} \frac{[2k + q_3]^{\mu_3} [2(k + q_3) + q_2]^{\mu_2}}{[k^2 - m_{\tilde{f}}^2] [(k + q_3)^2 - m_{\tilde{f}}^2]} \\ &\quad \times \frac{[2(k + q_{23}) + q_1]^{\mu_1}}{[(k + q_{23})^2 - m_{\tilde{f}}^2] [(k + q_{123})^2 - m_{\tilde{f}}^2]}. \end{aligned} \quad (\text{B.36})$$

After a shift of the loop momentum  $k \rightarrow -k - q_1 - q_2 - q_3$ , the relations of Eq. (B.25), (B.26) and (B.28) also holds for the sfermionic box factor. Evaluation of the numerator for the gluon permutation (1, 2, 3) yields

$$\begin{aligned} \overline{B}_{\Phi,\tilde{f}}^{\mu_1\mu_2\mu_3}(q_1, q_2, q_3, m_{\tilde{f}}) &= 8 D^{\mu_1\mu_2\mu_3} + 4 (2 q_1^{\mu_3} + 2 q_2^{\mu_3} + q_3^{\mu_3}) D^{\mu_1\mu_2} \\ &\quad + 8 q_1^{\mu_2} D^{\mu_1\mu_3} + 4 q_2^{\mu_2} D^{\mu_1\mu_3} + 4 q_1^{\mu_1} D^{\mu_2\mu_3} + 2 (2 q_1^{\mu_2} + q_2^{\mu_2}) (2 q_1^{\mu_3} \\ &\quad + 2 q_2^{\mu_3} + q_3^{\mu_3}) D^{\mu_1} + 2 q_1^{\mu_1} (2 q_1^{\mu_3} + 2 q_2^{\mu_3} + q_3^{\mu_3}) D^{\mu_2} + 4 q_1^{\mu_1} q_1^{\mu_2} D^{\mu_3} \\ &\quad + 2 q_1^{\mu_1} q_2^{\mu_2} D^{\mu_3} + q_1^{\mu_1} (2 q_1^{\mu_2} + q_2^{\mu_2}) (2 q_1^{\mu_3} + 2 q_2^{\mu_3} + q_3^{\mu_3}) D_0. \end{aligned} \quad (\text{B.37})$$



## B.2.5 Sfermion-box with $\mathcal{CP}$ -even Higgs vertex and $\tilde{q}\tilde{q}gg$ -vertex

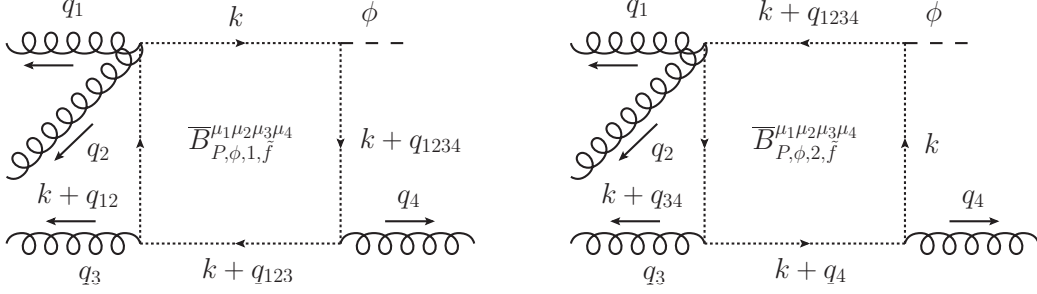


Figure B.8: *Sfermionic box-loops with opposite fermion flow and  $\tilde{q}\tilde{q}gg$  vertex.*

The cyclic permutation of the momentum set  $(q_{12}, q_3, q_4)$  provides three different box contributions. The first contributions with opposite loop-momentum are depicted in Fig. B.8. All distinct box diagrams and their partners with opposite loop momentum flow are described now in more detail:

### 1) Permutation $(q_{12}, q_3, q_4)$

$$\begin{aligned} \overline{B}_{P,\Phi,1,\tilde{f}}^{\mu_1\mu_2\mu_3\mu_4}(q_{12}, q_3, q_4, m_{\tilde{f}}) &= \int \frac{d^4k}{i\pi^2} \frac{g^{\mu_1\mu_2} [2(k+q_{12}) + q_3]^{\mu_3}}{[k^2 - m_{\tilde{f}}^2] [(k+q_{12})^2 - m_{\tilde{f}}^2]} \\ &\times \frac{[2(k+q_{123}) + q_4]^{\mu_4}}{[(k+q_{123})^2 - m_{\tilde{f}}^2] [(k+q_{1234})^2 - m_{\tilde{f}}^2]}, \quad (\text{B.38}) \end{aligned}$$

$$\begin{aligned} \overline{B}_{P,\Phi,2,\tilde{f}}^{\mu_4\mu_3\mu_2\mu_1}(q_4, q_3, q_{12}, m_{\tilde{f}}) &= \int \frac{d^4k}{i\pi^2} \frac{g^{\mu_1\mu_2} [2k + q_4]^{\mu_4}}{[k^2 - m_{\tilde{f}}^2] [(k+q_4)^2 - m_{\tilde{f}}^2]} \\ &\times \frac{[2(k+q_4) + q_3]^{\mu_3}}{[(k+q_{34})^2 - m_{\tilde{f}}^2] [(k+q_{1234})^2 - m_{\tilde{f}}^2]}, \quad (\text{B.39}) \end{aligned}$$

### 2) Permutation $(q_3, q_4, q_{12})$

$$\overline{B}_{P,\Phi,3,\tilde{f}}^{\mu_1\mu_2\mu_3\mu_4}(q_4, q_{12}, q_3, m_{\tilde{f}}) = \int \frac{d^4k}{i\pi^2} \frac{g^{\mu_1\mu_2} [2(k+q_{124}) + q_3]^{\mu_3}}{[k^2 - m_{\tilde{f}}^2] [(k+q_4)^2 - m_{\tilde{f}}^2]}$$

$$\times \frac{[2k + q_4]^{\mu_4}}{\left[ (k + q_{124})^2 - m_{\tilde{f}}^2 \right] \left[ (k + q_{1234})^2 - m_{\tilde{f}}^2 \right]}, \quad (\text{B.40})$$

$$\begin{aligned} \overline{B}_{P,\Phi,4,\tilde{f}}^{\mu_4\mu_1\mu_2\mu_3}(q_3, q_{12}, q_4, m_{\tilde{f}}) &= \int \frac{d^4k}{i\pi^2} \frac{g^{\mu_1\mu_2} [2k + q_3]^{\mu_3}}{\left[ k^2 - m_{\tilde{f}}^2 \right] \left[ (k + q_3)^2 - m_{\tilde{f}}^2 \right]} \\ &\times \frac{[2(k + q_{123}) + q_4]^{\mu_4}}{\left[ (k + q_{123})^2 - m_{\tilde{f}}^2 \right] \left[ (k + q_{1234})^2 - m_{\tilde{f}}^2 \right]}, \quad (\text{B.41}) \end{aligned}$$

### 3) Permutation $(q_4, q_{12}, q_3)$

$$\begin{aligned} \overline{B}_{P,\Phi,5,\tilde{f}}^{\mu_3\mu_4\mu_1\mu_2}(q_3, q_4, q_{12}, m_{\tilde{f}}) &= \int \frac{d^4k}{i\pi^2} \frac{g^{\mu_1\mu_2} [2k + q_3]^{\mu_3}}{\left[ k^2 - m_{\tilde{f}}^2 \right] \left[ (k + q_3)^2 - m_{\tilde{f}}^2 \right]} \\ &\times \frac{[2(k + q_3) + q_4]^{\mu_4}}{\left[ (k + q_4)^2 - m_{\tilde{f}}^2 \right] \left[ (k + q_{1234})^2 - m_{\tilde{f}}^2 \right]}, \quad (\text{B.42}) \end{aligned}$$

$$\begin{aligned} \overline{B}_{P,\Phi,6,\tilde{f}}^{\mu_1\mu_2\mu_3\mu_4}(q_{12}, q_4, q_3, m_{\tilde{f}}) &= \int \frac{d^4k}{i\pi^2} \frac{g^{\mu_1\mu_2} [2(k + q_{12}) + q_4]^{\mu_4}}{\left[ k^2 - m_{\tilde{f}}^2 \right] \left[ (k + q_{12})^2 - m_{\tilde{f}}^2 \right]} \\ &\times \frac{[2(k + q_{124}) + q_3]^{\mu_3}}{\left[ (k + q_{124})^2 - m_{\tilde{f}}^2 \right] \left[ (k + q_{1234})^2 - m_{\tilde{f}}^2 \right]}. \quad (\text{B.43}) \end{aligned}$$

Performing a shift of the loop momentum  $k \rightarrow -k - q_{1234}$  in the box tensors no. 2, 4, 6 gives

$$\overline{B}_{P,\Phi,1,\tilde{f}}^{\mu_1\mu_2\mu_3\mu_4} = +\overline{B}_{P,\Phi,2,\tilde{f}}^{\mu_4\mu_3\mu_2\mu_1} \equiv \overline{B}_{P,\Phi,a,\tilde{f}}^{\mu_1\mu_2\mu_3\mu_4}(q_{12}, q_3, q_4, m_{\tilde{f}}), \quad (\text{B.44})$$

$$\overline{B}_{P,\Phi,3,\tilde{f}}^{\mu_1\mu_2\mu_3\mu_4} = +\overline{B}_{P,\Phi,4,\tilde{f}}^{\mu_4\mu_3\mu_2\mu_1} \equiv \overline{B}_{P,\Phi,b,\tilde{f}}^{\mu_1\mu_2\mu_3\mu_4}(q_3, q_4, q_{12}, m_{\tilde{f}}), \quad (\text{B.45})$$

$$\overline{B}_{P,\Phi,5,\tilde{f}}^{\mu_1\mu_2\mu_3\mu_4} = +\overline{B}_{P,\Phi,6,\tilde{f}}^{\mu_4\mu_3\mu_2\mu_1} \equiv \overline{B}_{P,\Phi,c,\tilde{f}}^{\mu_1\mu_2\mu_3\mu_4}(q_4, q_{12}, q_3, m_{\tilde{f}}). \quad (\text{B.46})$$

Furthermore, all diagrams have a pentagon-like color structure, which is denoted by the index  $P$ . Due to the invariance property of the trace under cyclic permutations, the color structure is the same for all three contributions. For

a permutation such as  $(q_{12}, q_3, q_4)$ , it is given by

$$\begin{aligned}
& \text{tr} \left[ \{t^{a_1}, t^{a_2}\} t^{a_3} t^{a_4} \right] \overline{B}_{P,\Phi,1,\tilde{f}}^{\mu_1\mu_2\mu_3\mu_4} + \text{tr} \left[ t^{a_4} t^{a_3} \{t^{a_1}, t^{a_2}\} \right] \overline{B}_{P,\Phi,2,\tilde{f}}^{\mu_4\mu_3\mu_2\mu_1} \\
&= \left( \text{tr} [t^{a_1} t^{a_2} t^{a_3} t^{a_4}] + \text{tr} [t^{a_2} t^{a_1} t^{a_3} t^{a_4}] + \text{tr} [t^{a_4} t^{a_3} t^{a_1} t^{a_2}] \right. \\
&\quad \left. + \text{tr} [t^{a_4} t^{a_3} t^{a_2} t^{a_1}] \right) \overline{B}_{P,\Phi,a}^{\mu_1\mu_2\mu_3\mu_4}(q_{12}, q_3, q_4, m_{\tilde{f}}) \tag{B.47}
\end{aligned}$$

In the Fortran program *VBFNLO* all permutations are combined to one box factor

$$B_{P,\Phi,\tilde{f}}^{\mu_1\mu_2\mu_3\mu_4}(q_{12}, q_3, q_4, m_{\tilde{f}}) = \overline{B}_{P,\Phi,a,\tilde{f}}^{\mu_1\mu_2\mu_3\mu_4} + \overline{B}_{P,\Phi,b,\tilde{f}}^{\mu_3\mu_4\mu_1\mu_2} + \overline{B}_{P,\Phi,c,\tilde{f}}^{\mu_4\mu_1\mu_2\mu_3} \tag{B.48}$$

with

$$\begin{aligned}
& \overline{B}_{P,\Phi,a,\tilde{f}}^{\mu_1\mu_2\mu_3\mu_4}(q_{12}, q_3, q_4, m_{\tilde{f}}) \\
&= 4 g^{\mu_1\mu_2} D^{\mu_3\mu_4} + 2 g^{\mu_1\mu_2} (2 q_1^{\mu_3} + 2 q_2^{\mu_3} + q_3^{\mu_3}) D^{\mu_4} + 2 g^{\mu_1\mu_2} (2 q_1^{\mu_4} \\
&\quad + 2 q_2^{\mu_4} + 2 q_3^{\mu_4} + q_4^{\mu_4}) D^{\mu_3} + g^{\mu_1\mu_2} (2 q_1^{\mu_3} + 2 q_2^{\mu_3} + q_3^{\mu_3}) (2 q_1^{\mu_4} \\
&\quad + 2 q_2^{\mu_4} + 2 q_3^{\mu_4} + q_4^{\mu_4}) D_0, \tag{B.49}
\end{aligned}$$

$$\begin{aligned}
& \overline{B}_{P,\Phi,b,\tilde{f}}^{\mu_1\mu_2\mu_3\mu_4}(q_3, q_4, q_{12}, m_{\tilde{f}}) \\
&= 4 g^{\mu_1\mu_2} D^{\mu_3\mu_4} + 2 g^{\mu_1\mu_2} (2 q_1^{\mu_3} + 2 q_2^{\mu_3} + 2 q_4^{\mu_3} + q_3^{\mu_3}) D^{\mu_4} \\
&\quad + 2 g^{\mu_1\mu_2} q_4^{\mu_4} D^{\mu_3} + g^{\mu_1\mu_2} (2 q_1^{\mu_3} + 2 q_2^{\mu_3} + 2 q_4^{\mu_3} + q_3^{\mu_3}) q_4^{\mu_4} D_0, \tag{B.50}
\end{aligned}$$

$$\begin{aligned}
& \overline{B}_{P,\Phi,c,\tilde{f}}^{\mu_1\mu_2\mu_3\mu_4}(q_4, q_{12}, q_3, m_{\tilde{f}}) \\
&= 4 g^{\mu_1\mu_2} D^{\mu_3\mu_4} + 2 g^{\mu_1\mu_2} q_3^{\mu_3} D^{\mu_4} + 2 g^{\mu_1\mu_2} (2 q_3^{\mu_4} + q_4^{\mu_4}) D^{\mu_3} \\
&\quad + g^{\mu_1\mu_2} q_3^{\mu_3} (2 q_3^{\mu_4} + q_4^{\mu_4}) D_0. \tag{B.51}
\end{aligned}$$

## B.3 Five-point functions (Pentagons)

### B.3.1 Fermion-pentagon with Higgs vertex

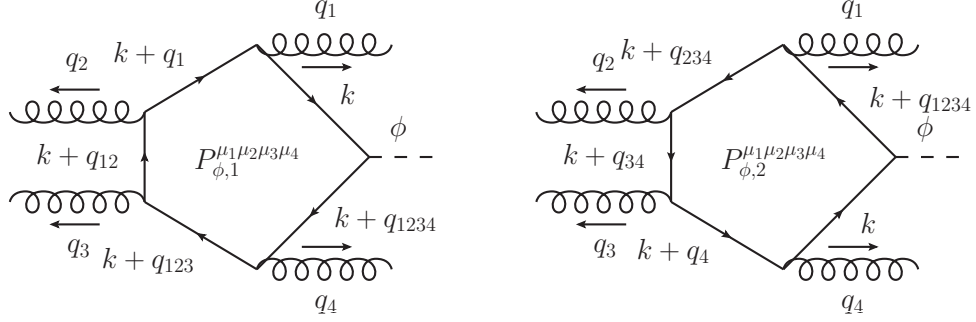


Figure B.9: *Five-point functions connected by charge-conjugation.*

The two five-point functions connected by charge conjugation for the gluon permutation (1,2,3,4) have the following expressions

$$\begin{aligned}
 P_{\Phi,1,f}^{\mu_1\mu_2\mu_3\mu_4}(q_1, q_2, q_3, q_4, m_f) &= \int \frac{d^4k}{i\pi^2} \text{tr} \left[ \frac{\mathcal{K} + m_f}{k^2 - m_f^2} \gamma^{\mu_1} \right. \\
 &\quad \times \frac{\mathcal{K} + \not{A}_1 + m_f}{(k + q_1)^2 - m_f^2} \gamma^{\mu_2} \frac{\mathcal{K} + \not{A}_{12} + m_f}{(k + q_{12})^2 - m_f^2} \gamma^{\mu_3} \\
 &\quad \left. \times \frac{\mathcal{K} + \not{A}_{123} + m_f}{(k + q_{123})^2 - m_f^2} \gamma^{\mu_4} \frac{\mathcal{K} + \not{A}_{1234} + m_f}{(k + q_{1234})^2 - m_f^2} \mathcal{V}_\Phi \right], \quad (\text{B.52})
 \end{aligned}$$

$$\begin{aligned}
 P_{\Phi,2,f}^{\mu_1\mu_2\mu_3\mu_4}(q_1, q_2, q_3, q_4, m_f) &= \int \frac{d^4k}{i\pi^2} \text{tr} \left[ \frac{\mathcal{K} + m_f}{k^2 - m_f^2} \gamma^{\mu_4} \right. \\
 &\quad \times \frac{\mathcal{K} + \not{A}_4 + m_f}{(k + q_4)^2 - m_f^2} \gamma^{\mu_3} \frac{\mathcal{K} + \not{A}_{34} + m_f}{(k + q_{34})^2 - m_f^2} \gamma^{\mu_2} \\
 &\quad \left. \times \frac{\mathcal{K} + \not{A}_{234} + m_f}{(k + q_{234})^2 - m_f^2} \gamma^{\mu_1} \frac{\mathcal{K} + \not{A}_{1234} + m_f}{(k + q_{1234})^2 - m_f^2} \mathcal{V}_\Phi \right], \quad (\text{B.53})
 \end{aligned}$$

where  $q_1, q_2, q_3$  and  $q_4$  are outgoing momenta ( $q_{ij} = q_i + q_j$  and analog for  $q_{ijk}$  and  $q_{ijkl}$ ). Using Furrry's theorem, one gets for the sum

$$\left( \text{tr} [t^{a_1} t^{a_2} t^{a_3} t^{a_4}] + \text{tr} [t^{a_4} t^{a_3} t^{a_2} t^{a_1}] \right) P_{\Phi,f}^{\mu_1\mu_2\mu_3\mu_4}(q_1, q_2, q_3, q_4, m_f). \quad (\text{B.54})$$

In total, there exist 12 pentagons related by charge conjugation. Due to the length of the expressions for the fermionic pentagons, the tensorial structure will be described in a very brief way. For all pentagons, tensor reduction methods developed by Denner and Dittmaier [34, 35] were applied, which avoid the inversion of small Gram determinants, in particular for planar configurations of the Higgs and the two final state partons. Furthermore, all pentagons are UV- and IR-finite and are implemented as independent functions in the gluon fusion part  $GGFLO$  of the program  $VBFNLO$  [4].

The evaluation of the Dirac-trace with  $\mathcal{V}_A = \gamma_5$  contains  $E^{\mu_1\mu_2}$ ,  $E^\mu$ ,  $E^0$ ,  $D^\mu$ ,  $D^0$  and  $C^0$  functions.

The pentagon contribution for the  $\mathcal{CP}$ -even Higgs bosons  $H_{\text{SM}}$ ,  $h$  and  $H$  with  $\mathcal{V}_{H_{\text{SM}},h,H} = \mathbb{1}$  is composed of  $E^{\mu_1\mu_2\mu_3\mu_4}$ ,  $E^{\mu_1\mu_2\mu_3}$ ,  $E^{\mu_1\mu_2}$ ,  $E^{\mu_1}$ ,  $E^0$ ,  $D^{\mu_1\mu_2}$ ,  $D^{\mu_1}$  and  $D^0$  functions.

### B.3.2 Sfermion-pentagon with $\mathcal{CP}$ -even Higgs vertex

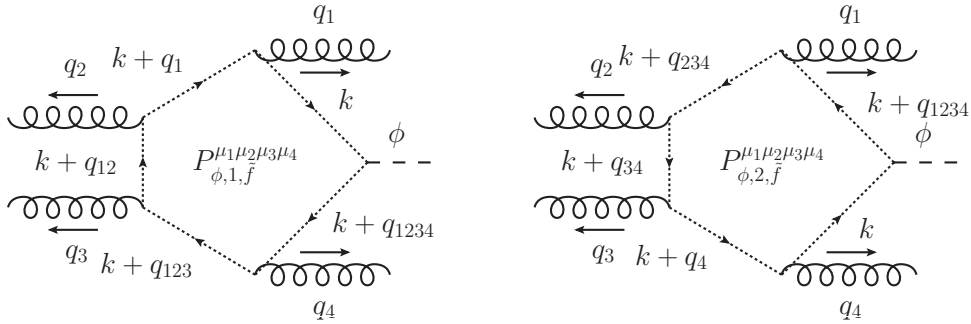


Figure B.10: *Sfermionic pentagon-loops with opposite fermion flow*

The generic five-point functions for sfermionic pentagon graphs with  $\mathcal{CP}$ -even Higgs vertex and opposite loop momentum, shown in Fig. B.10, have the following expressions

$$\begin{aligned}
P_{\Phi,1,\bar{f}}^{\mu_1\mu_2\mu_3\mu_4}(q_1, q_2, q_3, q_4, m_{\bar{f}}) &= \int \frac{d^4k}{i\pi^2} [2k + q_1]^{\mu_1} [2(k + q_1) + q_2]^{\mu_2} \\
&\times \frac{[2(k + q_{12}) + q_3]^{\mu_3} [2(k + q_{123}) + q_4]^{\mu_4}}{\left[ k^2 - m_{\bar{f}}^2 \right] \left[ \dots \right] \left[ \dots \right] \left[ \dots \right] \left[ (k + q_{1234})^2 - m_{\bar{f}}^2 \right]}, \quad (\text{B.55})
\end{aligned}$$

$$\begin{aligned}
P_{\Phi,2,\bar{f}}^{\mu_1\mu_2\mu_3\mu_4}(q_1, q_2, q_3, q_4, m_{\bar{f}}) &= \int \frac{d^4k}{i\pi^2} [2k + q_4]^{\mu_3} [2(k + q_4) + q_3]^{\mu_2} \\
&\times \frac{[2(k + q_{34}) + q_2]^{\mu_1} [2(k + q_{234}) + q_1]^{\mu_1}}{[k^2 - m_{\bar{f}}^2] [\dots] [\dots] [\dots] [(k + q_{1234})^2 - m_{\bar{f}}^2]}. \tag{B.56}
\end{aligned}$$

The shorthand notation  $[\dots]$  denotes intermediate propagators. After a shift of the loop momentum, both Pentagons can be replaced by one expression with the color structure of Eq. (B.54). The evaluated expression of the sfermionic pentagon is given by

$$\begin{aligned}
&P_{h,H,\bar{f}}^{\mu_1\mu_2\mu_3\mu_4}(q_1, q_2, q_3, q_4, m_{\bar{f}}) \\
&= 16E^{\mu_1\mu_2\mu_3\mu_4} + 8(2q_1^{\mu_4} + 2q_2^{\mu_4} + 2q_3^{\mu_4} + q_4^{\mu_4})E^{\mu_1\mu_2\mu_3} + 8(2q_1^{\mu_3} \\
&+ 2q_2^{\mu_3} + q_3^{\mu_3})E^{\mu_1\mu_2\mu_4} + 8(2q_1^{\mu_2} + q_2^{\mu_2})E^{\mu_1\mu_3\mu_4} + 8q_1^{\mu_1}E^{\mu_2\mu_3\mu_4} + 4(2q_1^{\mu_3} \\
&+ 2q_2^{\mu_3} + q_3^{\mu_3})(2q_1^{\mu_4} + 2q_2^{\mu_4} + 2q_3^{\mu_4} + q_4^{\mu_4})E^{\mu_1\mu_2} + 4(2q_1^{\mu_2} + q_2^{\mu_2})(2q_1^{\mu_4} \\
&+ 2q_2^{\mu_4} + 2q_3^{\mu_4} + q_4^{\mu_4})E^{\mu_1\mu_3} + 4q_1^{\mu_1}(2q_1^{\mu_4} + 2q_2^{\mu_4} + 2q_3^{\mu_4} + q_4^{\mu_4})E^{\mu_2\mu_3} \\
&+ 4(2q_1^{\mu_2} + q_2^{\mu_2})(2q_1^{\mu_3} + 2q_2^{\mu_3} + q_3^{\mu_3})E^{\mu_1\mu_4} + 4q_1^{\mu_1}(2q_1^{\mu_3} + 2q_2^{\mu_3} \\
&+ q_3^{\mu_3})E^{\mu_2\mu_4} + 4q_1^{\mu_1}(2q_1^{\mu_2} + q_2^{\mu_2})E^{\mu_3\mu_4} + 2(2q_1^{\mu_2} + q_2^{\mu_2})(2q_1^{\mu_3} + 2q_2^{\mu_3} \\
&+ q_3^{\mu_3})(2q_1^{\mu_4} + 2q_2^{\mu_4} + 2q_3^{\mu_4} + q_4^{\mu_4})E^{\mu_1} + 2q_1^{\mu_1}(2q_1^{\mu_3} + 2q_2^{\mu_3} + q_3^{\mu_3})(2q_1^{\mu_4} \\
&+ 2q_2^{\mu_4} + 2q_3^{\mu_4} + q_4^{\mu_4})E^{\mu_2} + 2q_1^{\mu_1}(2q_1^{\mu_2} + q_2^{\mu_2})(2q_1^{\mu_4} + 2q_2^{\mu_4} + 2q_3^{\mu_4} \\
&+ q_4^{\mu_4})E^{\mu_3} + 2q_1^{\mu_1}(2q_1^{\mu_2} + q_2^{\mu_2})(2q_1^{\mu_3} + 2q_2^{\mu_3} + q_3^{\mu_3})E^{\mu_4} + q_1^{\mu_1}(2q_1^{\mu_2} \\
&+ q_2^{\mu_2})(2q_1^{\mu_3} + 2q_2^{\mu_3} + q_3^{\mu_3})(2q_1^{\mu_4} + 2q_2^{\mu_4} + 2q_3^{\mu_4} + q_4^{\mu_4})E_0 \tag{B.57}
\end{aligned}$$

## B.4 Six-point functions (Hexagons)

The hexagons  $H_{\Phi,p}^{\mu_1\mu_2\mu_3\mu_4\mu_5}(q_1, q_2, q_3, q_4, q_5, m_p)$  are computed using traditional methods, that is, computing the Feynman diagrams and giving the result in terms of tensor coefficient integrals  $F_{ij}$  of six-point functions up to rank five for the  $\mathcal{CP}$ -even case and up to rank three for the  $\mathcal{CP}$ -odd case. In the process, some simplification has been used, the scalar products between of loop momenta and external momenta are rewritten in terms of propagators and some simplification can be done. Furthermore, tensor reduction methods of Denner and Dittmaier [34, 35] were used. In the hexagon subroutine also

appear  $E_{ij}$  and some  $D_{ij}$  functions. Moreover, all the gluons are kept off-shell to be able to attach to them some external current. For more details see Ref. [36]. The five external gluons give rise to  $5! = 120$  hexagons, which are of course proportional to 120 different color traces of the form

$$\begin{aligned} \text{tr}[t^{a_i} t^{a_j} t^{a_k} t^{a_l} t^{a_m}] \quad \text{with} \quad i, j, k, l, m = 1, \dots, 5 \\ \text{and} \quad i \neq j \neq k \neq l \neq m . \end{aligned} \quad (\text{B.58})$$

In total there exist 60 hexagons related by charge conjugation. With the permutation (1,2,3,4,5) of the attached gluons the color structure for a sum of two hexagons reads as follows

$$\begin{aligned} \left( \text{tr}[t^{a_1} t^{a_2} t^{a_3} t^{a_4} t^{a_5}] - \text{tr}[t^{a_5} t^{a_4} t^{a_3} t^{a_2} t^{a_1}] \right) \\ \times H_{\Phi, p}^{\mu_1 \mu_2 \mu_3 \mu_4 \mu_5}(q_1, q_2, q_3, q_4, q_5, m_p) . \end{aligned} \quad (\text{B.59})$$





# Appendix C

## SU( $N$ ) identities

---

This appendix contains a summary of useful identities of the SU( $N$ ) algebra, which were used in processes, explained in former chapters. For more details see references [14, 54, 55, 56].

### C.1 SU( $N$ ) tensors

$$\delta^{a_1 a_2} = 2 \operatorname{tr}(t^{a_1} t^{a_2}) , \quad (\text{C.1})$$

$$d^{a_1 a_2 a_3} = 2 \operatorname{tr}(\{t^{a_1}, t^{a_2}\} t^{a_3}) , \quad (\text{C.2})$$

$$f^{a_1 a_2 a_3} = 2 \operatorname{i} \operatorname{tr}(t^{a_1} [t^{a_3}, t^{a_2}]) . \quad (\text{C.3})$$

### C.2 Traces of color generators

$$\operatorname{tr}[t^a] = 0 , \quad (\text{C.4})$$

$$\operatorname{tr}[t^{a_1} t^{a_2}] = T_F \delta^{a_1 a_2} = \frac{1}{2} \delta^{a_1 a_2} , \quad (\text{C.5})$$

$$\operatorname{tr}[t^{a_1} t^{a_2} t^{a_3}] = \frac{1}{4} (d^{a_1 a_2 a_3} + \operatorname{i} f^{a_1 a_2 a_3}) , \quad (\text{C.6})$$

$$\begin{aligned} \operatorname{tr}[t^{a_1} t^{a_2} t^{a_3} t^{a_4}] &= \frac{1}{4N} \delta^{a_1 a_2} \delta^{a_3 a_4} \\ &+ \frac{1}{8} (d^{a_1 a_2 m} + \operatorname{i} f^{a_1 a_2 m}) (d^{a_3 a_4 m} + \operatorname{i} f^{a_3 a_4 m}) , \end{aligned} \quad (\text{C.7})$$

$$\begin{aligned}
\text{tr}[t^{a_1} t^{a_2} t^{a_3} t^{a_4} t^{a_5}] &= \frac{1}{8N} (d^{a_1 a_2 a_3} + i f^{a_1 a_2 a_3}) \delta^{a_4 a_5} \\
&+ \frac{1}{8N} \delta^{a_1 a_2} (d^{a_3 a_4 a_5} + i f^{a_3 a_4 a_5}) + \frac{1}{16} (d^{a_1 a_2 m} + i f^{a_1 a_2 m}) \\
&\times (d^{m a_3 n} + i f^{m a_3 n}) (d^{n a_4 a_5} + i f^{n a_4 a_5}) . \tag{C.8}
\end{aligned}$$

### C.3 Convolutions of $d^{a_1 a_2 a_3}$ and $f^{a_1 a_2 a_3}$ with $t^a$

$$\begin{aligned}
&d^{a_1 a_2 m} d^{m a_3 n} t_{i_2 i_1}^n \\
&= (t^{a_1} t^{a_2} t^{a_3} + t^{a_2} t^{a_1} t^{a_3} + t^{a_3} t^{a_1} t^{a_2} + t^{a_3} t^{a_2} t^{a_1})_{i_2 i_1} \\
&- \frac{1}{3} d^{a_1 a_2 a_3} \delta_{i_2 i_1} - \frac{2}{3} \delta^{a_1 a_2} t_{i_2 i_1}^{a_3} , \tag{C.9}
\end{aligned}$$

$$\begin{aligned}
&f^{a_1 a_2 m} f^{m a_3 n} t_{i_2 i_1}^n \\
&= (-t^{a_1} t^{a_2} t^{a_3} + t^{a_2} t^{a_1} t^{a_3} + t^{a_3} t^{a_1} t^{a_2} - t^{a_3} t^{a_2} t^{a_1})_{i_2 i_1} , \tag{C.10}
\end{aligned}$$

$$\begin{aligned}
&d^{a_1 a_2 m} f^{m a_3 n} t_{i_2 i_1}^n \\
&= i(-t^{a_1} t^{a_2} t^{a_3} - t^{a_2} t^{a_1} t^{a_3} + t^{a_3} t^{a_1} t^{a_2} + t^{a_3} t^{a_2} t^{a_1})_{i_2 i_1} \tag{C.11}
\end{aligned}$$

$$\begin{aligned}
&f^{a_1 a_2 m} d^{m a_3 n} t_{i_2 i_1}^n \\
&= i(-t^{a_1} t^{a_2} t^{a_3} + t^{a_2} t^{a_1} t^{a_3} - t^{a_3} t^{a_1} t^{a_2} + t^{a_3} t^{a_2} t^{a_1})_{i_2 i_1} \\
&- \frac{1}{3} f^{a_1 a_2 a_3} \delta_{i_2 i_1} . \tag{C.12}
\end{aligned}$$

### C.4 Jacobi identities

$$d^{a_1 a_2 m} f^{m a_3 a_4} + d^{a_2 a_3 m} f^{m a_1 a_4} + d^{a_3 a_1 m} f^{m a_2 a_4} = 0 , \tag{C.13}$$

$$f^{a_1 a_2 m} f^{m a_3 a_4} + f^{a_1 a_4 m} f^{m a_2 a_3} + f^{a_1 a_3 m} f^{m a_4 a_2} = 0 . \tag{C.14}$$

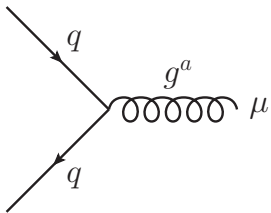
# Appendix D

## QCD- and SQCD Vertices

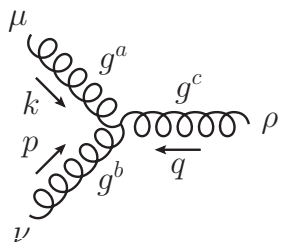
---

This Appendix illustrates only the vertices of the QCD and SQCD used in former calculations. Further vertices, especially of the SQCD, can be looked up in Ref. [10].

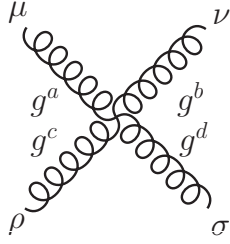
### D.1 QCD vertices



$$ig_S \gamma^\mu t^a \quad (D.1)$$

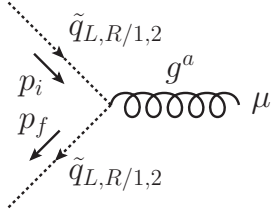


$$g_S f^{abc} \left[ g^{\mu\nu} (k - p)^\rho + g^{\nu\rho} (p - q)^\mu + g^{\rho\mu} (q - k)^\nu \right] \quad (D.2)$$

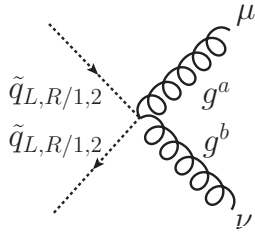


$$\begin{aligned}
 & -ig_S^2 \left[ f^{abe} f^{cde} (g^{\mu\rho} g^{\nu\sigma} - g^{\mu\sigma} g^{\nu\rho}) \right. \\
 & \quad + f^{ace} f^{bde} (g^{\mu\nu} g^{\rho\sigma} - g^{\mu\sigma} g^{\nu\rho}) \\
 & \quad \left. + f^{ade} f^{bce} (g^{\mu\rho} g^{\nu\sigma} - g^{\mu\rho} g^{\nu\sigma}) \right] \quad (D.3)
 \end{aligned}$$

## D.2 SQCD vertices (only squarks)



$$ig_S t^a (p_i + p_f)^\mu \quad (D.4)$$



$$ig_S^2 \{t^a, t^b\} g^{\mu\nu} \quad (D.5)$$

# Appendix E

## Effective Lagrangian

---

The calculation of Higgs + 2 jet and 3 jet via gluon fusion is quite involved, due to the fact, that already at leading order the Higgs boson is produced via a quark loop. For Higgs masses smaller than the threshold for the creation of a top-quark pair,  $m_\phi \lesssim 2 m_t$ , and jet transverse energies smaller than the top-quark mass,  $p_\perp \lesssim m_t$  [57] it is possible to replace different quark loop topologies by effective vertices [58]. In this connection low-energy theorems for Higgs boson interactions are used to relate amplitudes of two processes which differ by the insertions of a zero momentum Higgs boson [59, 60]. A direct comparison between loop and effective theory induced production of the  $\mathcal{CP}$ -even and  $\mathcal{CP}$ -odd Higgs boson with two jets is shown in plot E.1. The striking peak, which is absent in the effective limit, arises due to threshold enhancement at  $m_H \approx 2 m_t$ . For that reason, finite width effects were included to control the behavior of this resonance. The threshold enhancement is smoother in the case of the  $\mathcal{CP}$ -even Higgs boson, due to its large width, which is caused by additional contributions of decays to  $W$  and  $Z$  gauge bosons. For the  $\mathcal{CP}$ -odd case those decays are forbidden at tree-level. The effective Lagrangian density for the  $\mathcal{CP}$ -even Higgs boson  $H$  can be derived from the  $\gamma\gamma - H$  coupling, which is mediated by a triangle fermion loop. Similar to that, one can derive the effective Lagrangian of the  $\mathcal{CP}$ -odd Higgs boson  $A$  from the anomaly of the axial-vector current [61, 62]. Then, it is quite straightforward to generalize both Lagrangians to the non-Abelian  $SU(3)$  group. Hence, the effective theory is a powerful tool to examine QCD-processes without enormous numerical effort. For more details see also Refs. [15, 63, 64]. The effective Lagrangians for both Higgs bosons read as

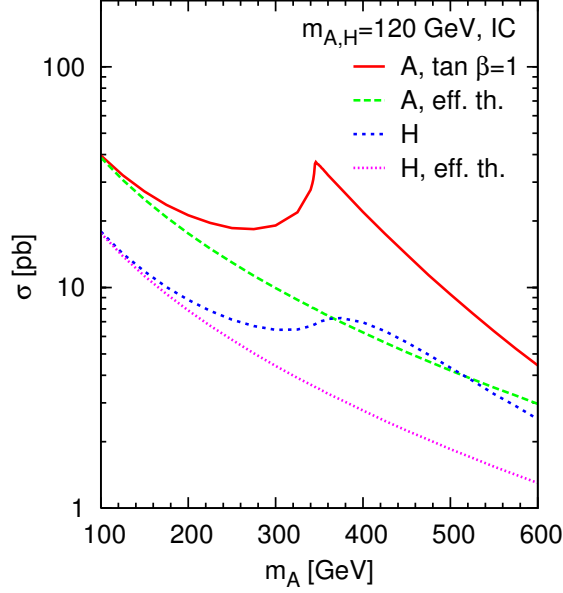


Figure E.1: Comparison of cross sections of the  $\mathcal{CP}$ -odd and  $\mathcal{CP}$ -even Higgs coupling in both loop-induced and effective theory. Here, the inclusive cuts (IC) of Eq. (5.1) were applied.

$$\begin{aligned}
\mathcal{L}_{\text{eff}} &= \mathcal{L}_{H^0 gg} + \mathcal{L}_{A^0 gg} \\
&= \frac{1}{v} \frac{\alpha_s}{12\pi} G_{\mu_1\mu_2}^a G^{\mu_1\mu_2 a} H + \frac{1}{v} \frac{\alpha_s}{8\pi} G_{\mu_1\mu_2}^a \tilde{G}^{\mu_1\mu_2 a} A
\end{aligned} \tag{E.1}$$

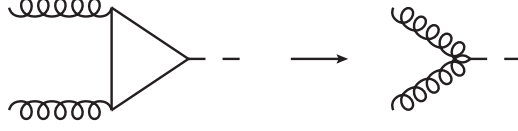
with

$$\tilde{G}^{a\mu_1\mu_2} = \frac{1}{2} \epsilon^{\mu_1\mu_2\mu_3\mu_4} G_{\mu_3\mu_4}^a, \quad \alpha_s = \frac{g_s^2}{4\pi}, \quad \frac{1}{v} = \left(\sqrt{2}G_F\right)^{1/2}, \tag{E.2}$$

where  $G_{\alpha\beta}^a$  denotes the non-Abelian field strength tensor of the SU(3) gluon field,  $v$  the vacuum expectation value and  $G_F$  the Fermi constant.

The effective Lagrangians generate vertices involving two, three or four gluons and, of course, the Higgs bosons. Up to the box diagrams, the full loop and the effective theory can be related to each other very easily, because their color structure is equal.

- **Effective  $gg\phi$  vertex  $\leftrightarrow$  triangle loops**



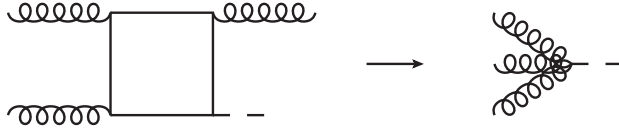
The effective  $gg\phi$  interactions for both Higgs bosons without couplings constants are [65]

$$T_{H,\text{eff}}^{\mu_1\mu_2}(q_1, q_2) = \frac{1}{3}\delta^{a_1a_2}(g^{\mu_1\mu_2}q_1 \cdot q_2 - q_1^{\mu_1}q_2^{\mu_2}) \quad \text{and} \quad (\text{E.3})$$

$$T_{A,\text{eff}}^{\mu_1\mu_2}(q_1, q_2) = \frac{1}{2}\delta^{a_1a_2}\varepsilon^{\mu_1\mu_2\mu_3\mu_4}q_{1,\mu_3}q_{2,\mu_4} \quad (\text{E.4})$$

To involve full mass dependence, one has to replace the effective vertices by the expression  $\delta^{a_1a_2}T_\phi^{\mu_1\mu_2}(q_1, q_2, m_t)$  (B.5) containing two charge-conjugated triangle loops

- **effective  $ggg\phi$  vertex  $\leftrightarrow$  box loops**

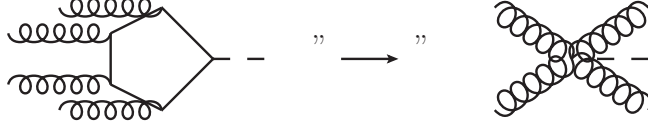


The tensor structure of the effective  $ggg\phi$  interaction corresponds exactly to that of a three-gluon vertex (D.2)

$$B_{H,\text{eff}}^{\mu_1\mu_2\mu_3}(q_1, q_2, q_3) = f^{a_1a_2a_3}\left[g^{\mu_1\mu_2}(q_2 - q_1)^{\mu_3} + g^{\mu_2\mu_3}(q_3 - q_2)^{\mu_1} + g^{\mu_3\mu_1}(q_1 - q_3)^{\mu_2}\right]. \quad (\text{E.5})$$

Inserting a box diagram denoted by  $f^{a_1a_2a_3}B_\phi^{\mu_1\mu_2\mu_3}(q_1, q_2, q_3, m_t)$  (B.28) into the effective vertex brings the full mass dependence back. In total, however, there are six box graphs with different permutations of the external momenta. These can be reduced via Furry's theorem [29] to three boxes with cyclicly permuted gluons.

- **effective  $gggg\phi$  vertex  $\leftrightarrow$  pentagon loops**



The effective  $gggg\phi$  interaction with  $\phi = H_{\text{SM}}, h^0, H^0$  is a copy of the four-gluon vertex (D.3)

$$\begin{aligned}
P_{H, \text{eff}}^{\mu_1 \mu_2 \mu_3 \mu_4}(q_1, q_2, q_3, q_4) = & \left[ f^{a_1 a_2 m} f^{a_3 a_4 m} (g^{\mu_1 \mu_3} g^{\mu_2 \mu_4} - g^{\mu_1 \mu_4} g^{\mu_2 \mu_3}) \right. \\
& + f^{a_1 a_3 m} f^{a_2 a_4 m} (g^{\mu_1 \mu_2} g^{\mu_3 \mu_4} - g^{\mu_1 \mu_4} g^{\mu_2 \mu_3}) \\
& \left. + f^{a_1 a_4 m} f^{a_2 a_3 m} (g^{\mu_1 \mu_3} g^{\mu_2 \mu_4} - g^{\mu_1 \mu_3} g^{\mu_2 \mu_4}) \right] \quad (\text{E.6})
\end{aligned}$$

For the  $\mathcal{CP}$ -odd Higgs boson  $A^0$ , there exists no effective vertex. It vanishes due to the anti-symmetry of the Levi-Civita symbol and structure constants and the Bose symmetry of the four attached gluons. A detailed proof is described in Ref. [3]. The non existence of this vertex can also be explained in a geometrical way. The four polarization vectors contain only space-like entries and hence span a three-dimensional subspace of the Minkowski vector space. Due to the fact that the maximal number of basis vectors is three, the fourth vector has to be a linear combination of the basis vectors. For this case the contraction of the four polarization vectors with the Levi-Civita symbol is exactly zero. The full theory contains  $4! = 24$  pentagons. Furry's theorem reduces the number of pentagons to 12. In chapter 3.3.3 it is shown that only six different color traces exist, which can be combined further to three real-valued color factors  $c_i$  (3.31). By means of  $c_1$  (3.32),

$$c_1 = \frac{1}{4} \left( \frac{2}{N} \delta^{a_1 a_2} \delta^{a_3 a_4} + d^{a_1 a_2 m} d^{a_3 a_4 m} - f^{a_1 a_2 m} f^{a_3 a_4 m} \right), \quad (\text{E.7})$$

one can see that the additional two terms spoil the simplicity of the color structure of a four-gluon vertex. Therefore, diagrams with a pentagon insertion have to be treated separately.



# Appendix F

## $gg \rightarrow ggg\Phi$

---

### F.1 Remaining color factors for diagrams with pentagons

The momenta configuration of the gluon current (3.10) is denoted by squared brackets. Furthermore, the structure constants  $f$  are contracted via the index  $m$  with the  $c_i$  of Eq. (3.31) using the following prescription

$$c_i f^{ma_p a_r} = \text{tr} [t^{a_j} t^{a_k} t^{a_l} t^m] f^{ma_p a_r}$$

with  $j, k, l, m, p, r = 1, \dots, 5$  and  $j \neq k \neq l \neq p \neq r$ .

Here the index  $i = 1, 2, 3$  denotes the corresponding order of the color generators inside the trace for a given  $c_i$ . The remaining permutations are

◦ permutation:  $\{3, 4, 5, [1, 2]\}$

$$c_1 f^{ma_1 a_2} = -i \left( \text{tr} [t^{a_3} t^{a_4} t^{a_5} t^{a_1} t^{a_2}] - \text{tr} [t^{a_3} t^{a_4} t^{a_5} t^{a_2} t^{a_1}] \right. \\ \left. + \text{tr} [t^{a_3} t^{a_1} t^{a_2} t^{a_5} t^{a_4}] - \text{tr} [t^{a_3} t^{a_2} t^{a_1} t^{a_5} t^{a_4}] \right), \quad (\text{F.1})$$

$$c_2 f^{ma_1 a_2} = -i \left( \text{tr} [t^{a_3} t^{a_5} t^{a_1} t^{a_2} t^{a_4}] - \text{tr} [t^{a_3} t^{a_5} t^{a_2} t^{a_1} t^{a_4}] \right. \\ \left. + \text{tr} [t^{a_3} t^{a_4} t^{a_1} t^{a_2} t^{a_5}] - \text{tr} [t^{a_3} t^{a_4} t^{a_2} t^{a_1} t^{a_5}] \right), \quad (\text{F.2})$$

$$c_3 f^{ma_1 a_2} = -i \left( \text{tr} [t^{a_3} t^{a_1} t^{a_2} t^{a_4} t^{a_5}] - \text{tr} [t^{a_3} t^{a_2} t^{a_1} t^{a_4} t^{a_5}] \right. \\ \left. + \text{tr} [t^{a_3} t^{a_5} t^{a_4} t^{a_1} t^{a_2}] - \text{tr} [t^{a_3} t^{a_5} t^{a_4} t^{a_2} t^{a_1}] \right), \quad (\text{F.3})$$

◦ permutation:  $\{2, 4, 5, [1, 3]\}$

$$c_1 f^{ma_1a_3} = -i \left( \text{tr} [t^{a_2} t^{a_4} t^{a_5} t^{a_1} t^{a_3}] - \text{tr} [t^{a_2} t^{a_4} t^{a_5} t^{a_3} t^{a_1}] \right. \\ \left. + \text{tr} [t^{a_2} t^{a_1} t^{a_3} t^{a_5} t^{a_4}] - \text{tr} [t^{a_2} t^{a_3} t^{a_1} t^{a_5} t^{a_4}] \right), \quad (\text{F.4})$$

$$c_2 f^{ma_1a_3} = -i \left( \text{tr} [t^{a_2} t^{a_5} t^{a_1} t^{a_3} t^{a_4}] - \text{tr} [t^{a_2} t^{a_5} t^{a_3} t^{a_1} t^{a_4}] \right. \\ \left. + \text{tr} [t^{a_2} t^{a_4} t^{a_1} t^{a_3} t^{a_5}] - \text{tr} [t^{a_2} t^{a_4} t^{a_3} t^{a_1} t^{a_5}] \right), \quad (\text{F.5})$$

$$c_3 f^{ma_1a_3} = -i \left( \text{tr} [t^{a_2} t^{a_1} t^{a_3} t^{a_4} t^{a_5}] - \text{tr} [t^{a_2} t^{a_3} t^{a_1} t^{a_4} t^{a_5}] \right. \\ \left. + \text{tr} [t^{a_2} t^{a_5} t^{a_4} t^{a_1} t^{a_3}] - \text{tr} [t^{a_2} t^{a_5} t^{a_4} t^{a_3} t^{a_1}] \right), \quad (\text{F.6})$$

◦ permutation:  $\{2, 3, 5, [1, 4]\}$

$$c_1 f^{ma_1a_4} = -i \left( \text{tr} [t^{a_2} t^{a_3} t^{a_5} t^{a_1} t^{a_4}] - \text{tr} [t^{a_2} t^{a_3} t^{a_5} t^{a_4} t^{a_1}] \right. \\ \left. + \text{tr} [t^{a_2} t^{a_1} t^{a_4} t^{a_5} t^{a_3}] - \text{tr} [t^{a_2} t^{a_4} t^{a_1} t^{a_5} t^{a_3}] \right), \quad (\text{F.7})$$

$$c_2 f^{ma_1a_4} = -i \left( \text{tr} [t^{a_2} t^{a_5} t^{a_1} t^{a_4} t^{a_3}] - \text{tr} [t^{a_2} t^{a_5} t^{a_4} t^{a_1} t^{a_3}] \right. \\ \left. + \text{tr} [t^{a_2} t^{a_3} t^{a_1} t^{a_4} t^{a_5}] - \text{tr} [t^{a_2} t^{a_3} t^{a_4} t^{a_1} t^{a_5}] \right), \quad (\text{F.8})$$

$$c_3 f^{ma_1a_4} = -i \left( \text{tr} [t^{a_2} t^{a_1} t^{a_4} t^{a_3} t^{a_5}] - \text{tr} [t^{a_2} t^{a_4} t^{a_1} t^{a_3} t^{a_5}] \right. \\ \left. + \text{tr} [t^{a_2} t^{a_5} t^{a_3} t^{a_1} t^{a_4}] - \text{tr} [t^{a_2} t^{a_5} t^{a_3} t^{a_4} t^{a_1}] \right), \quad (\text{F.9})$$

◦ permutation:  $\{(2, 3, 4, (1, 5))\}$

$$c_1 f^{ma_1a_5} = -i \left( \text{tr} [t^{a_2} t^{a_3} t^{a_4} t^{a_1} t^{a_5}] - \text{tr} [t^{a_2} t^{a_3} t^{a_4} t^{a_5} t^{a_1}] \right. \\ \left. + \text{tr} [t^{a_2} t^{a_1} t^{a_5} t^{a_4} t^{a_3}] - \text{tr} [t^{a_2} t^{a_5} t^{a_1} t^{a_4} t^{a_3}] \right), \quad (\text{F.10})$$

$$c_2 f^{ma_1a_5} = -i \left( \text{tr} [t^{a_2} t^{a_4} t^{a_1} t^{a_5} t^{a_3}] - \text{tr} [t^{a_2} t^{a_4} t^{a_5} t^{a_1} t^{a_3}] \right. \\ \left. + \text{tr} [t^{a_2} t^{a_3} t^{a_1} t^{a_5} t^{a_4}] - \text{tr} [t^{a_2} t^{a_3} t^{a_5} t^{a_1} t^{a_4}] \right), \quad (\text{F.11})$$

$$c_3 f^{ma_1a_5} = -i \left( \text{tr} [t^{a_2} t^{a_1} t^{a_5} t^{a_3} t^{a_4}] - \text{tr} [t^{a_2} t^{a_5} t^{a_1} t^{a_3} t^{a_4}] \right. \\ \left. + \text{tr} [t^{a_2} t^{a_4} t^{a_3} t^{a_1} t^{a_5}] - \text{tr} [t^{a_2} t^{a_4} t^{a_3} t^{a_5} t^{a_1}] \right), \quad (\text{F.12})$$

◦ permutation:  $\{(1, 4, 5, (2, 3))\}$

$$c_1 f^{ma_2a_3} = -i \left( \text{tr} [t^{a_1} t^{a_4} t^{a_5} t^{a_2} t^{a_3}] - \text{tr} [t^{a_1} t^{a_4} t^{a_5} t^{a_3} t^{a_2}] \right. \\ \left. + \text{tr} [t^{a_1} t^{a_2} t^{a_3} t^{a_5} t^{a_4}] - \text{tr} [t^{a_1} t^{a_3} t^{a_2} t^{a_5} t^{a_4}] \right), \quad (\text{F.13})$$

$$c_2 f^{ma_2a_3} = -i \left( \text{tr} [t^{a_1} t^{a_5} t^{a_2} t^{a_3} t^{a_4}] - \text{tr} [t^{a_1} t^{a_5} t^{a_3} t^{a_2} t^{a_4}] \right. \\ \left. + \text{tr} [t^{a_1} t^{a_4} t^{a_2} t^{a_3} t^{a_5}] - \text{tr} [t^{a_1} t^{a_4} t^{a_3} t^{a_2} t^{a_5}] \right), \quad (\text{F.14})$$

$$c_3 f^{ma_2a_3} = -i \left( \text{tr} [t^{a_1} t^{a_2} t^{a_3} t^{a_4} t^{a_5}] - \text{tr} [t^{a_1} t^{a_3} t^{a_2} t^{a_4} t^{a_5}] \right. \\ \left. + \text{tr} [t^{a_1} t^{a_5} t^{a_4} t^{a_2} t^{a_3}] - \text{tr} [t^{a_1} t^{a_5} t^{a_4} t^{a_3} t^{a_2}] \right), \quad (\text{F.15})$$

◦ permutation:  $\{(1, 3, 5, (2, 4))\}$

$$c_1 f^{ma_2a_4} = -i \left( \text{tr} [t^{a_1} t^{a_3} t^{a_5} t^{a_2} t^{a_4}] - \text{tr} [t^{a_1} t^{a_3} t^{a_5} t^{a_4} t^{a_2}] \right. \\ \left. + \text{tr} [t^{a_1} t^{a_2} t^{a_4} t^{a_5} t^{a_3}] - \text{tr} [t^{a_1} t^{a_4} t^{a_2} t^{a_5} t^{a_3}] \right), \quad (\text{F.16})$$

$$c_2 f^{ma_2a_4} = -i \left( \text{tr} [t^{a_1} t^{a_5} t^{a_2} t^{a_4} t^{a_3}] - \text{tr} [t^{a_1} t^{a_5} t^{a_4} t^{a_2} t^{a_3}] \right. \\ \left. + \text{tr} [t^{a_1} t^{a_3} t^{a_2} t^{a_4} t^{a_5}] - \text{tr} [t^{a_1} t^{a_3} t^{a_4} t^{a_2} t^{a_5}] \right), \quad (\text{F.17})$$

$$c_3 f^{ma_2a_4} = -i \left( \text{tr} [t^{a_1} t^{a_2} t^{a_4} t^{a_3} t^{a_5}] - \text{tr} [t^{a_1} t^{a_4} t^{a_2} t^{a_3} t^{a_5}] \right. \\ \left. + \text{tr} [t^{a_1} t^{a_5} t^{a_3} t^{a_2} t^{a_4}] - \text{tr} [t^{a_1} t^{a_5} t^{a_3} t^{a_4} t^{a_2}] \right), \quad (\text{F.18})$$

◦ permutation:  $\{(1, 3, 4, (2, 5))\}$

$$c_1 f^{ma_2a_5} = -i \left( \text{tr} [t^{a_1} t^{a_3} t^{a_4} t^{a_2} t^{a_5}] - \text{tr} [t^{a_1} t^{a_3} t^{a_4} t^{a_5} t^{a_2}] \right. \\ \left. + \text{tr} [t^{a_1} t^{a_2} t^{a_5} t^{a_4} t^{a_3}] - \text{tr} [t^{a_1} t^{a_5} t^{a_2} t^{a_4} t^{a_3}] \right), \quad (\text{F.19})$$

$$c_2 f^{ma_2a_5} = -i \left( \text{tr} [t^{a_1} t^{a_4} t^{a_2} t^{a_5} t^{a_3}] - \text{tr} [t^{a_1} t^{a_4} t^{a_5} t^{a_2} t^{a_3}] \right. \\ \left. + \text{tr} [t^{a_1} t^{a_3} t^{a_2} t^{a_5} t^{a_4}] - \text{tr} [t^{a_1} t^{a_3} t^{a_5} t^{a_2} t^{a_4}] \right), \quad (\text{F.20})$$

$$c_3 f^{ma_2a_5} = -i \left( \text{tr} [t^{a_1} t^{a_2} t^{a_5} t^{a_3} t^{a_4}] - \text{tr} [t^{a_1} t^{a_5} t^{a_2} t^{a_3} t^{a_4}] \right. \\ \left. + \text{tr} [t^{a_1} t^{a_4} t^{a_3} t^{a_2} t^{a_5}] - \text{tr} [t^{a_1} t^{a_4} t^{a_3} t^{a_5} t^{a_2}] \right), \quad (\text{F.21})$$

◦ permutation:  $\{(1, 2, 5, (3, 4))\}$

$$c_1 f^{ma_3a_4} = -i \left( \text{tr} [t^{a_1} t^{a_2} t^{a_5} t^{a_3} t^{a_4}] - \text{tr} [t^{a_1} t^{a_2} t^{a_5} t^{a_4} t^{a_3}] \right. \\ \left. + \text{tr} [t^{a_1} t^{a_3} t^{a_4} t^{a_5} t^{a_2}] - \text{tr} [t^{a_1} t^{a_4} t^{a_3} t^{a_5} t^{a_2}] \right), \quad (\text{F.22})$$

$$c_2 f^{ma_3a_4} = -i \left( \text{tr} [t^{a_1} t^{a_5} t^{a_3} t^{a_4} t^{a_2}] - \text{tr} [t^{a_1} t^{a_5} t^{a_4} t^{a_3} t^{a_2}] \right. \\ \left. + \text{tr} [t^{a_1} t^{a_2} t^{a_3} t^{a_4} t^{a_5}] - \text{tr} [t^{a_1} t^{a_2} t^{a_4} t^{a_3} t^{a_5}] \right), \quad (\text{F.23})$$

$$c_3 f^{ma_3a_4} = -i \left( \text{tr} [t^{a_1} t^{a_3} t^{a_4} t^{a_2} t^{a_5}] - \text{tr} [t^{a_1} t^{a_4} t^{a_3} t^{a_2} t^{a_5}] \right. \\ \left. + \text{tr} [t^{a_1} t^{a_5} t^{a_2} t^{a_3} t^{a_4}] - \text{tr} [t^{a_1} t^{a_5} t^{a_2} t^{a_4} t^{a_3}] \right), \quad (\text{F.24})$$

◦ permutation:  $\{(1, 2, 4, (3, 5))\}$

$$c_1 f^{ma_3a_5} = -i \left( \text{tr} [t^{a_1} t^{a_2} t^{a_4} t^{a_3} t^{a_5}] - \text{tr} [t^{a_1} t^{a_2} t^{a_4} t^{a_5} t^{a_3}] \right. \\ \left. + \text{tr} [t^{a_1} t^{a_3} t^{a_5} t^{a_4} t^{a_2}] - \text{tr} [t^{a_1} t^{a_5} t^{a_3} t^{a_4} t^{a_2}] \right), \quad (\text{F.25})$$

$$c_2 f^{ma_3a_5} = -i \left( \text{tr} [t^{a_1} t^{a_4} t^{a_3} t^{a_5} t^{a_2}] - \text{tr} [t^{a_1} t^{a_4} t^{a_5} t^{a_3} t^{a_2}] \right. \\ \left. + \text{tr} [t^{a_1} t^{a_2} t^{a_3} t^{a_5} t^{a_4}] - \text{tr} [t^{a_1} t^{a_2} t^{a_5} t^{a_3} t^{a_4}] \right), \quad (\text{F.26})$$

$$c_3 f^{ma_3a_5} = -i \left( \text{tr} [t^{a_1} t^{a_3} t^{a_5} t^{a_2} t^{a_4}] - \text{tr} [t^{a_1} t^{a_5} t^{a_3} t^{a_2} t^{a_4}] \right. \\ \left. + \text{tr} [t^{a_1} t^{a_4} t^{a_2} t^{a_3} t^{a_5}] - \text{tr} [t^{a_1} t^{a_4} t^{a_2} t^{a_5} t^{a_3}] \right). \quad (\text{F.27})$$

# Bibliography

---

- [1] V. Del Duca, W. Kilgore, C. Oleari, C. Schmidt, and D. Zeppenfeld, “*H + 2 jets via gluon fusion*,” *Phys. Rev. Lett.* **87** (2001) 122001, [hep-ph/0105129](#).
- [2] V. Del Duca, W. Kilgore, C. Oleari, C. Schmidt, and D. Zeppenfeld, “*Gluon-fusion contributions to H + 2 jet production*,” *Nucl. Phys.* **B616** (2001) 367–399, [arXiv:hep-ph/0108030](#).
- [3] M. Kubocz, “*Produktion des CP-ungeraden Higgs-Bosons im Prozess pp → A<sup>0</sup>jjX*,” Master’s thesis, Institut für Theoretische Physik, Universität Karlsruhe, <http://www-itp.particle.uni-karlsruhe.de/diplomatheses.de.shtml>, 2006.
- [4] K. Arnold, M. Bahr, G. Bozzi, F. Campanario, T. Englert, C. and Figy, N. Greiner, C. Hackstein, V. Hankele, B. Jager, G. Klamke, M. Kubocz, C. Oleari, S. Platzer, S. Prestel, M. Worek, and D. Zeppenfeld, “*VBFNLO: A parton level Monte Carlo for processes with electroweak bosons*,” [arXiv:0811.4559 \[hep-ph\]](#).
- [5] S. P. Martin, “A Supersymmetry Primer,” [arXiv:hep-ph/9709356](#).
- [6] A. Djouadi, “The Anatomy of electro-weak symmetry breaking. II. The Higgs bosons in the minimal supersymmetric model,” *Phys. Rept.* **459** (2008) 1–241, [arXiv:hep-ph/0503173](#).
- [7] R. D. Peccei and H. R. Quinn, “CP Conservation in the Presence of Instantons,” *Phys. Rev. Lett.* **38** (1977) 1440–1443.
- [8] J. F. Gunion, H. E. Haber, G. L. Kane, and S. Dawson, “*The Higgs Hunter’s Guide*,” 1990.
- [9] X. T. H. Baer, “*Weak Scale Supersymmetry*,” 2006.

- [10] P. R. M. Drees, R. M. Gonbole, “*Theory and Phenomenology of Sparticles,*” 2004.
- [11] D. J. Gross and F. Wilczek, “Asymptotically Free Gauge Theories. 1,” *Phys. Rev.* **D8** (1973) 3633–3652.
- [12] H. D. Politzer, “Reliable perturbative results for strong interactions?,” *Phys. Rev. Lett.* **30** (1973) 1346–1349.
- [13] **CTEQ** Collaboration, R. Brock *et al.*, “Handbook of perturbative QCD: Version 1.0,” *Rev. Mod. Phys.* **67** (1995) 157–248.
- [14] M. E. P. und D. V. Schroeder, *An Introduction to Quantum Field Theory.* Westview Press, Boulder, 1995.
- [15] M. Spira, A. Djouadi, D. Graudenz, and P. M. Zerwas, “*Higgs boson production at the LHC,*” *Nucl. Phys.* **B453** (1995) 17–82, [arXiv:hep-ph/9504378](#).
- [16] M. Spira, “*QCD effects in Higgs physics,*” *Fortsch. Phys.* **46** (1998) 203–284, [arXiv:hep-ph/9705337](#).
- [17] R. V. Harlander and W. B. Kilgore, “*Next-to-next-to-leading order Higgs production at hadron colliders,*” *Phys. Rev. Lett.* **88** (2002) 201801, [arXiv:hep-ph/0201206](#).
- [18] C. Anastasiou and K. Melnikov, “*Higgs boson production at hadron colliders in NNLO QCD,*” *Nucl. Phys.* **B646** (2002) 220–256, [arXiv:hep-ph/0207004](#).
- [19] T. Figy, C. Oleari, and D. Zeppenfeld, “*Next-to-leading order jet distributions for Higgs boson production via weak-boson fusion,*” *Phys. Rev.* **D68** (2003) 073005, [arXiv:hep-ph/0306109](#).
- [20] T. Figy, V. Hankele, and D. Zeppenfeld, “*Next-to-leading order QCD corrections to Higgs plus three jet production in vector-boson fusion,*” *JHEP* **02** (2008) 076, [arXiv:0710.5621](#) [hep-ph].
- [21] J. M. Campbell, R. K. Ellis, and G. Zanderighi, “*Next-to-leading order Higgs + 2 jet production via gluon fusion,*” *JHEP* **10** (2006) 028, [arXiv:hep-ph/0608194](#).

- [22] Z. Kunszt, “Associated Production of Heavy Higgs Boson with Top Quarks,” *Nucl. Phys.* **B247** (1984) 339.
- [23] W. J. Marciano and F. E. Paige, “Associated production of Higgs bosons with  $t$  anti- $t$  pairs,” *Phys. Rev. Lett.* **66** (1991) 2433–2435.
- [24] S. L. Glashow, D. V. Nanopoulos, and A. Yildiz, “Associated Production of Higgs Bosons and Z Particles,” *Phys. Rev.* **D18** (1978) 1724–1727.
- [25] T. Han and S. Willenbrock, “QCD correction to the  $p p \rightarrow W H$  and  $Z H$  total cross-sections,” *Phys. Lett.* **B273** (1991) 167–172.
- [26] K. Hagiwara and D. Zeppenfeld, “Helicity Amplitudes for Heavy Lepton Production in  $e^+ e^-$  Annihilation,” *Nucl. Phys.* **B274** (1986) 1.
- [27] K. Hagiwara and D. Zeppenfeld, “Amplitudes for Multiparton Processes Involving a Current at  $e^+ e^-$ ,  $e^+ p$ , and Hadron Colliders,” *Nucl. Phys.* **B313** (1989) 560.
- [28] H. Murayama, I. Watanabe, and K. Hagiwara, “HELAS: HELicity amplitude subroutines for Feynman diagram evaluations,”. KEK-91-11.
- [29] W. H. Furry, “A symmetry theorem in the positron theory,” *Phys. Rev.* **51** (1936) 125.
- [30] M. Kubocz and D. Zeppenfeld, “Gluon-fusion contributions to  $\phi + 2$  jet production,” 2009, in preparation.
- [31] F. Maltoni and T. Stelzer, “MadEvent: Automatic event generation with MadGraph,” *JHEP* **02** (2003) 027, [arXiv:hep-ph/0208156](https://arxiv.org/abs/hep-ph/0208156).
- [32] G. Passarino and M. J. G. Veltman, “One Loop Corrections for  $e^+ e^-$  Annihilation Into  $\mu^+ \mu^-$  in the Weinberg Model,” *Nucl. Phys.* **B160** (1979) 151.
- [33] G. ’t Hooft and M. J. G. Veltman, “Scalar One Loop Integrals,” *Nucl. Phys.* **B153** (1979) 365–401.
- [34] A. Denner and S. Dittmaier, “Reduction of one-loop tensor 5-point integrals,” *Nucl. Phys.* **B658** (2003) 175–202, [arXiv:hep-ph/0212259](https://arxiv.org/abs/hep-ph/0212259).

- [35] A. Denner and S. Dittmaier, “*Reduction schemes for one-loop tensor integrals,*” *Nucl. Phys.* **B734** (2006) 62–115, [arXiv:hep-ph/0509141](#).
- [36] F. Campanario, “private communication.”.
- [37] T. Hahn, “*Generating Feynman diagrams and amplitudes with FeynArts 3,*” *Comput. Phys. Commun.* **140** (2001) 418–431, [arXiv:hep-ph/0012260](#).
- [38] T. Hahn and C. Schappacher, “*The implementation of the minimal supersymmetric standard model in FeynArts and FormCalc,*” *Comput. Phys. Commun.* **143** (2002) 54–68, [arXiv:hep-ph/0105349](#).
- [39] T. Hahn and M. Perez-Victoria, “*Automatized one-loop calculations in four and D dimensions,*” *Comput. Phys. Commun.* **118** (1999) 153–165, [arXiv:hep-ph/9807565](#).
- [40] J. Pumplin *et al.*, “*New generation of parton distributions with uncertainties from global QCD analysis,*” *JHEP* **07** (2002) 012, [arXiv:hep-ph/0201195](#).
- [41] C. A. et al. (Particle Data Group) *Physics Letters* **B667**, **1** (2008) and **2009 partial update for the 2010 edition** .
- [42] V. Del Duca, A. Frizzo, and F. Maltoni, “*Higgs boson production in association with three jets,*” *JHEP* **05** (2004) 064, [arXiv:hep-ph/0404013](#).
- [43] G. Klamke and D. Zeppenfeld, “*H<sub>jj</sub> production: Signals and CP measurements,*” [arXiv:0705.2983 \[hep-ph\]](#).
- [44] T. Plehn, D. L. Rainwater, and D. Zeppenfeld, “*Determining the structure of Higgs couplings at the LHC,*” *Phys. Rev. Lett.* **88** (2002) 051801, [arXiv:hep-ph/0105325](#).
- [45] V. Hankele, G. Klamke, and D. Zeppenfeld, “*Higgs + 2 jets as a probe for CP properties,*” [arXiv:hep-ph/0605117](#).
- [46] K. Gunnar. PhD thesis.



- [47] S. Heinemeyer, W. Hollik, and G. Weiglein, “*FeynHiggs: a program for the calculation of the masses of the neutral CP-even Higgs bosons in the MSSM,*” *Comput. Phys. Commun.* **124** (2000) 76–89, [arXiv:hep-ph/9812320](#).
- [48] S. Heinemeyer, W. Hollik, and G. Weiglein, “*The Masses of the neutral CP - even Higgs bosons in the MSSM: Accurate analysis at the two loop level,*” *Eur. Phys. J.* **C9** (1999) 343–366, [arXiv:hep-ph/9812472](#).
- [49] G. Degrandi, S. Heinemeyer, W. Hollik, P. Slavich, and G. Weiglein, “*Towards high-precision predictions for the MSSM Higgs sector,*” *Eur. Phys. J.* **C28** (2003) 133–143, [arXiv:hep-ph/0212020](#).
- [50] M. Frank *et al.*, “*The Higgs boson masses and mixings of the complex MSSM in the Feynman-diagrammatic approach,*” *JHEP* **02** (2007) 047, [arXiv:hep-ph/0611326](#).
- [51] K. Odagiri, “*On azimuthal spin correlations in Higgs plus jet events at LHC,*” *JHEP* **03** (2003) 009, [arXiv:hep-ph/0212215](#).
- [52] V. Del Duca *et al.*, “*Monte Carlo studies of the jet activity in Higgs + 2jet events,*” *JHEP* **10** (2006) 016, [arXiv:hep-ph/0608158](#).
- [53] V. Del Duca, “*Higgs production in association with two jets at the LHC,*” *Acta Phys. Polon.* **B39** (2008) 1549–1554.
- [54] V. I. Borodulin, R. N. Rogalev, and S. R. Slabospitsky, “*CORE: Compendium of Relations: Version 2.1,*” [arXiv:hep-ph/9507456](#).
- [55] P. Cvitanovic, “*Group Theory for Feynman Diagrams in Nonabelian Gauge Theories: Exceptional Groups,*” *Phys. Rev.* **D14** (1976) 1536–1553.
- [56] T. Muta, *Foundations of Quantum Chromodynamics*. World Scientific Publishing Co. Pte. Ltd., 2000.
- [57] V. Del Duca, W. Kilgore, C. Oleari, C. R. Schmidt, and D. Zeppenfeld, “*Kinematical limits on Higgs boson production via gluon fusion in association with jets,*” *Phys. Rev.* **D67** (2003) 073003, [arXiv:hep-ph/0301013](#).

- [58] J. R. Ellis, M. K. Gaillard, and D. V. Nanopoulos, “A Phenomenological Profile of the Higgs Boson,” *Nucl. Phys.* **B106** (1976) 292.
- [59] S. Dawson and H. E. Haber, “A primer on Higgs boson low-energy theorems,”. To appear in Proc. of Workshop on High Energy Physics Phenomenology, Bombay, India, Jan 2-15, 1989.
- [60] M. A. Shifman, A. I. Vainshtein, M. B. Voloshin, and V. I. Zakharov, “Low-Energy Theorems for Higgs Boson Couplings to Photons,” *Sov. J. Nucl. Phys.* **30** (1979) 711–716.
- [61] J. S. Bell and R. Jackiw, “A PCAC puzzle:  $\pi^0 \rightarrow \gamma \gamma$  in the sigma model,” *Nuovo Cim.* **A60** (1969) 47–61.
- [62] S. L. Adler, “Axial vector vertex in spinor electrodynamics,” *Phys. Rev.* **177** (1969) 2426–2438.
- [63] S. Dawson, “Radiative corrections to Higgs boson production,” *Nucl. Phys.* **B359** (1991) 283–300.
- [64] R. P. Kauffman and W. Schaffer, “QCD corrections to production of Higgs pseudoscalars,” *Phys. Rev.* **D49** (1994) 551–554, [arXiv:hep-ph/9305279](https://arxiv.org/abs/hep-ph/9305279).
- [65] R. P. Kauffman, S. V. Desai, and D. Risal, “Amplitudes for Higgs bosons plus four partons,” [arXiv:hep-ph/9903330](https://arxiv.org/abs/hep-ph/9903330).

# Acknowledgements

---

My special thanks go to Prof. Dr. Dieter Zeppenfeld, for giving me the opportunity to work on this very interesting topic. I am particularly grateful for his advice, his interest in my work, and also for support in many respects. Special thanks go to Prof. Dr. Margarete Mühlleitner for the short-term acceptance of proofreading.

Also special thanks go to Gunnar Klämke for the great and important cooperation during my PhD thesis, to my room mates Christian Schappacher and Francisco Campanario for many important discussions (in English), the willingness to help and for the fantastic atmosphere, to which also our former room mate Luca D'Errico contributed a lot. Therefore also special thanks to Luca.

Special thanks to Christian Schappacher and Francisco Campanario for carefully reading of my Diss. and for giving me helpful advices.

Special thanks to Simon Plätzer for the help in technical questions about computer and other stuff and for interesting discussions.

Special thanks to Malin Sjö Dahl for the powerful color algebra mathematica package.

Special thanks to Anastasija Bierweiler, Philipp Maierhöfer, Cornelius Rampf and Gunnar Klämke for interesting discussions during the lunch time and leisure time.

I want to thank the Graduiertenkolleg "Hochenergiephysik und Teilchenastrophysik" and the Landesgraduiertenkolleg for its financial support.

I want to thank all members of the ITP for the fantastic atmosphere and helpfulness.

I am deeply grateful to my parents and grandparents for the tremendous encouragement during the whole study.